Loan Printing 7/23/73 Give to Pe?

(15)

OC
DI. 765

TID-26342

THIS DOCUMENT CONFIRMED AS UNCLASSIFIED
DIVISION OF CLASSIFICATION
BY J L Cucchiara / pab
DATE 8/1/73

Si–Au SCHOTTKY BARRIER NUCLEAR BATTERY

November 1972

MASTER

Thayer School of Engineering
Dartmouth College
Hanover, New Hampshire

DISTRIBUTION OF THIS DOCUMENT IS UNLIMITED

S1506

UNITED STATES ATOMIC ENERGY COMMISSION • TECHNICAL INFORMATION CENTER

DISCLAIMER

NOTICE

Available from the National Technical Information Service, U. S. Department of Commerce, Springfield, Virginia 22151.

Price: Paper Copy $7.60
Microfiche $0.95

Printed in the United States of America
USAEC Technical Information Center, Oak Ridge, Tennessee

TID-26342
Distribution Category UC-33

Si-Au SCHOTTKY BARRIER NUCLEAR BATTERY

A Thesis
Submitted to the Faculty
in partial fulfillment of the requirement
for the degree of
Doctor of Engineering

by

ANTHONY N. TSE

Thayer School of Engineering
Dartmouth College
Hanover, New Hampshire

November 1972

EXAMINING COMMITTEE

Graham B. Wallis
Graham B. Wallis, Chairman

John J. Pinajian
John J. Pinajian, Lab Adv.

Edward S. Brown
Edward Stickney Brown

Fred K. Manasse
Fred K. Manasse

John W. Strohbehn
John W. Strohbehn

Carl F. Tormey
Dean, Thayer School of Engineering

THAYER SCHOOL OF ENGINEERING
DARTMOUTH COLLEGE

Si-Au Schottky Barrier Nuclear Battery

by

Anthony N. Tse

Doctor of Engineering

NOVEMBER 1972

ABSTRACT

A long-life, high-power-density, high-reliability, compact microwatt battery is needed in many applications. In the field of medicine, for example, such a battery could power an artificial pacemaker which would greatly extend the residence time of the device.

Various alternatives are analyzed and discussed. Betavoltaic conversion systems with Si-Au Schottky barrier cells coupled with ^{147}Pm metal foil were selected for investigation. Characterization experiments were performed to obtain optimized silicon resistivity and promethium metal foil thickness. Radiation dose rates were measured and the safety aspects of the battery were analyzed. A prototype battery was assembled and tested. The economics of the battery were demonstrated for special applications.

It is concluded that a microwatt nuclear battery can be built with a conversion efficiency of 1 to 2%, a power density of 60 to 300 $\mu W/cm^3$ depending on the power level, and a useful life of 5 to 10 years. Further research areas are recommended.

Acknowledgments

I would like to express my special appreciation to Dr. John J. Pinajian and Professor Fred K. Manasse for their continuous guidance on the entire project; to Mr. J. H. Gillette, Superintendent of the Isotopes Development Center, Oak Ridge National Laboratory,* and Mr. A. F. Rupp, Director of the Isotopes Development Center, for making available the facility to conduct this work; to Mr. E. H. Kobisk, Mr. F. N. Case, and their staff members of the Isotopes Division for their assistance in the experimental work; and to Dr. Granvil C. Kyker of Oak Ridge Associated Universities for providing both an opportunity and a USAEC fellowship to perform this work at Oak Ridge National Laboratory. I would like to thank Professor Graham B. Wallis, Chairman, and Professors Edward S. Brown and John W. Strohbehn, members of the Doctoral Committee, for discussing and criticizing the work. Special thanks to Mr. C. E. McFarland of ORNL for his continuous assistance in the project. My thanks also to Mary M. Stooksbury and Susan K. Whatley for typing this thesis.

Finally, I would like to thank my wife for her encouragement, patience, and understanding, which helped to make my study possible.

*Operated by Union Carbide Corporation for the U. S. Atomic Energy Commission.

CONTENTS

Page

LIST OF TABLES

LIST OF FIGURES

1. INTRODUCTION

Mankind has successfully developed and utilized energy sources from the days fire was discovered. Long before the steam engine, energy from wind and water was utilized for ship propulsion and windmill and water mill operations. More recently, all kinds and all sizes of power sources, from thousands of megawatt power plants to milliwatt batteries, from coal burning to solar, chemical, and nuclear energy, have been developed.

Among all power sources, batteries have been used extensively. A battery is a device that converts various types of energy directly into electrical energy without the use of moving parts. Based on their energy sources, batteries can be divided into three major groups: chemical, solar, and nuclear.

Chemical batteries make use of spontaneous chemical reactions in which the oxidation reactions take place at two electrodes. They can be classified further as primary and secondary (storage) batteries. A primary battery is a source of electrochemical power in which the reactions are not reversible; it is therefore incapable of being recharged. Secondary batteries can be recharged to store chemical energy which may be converted to electrical energy. Chemical batteries are convenient, low cost, and readily available for many applications. However, for remote, long-life applications such as space and undersea exploration, automatic weather stations in the arctic, implantable prosthetic devices, etc., chemical batteries are less satisfactory because they have relatively low energy content and are severely limited by extreme environmental temperatures. Many chemical batteries also deteriorate over a period of 2-4 years independent of the energy which they deliver.

Solar batteries are solid-state devices which change radiant energy of light into electrical energy by a photoelectric process. This type of battery has been used for space applications, e.g., as the power source for artificial satellites.

Nuclear batteries make use of the charged particles emitted from the decay of radioisotopes to convert the decay energy into electricity through thermal, ionization, or charge collection processes. The main advantages for nuclear batteries are:

(1) high energy content — about 10^8 joules/gram for nuclear fuel compared to 10^3 joules/gram for the best chemical fuels,

(2) insensitivity to environmental conditions — particularly temperature, and

(3) long useful life — since nuclear energy is converted into electricity by physical processes, the useful life of a nuclear system with long-lived radioisotopes (tens of years) can be extended until the failure of a component due to material problems.

However, nuclear batteries have inherently higher cost and more safety problems, and therefore, nuclear batteries are used only if chemical batteries are unable to meet the requirements.

In the microwatt range, which is the concern of this thesis, the choice of battery systems is much narrower. In almost all applications, such as power sources for wrist watches, micro-electronic circuits, and implantable prosthetic devices, microwatt batteries should have light weight, small size, and long life. With such constraints, most chemical batteries except mercury cells will not meet the specifications. This

is partly because most chemical systems have relatively low energy content and partly because the deterioration of active chemicals in the system limits the useful life of the battery even at very low drain. Solar batteries cannot be used for most applications because of the limitation of a continuing supply of light energy. Therefore, for the types of applications of interest here, only mercury cells and nuclear battery systems are considered to be candidates for long-life microwatt batteries. The comparison between the two systems will be analyzed after a review of potential applications of such a battery and a brief discussion of pacemakers.

Microwatt batteries have found many applications in industry and in the field of medicine. For example, they are used as power sources for wrist watches and artificial pacemakers. In the case of the wrist watch, a mercury cell will be able to power the watch for at least one year. Since the battery in the watch can be easily replaced, it is not necessary to use a 5 to 10 year life nuclear battery. Not only does the nuclear battery cost at least 100 times what the chemical battery does, but the risk of being irradiated by the radiation and the risk of contaminating the environment under accidental conditions become a problem. On the other hand, in the cases of the pacemaker or other implantable prosthetic devices, surgical operations are involved in battery replacement. Experience with the present mercury-cell-powered pacemakers shows the battery power source has significant incidence of failures between 18 and 24 months.[1] If a power source with a useful life of 5 years or longer can be made available to patients who require pacemakers, the implanting operations necessary to replace the mercury cell every two years can be reduced in number. In this case, because of the professional and hospital

charges involved in each replacement, a long-life battery may be competitive, even at a higher cost. Also, the risk of being irradiated may be compensated by the benefits received due to the reduction in number of operations. The risk in environmental contamination can be minimized because a pacemaker battery can be relatively large ($\sim$5 cm^3) compared to a wrist watch battery, and the containment capsule of the nuclear battery can be designed and tested against rupture from any foreseeable accidents. Therefore, for special applications in which the criterion of inaccessibility can be established, nuclear batteries may compete favorably with chemical batteries.

The implantable cardiac pacemaker has been used clinically for more than a decade. At present, a long-life microwatt battery is needed by the pacemaker manufacturers. Since a definite need for a long-life pacemaker battery exists, the design considerations in this thesis will be based on such an application. One has to realize, however, that the pacemaker battery is only one example of many potential applications for microwatt nuclear batteries.

It is perhaps appropriate to discuss briefly artificial pacemakers. The task of a pacemaker for artificial stimulation of the heart is to deliver short electrical pulses at the desired heart rate. The pulses are fed to electrodes in contact with the ventricular wall. Two heart diseases, heart block and Adams-Stokes attack, can be treated adequately with an artificial pacemaker, and most users can live active, normal lives with such an implant. Heart block is a disease due to the failure of the connective cells between the atrial and the ventricular parts of the heart so that the stimulation can not pass from the atrium to the

ventricle. The disease is not immediately fatal. The ventricles will beat with their own rhythm but at a slower rate; therefore, the circulation will be insufficient and may lead to permanent invalidism. Adams-Stokes attack is characterized by periods of unconsciousness caused by sudden interruption of the action of the heart. If the attack lasts too long, it may cause severe injury to the brain and can be fatal.

The pacemaking pulses are usually square pulses lasting from 0.7 to 2 milliseconds with a frequency of about 70 pulses per minute. The power requirements are about 50 microwatts for an asynchronous cardiac pacemaker and about 200 microwatts for a synchronous pacemaker. A synchronous pacemaking system is programmed from atrial activity and requires an additional electrode to sense the atrial potential. This signal is amplified and triggers the pulse generator to deliver a stimulus to the ventricles. Another type of pulse generator is programmed from ventricular activity. When the beat rate of the heart remains above a preset frequency, the output pulse from the generator is suppressed by the ventricular programmed systems. These pacemakers work on the demand principle and are referred to as demand pacemakers.

For the purposes of establishing reasonable competitiveness in the market place, comparison between mercury cells and nuclear battery systems can be made based on the energy content, the power requirements, and the weight constraints of a pacemaker battery. The maximum power density of mercury cells is about 45 watt-hours per pound which is approximately 360 joules/gram. For a 200-microwatt pacemaker battery with 5 years operational life, the total energy required would be 32,000 joules. The weight of the mercury system alone would have to be at least 90 grams to

have enough energy to operate the pacemaker for five years. This weight will far exceed the present total system weight of 60 grams and the design goal of 30 grams (see Chapter 2 for weight specification and design goal). On the other hand, if a nuclear system with ^{147}Pm is used, since the energy density of pure ^{147}Pm is about 10^8 joules/gram, with conversion efficiency of 1% (present state-of-the-art), the nuclear system would require only milligram quantities of ^{147}Pm to operate a pacemaker for five years. With the conversion system and shielding material, the promethium battery system would yield an energy density of 1300 joules/gram. The weight of the promethium system would be 30 grams for 5-year operation. Figure 1.1 presents the energy content versus system weight for two chemical systems — mercury and Leclanche cells, two nuclear systems, ^{147}Pm with betavoltaic conversion and ^{238}Pu with thermoelectric conversion, and the energy content of pure radioisotope fuels (the upper limit possible by development of improved energy conversion systems). The energies required for a 200-μwatt pacemaker battery for both 2-year and 5-year operation are indicated. The weight specification and the design goal for a pacemaker battery are also plotted.

The curves for chemical batteries are straight lines because their weights are almost directly proportional to the amount of active chemicals contained in the battery. For nuclear systems, the energy content is directly proportional to the amount of radioactive fuels whose weight is on the order of milligrams and therefore is negligible. A large fraction of the system weight is radiation shielding material. Since the thickness is thin (on the order of millimeters), if higher order terms are neglected, the weight of the shielding material would be proportional to its thickness. For a point radiation source with monoenergetic

x or γ radiations, the attenuation of radiation can be expressed as

$$I/I_o = e^{-\mu t} \tag{1.1}$$

where I_o is the initial photon flux, μ and t are the attenuation coefficient and thickness of the shield, respectively, and I is the attenuated photon flux emerged from the shielding material. The thickness of the shield can then be obtained by inverting the above equation,

$$t = \frac{1}{\mu} \ln \frac{I_o}{I} \tag{1.2}$$

Equation (1.2) indicates that the shielding thickness is dependent on the logarithm of I_o because I is a fixed value (it is the permissible radiation

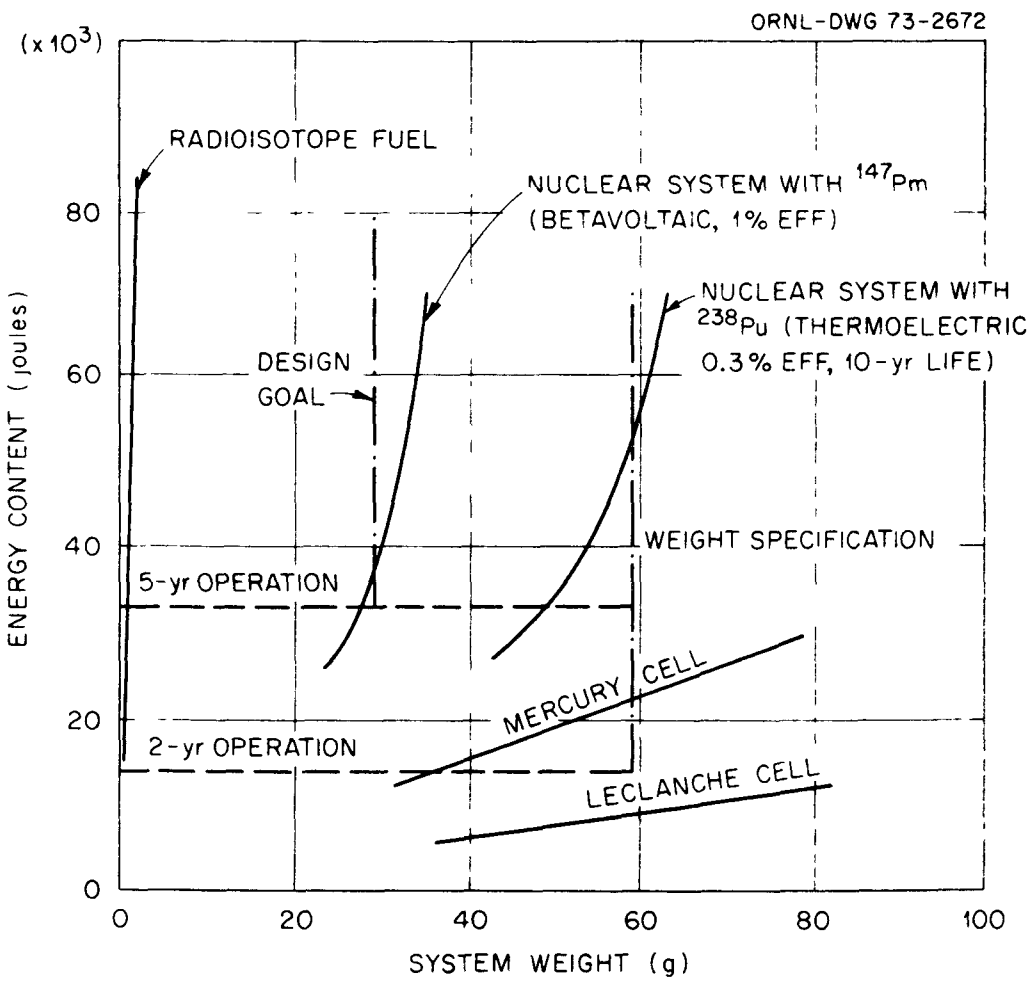

Fig. 1.1. Energy Content and Weight of Nuclear and Chemical Systems Compared With Design Specifications for Artificial Pacemaker Batteries.

leakage). Since energy content is approximately proportional to photon flux (I_o), and system weight is approximately proportional to shielding thickness (for thin shell capsules), Equation (1.2) shows that the system weight is dependent on the logarithm of the energy content.

Figure 1.1 shows that within the weight specification, both nuclear systems have enough energy content to operate the battery for at least five years, while the mercury system can only operate for about three years. Therefore, based on the energy content, nuclear systems have at least a 3 to 1 weight advantage over chemical systems. Figure 1.2 compares the power densities of two nuclear systems and a mercury cell versus operational period. Two curves were plotted for mercury cells at different power levels. At 200 μwatts, the power required for synchronous pacemakers, mercury cells can be operated for about two years. At 50 μwatts, for

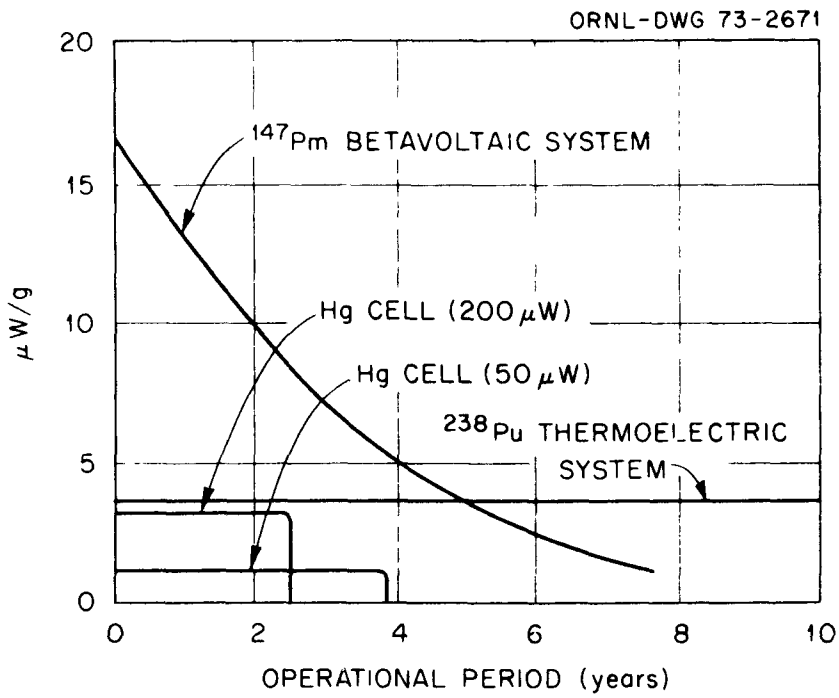

Fig. 1.2. Power Density Versus Time For Nuclear and Mercury Systems.

fixed rate or asynchronous pacemakers, the same mercury cells can last 40 months (as tested by Medtronic, Inc., of Minneapolis, Minnesota). This figure indicates that both nuclear systems are superior to the mercury cell. The comparison between the ^{238}Pu thermoelectric and the ^{147}Pm betavoltaic system will be discussed in Chapters 4 and 5.

The breakeven cost for batteries with longer useful life than mercury cells can be evaluated as follows. For pacemakers using 2-year life mercury cells, the cost of the battery is negligible compared to the cost of $1600 for the pacemaker and its implantation (see Chapter 13 for detailed cost analysis). A patient would require five pacemakers and implantations for a period of 10 years at a total cost of about $8000. If a 5-year life battery existed, only two pacemakers and implantations would be necessary at a cost of $3200 plus two batteries. Therefore, the breakeven cost of a 5-year battery would be about 1/2 × (8000-3200) = $2400. (Considering the "time-value" of money will not make much difference to this estimate.) Similarly, the breakeven cost of a 10-year life battery would be $6400. Figure 1.3 shows the breakeven cost of a long-life battery compared to mercury cells. If a battery can be built for less than the breakeven cost, there would be an economic advantage over mercury cells. In addition, it is likely that at least some patients would be willing to pay a premium for the convenience of fewer operations; in this case the first nuclear batteries which are introduced commercially could be sold for more than the "breakeven" cost described above.

The selection of radioisotopes for nuclear batteries depends on many factors which will be discussed in Chapter 7. The most important factor is the half-life, the time it takes to reduce the disintegration

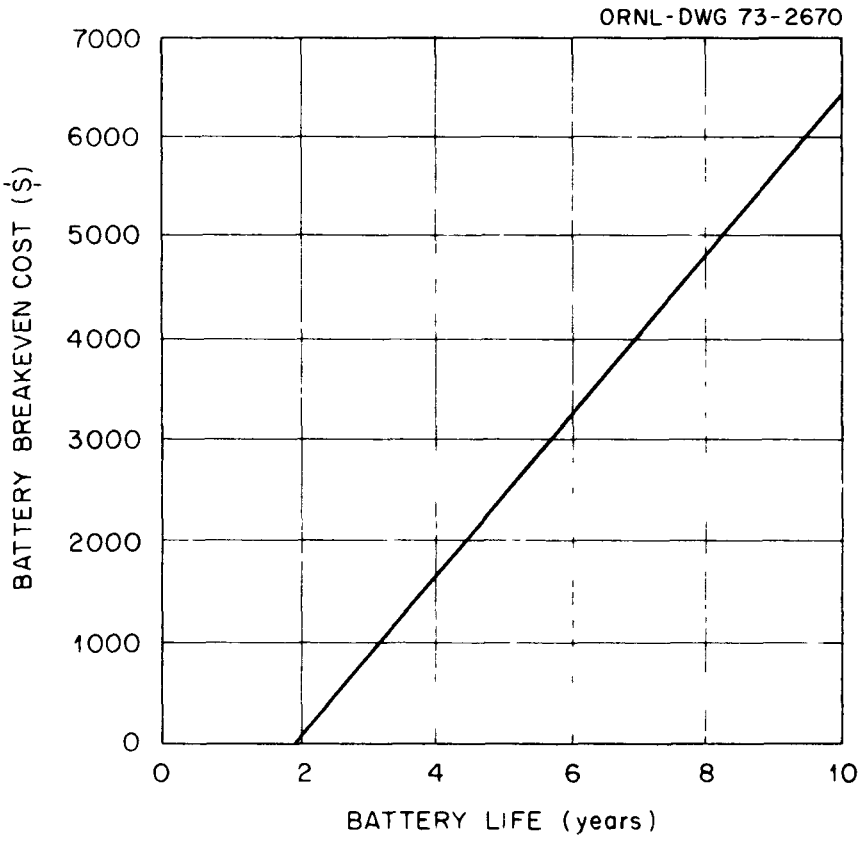

Fig. 1.3. Battery Life Versus Breakeven Cost.

rate of a radioisotope by a factor of 2. The half-life of radioisotopes varies from a fraction of a second to millions of years. By selecting the proper radioisotope, one might expect to have an energy source with the desired useful life.

With a suitable radioisotope power source, a conversion system is required to transfer the decay energy into electrical energy. Figure 1.4 shows six major methods of energy conversion associated with a radioisotope energy source. Each of the methods, except the dynamic conversion system, will be discussed in Chapter 4. The dynamic system is efficient only in kilowatt (electric) conversion levels.

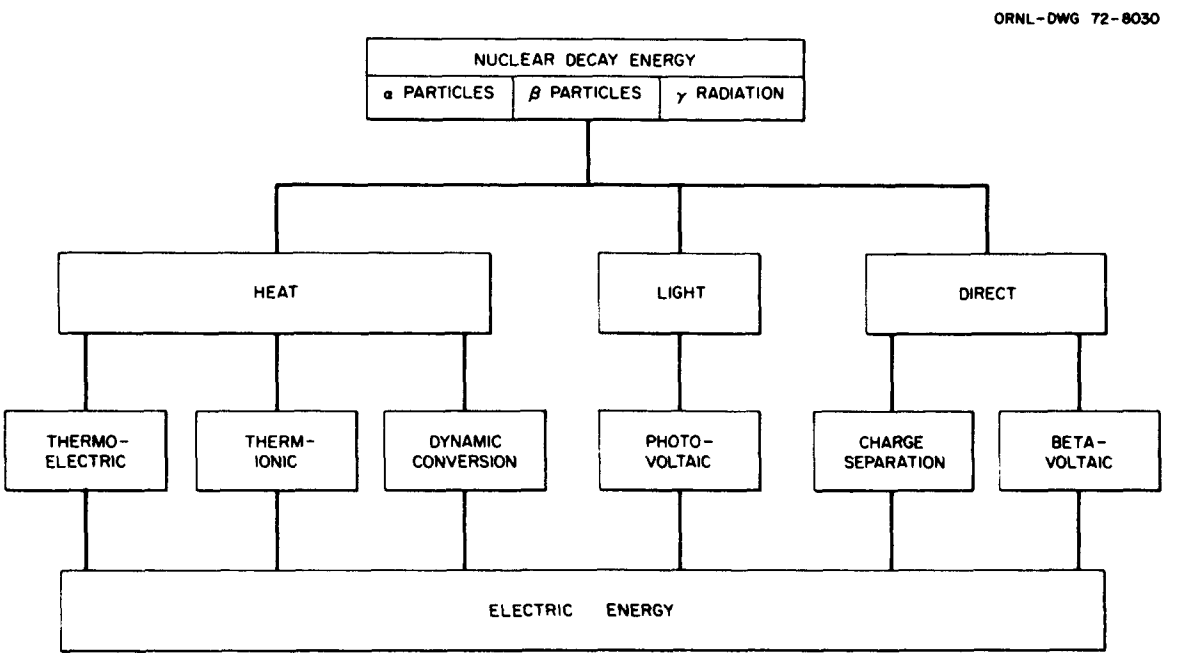

Fig. 1.4. Radionuclide — Electric Energy Conversion Systems.

The need for a long-life, high-power-density, high-reliability, compact microwatt battery can be evidenced by the effort made recently by the British, the French, and the United States. The British nuclear battery, designed by the Atomic Energy Research Establishment (AERE) at Harwell, uses a ^{238}Pu radioisotope source and a thermoelectric conversion system.[2] A power supply malfunction has been reported after 3 months' operation. The French unit, manufactured by Societe Alcated in Paris, also uses ^{238}Pu and thermoelectric conversion and has been implanted successfully.[3-5] In the United States the United States Atomic Energy Commission (USAEC) initiated interest in developing microwatt radioisotope-fueled generators in early 1964. Nuclear Materials and Equipment Corporation (NUMEC), under contract with the USAEC, developed a thermoelectric battery fueled with ^{238}Pu.[6] Table 1.1 summarizes the batteries developed

Table 1.1 Nuclear Batteries Developed for Pacemaker Applications

Country	Radioisotope Source			Conversion System		Output		
	Radionuclide	Weight (or Activity)	Thermal Power (mW)	Method	Material	Power (μW)	Voltage (V)	Efficiency (%)
Britain	^{238}Pu[a]	180 mg	90	TE	Bi-Te	400	0.25	0.45
France	^{238}Pu[a]	150 mg	75	TE	Bi-Te	240	0.9	0.32
United States								
NUMEC[b]	^{238}Pu[a]	500 mg	250	TE	Cupron Sp.-Tophel Sp.	240	6	0.1
McDonald Douglas	^{147}Pm[c]	73 Ci	26	BV	Silicon pn Junction	200	3.3	0.77

[a] Power density of ^{238}Pu = 0.5 W/g.

[b] NUMEC is Nuclear Materials and Equipment Corporation

[c] Activity power ratio of ^{147}Pm = 2786 Ci/W.

TE = Thermoelectric

BV = Betavoltaic

throughout the world. In mid-1972, the U.S. Senate approved $1 million for the nuclear pacemaker development program.[7]

The major contributions of the present work are:

(1) Experimental determination of the feasibility of an entirely new microwatt battery which combines the Schottky barrier effect with a radioactive energy source.

(2) Analysis of the characteristics of a prototype and predictions of the expected performance of a marketable production battery which shows that the device is competitive with alternative systems and offers potential for improvements over existing devices.

(3) Use of a new radioisotope form, ^{147}Pm metal, which is more compact and versatile than the usual promethium oxide.

(4) An approximate economic analysis which indicates that the most promising initial market for such a device lies in the area of artificial pacemakers. The ^{147}Pm Schottky barrier battery is significantly smaller than existing pacemaker power sources and should have a life which is two or three times greater, thus saving the cost and trauma of several surgical operations.

This thesis is divided into four major parts. The first part, Chapters 1 through 5, describes the need, specifications, parameters, and alternatives of the microwatt nuclear battery based on potential applications as a pacemaker battery. The second part, Chapters 6 through 8, describes the Schottky barriers, radioisotopes, and experimental instrumentations. Chapters 9 through 13 give detailed discussions of the characterization experiments as well as the design and construction of the prototype battery. The last part, Chapters 14 to 16, presents an improved design, recommendations for further research, and conclusions.

2. DEFINITION OF THE PROBLEM, ITS SPECIFICATIONS, AND DESIGN PARAMETERS

2.1 Objectives

The need for a long-life, high-power-density, maintenance-free microwatt power generator was discussed in the previous chapter, and the radioisotope-fueled battery was shown to be an extremely attractive candidate. In 1964, the USAEC contracted NUMEC to develop a power supply, a thermoelectric device with ^{238}Pu as fuel, for cardiac pacemakers. Since then, alternative devices were developed by many investigators. In 1969, Sanders Associates and Dartmouth College jointly sponsored a program to develop a Schottky diode betavoltaic device for a pacemaker battery and possibly other military-related (classified) applications. The selection of the Schottky barrier betavoltaic system over other conversion methods will be discussed in detail in Chapters 4 and 5. By early 1971, it was realized that to perform this broad program, a significantly large amount of effort and money would be necessary to build various metal semiconductor Schottky barrier devices (most of them are unavailable at the present time), and to investigate the betavoltaic effect with different beta decay radioisotopes. It was advantageous to first build a prototype battery by using existing Schottky barrier cells and to prove the feasibility of a Schottky barrier nuclear battery — this became the topic for this thesis, the result of which could then serve as a guide to determine whether a broad research program should be initiated.

Therefore, the specific objectives of this dissertation are:

(1) to demonstrate the feasibility of a long-lived battery using the betavoltaic effect on Schottky barriers and a radioisotope source,

(2) to build a prototype nuclear Schottky barrier battery, and

(3) to show that the Schottky barrier betavoltaic conversion system has potential for successful commercial development.

Si-Au Schottky cells have been selected for this demonstration because they are the best understood and most readily available among all other semiconductors. Due to the radiation damage problem, ^{147}Pm is selected as the energy source.

The long-range objective of the overall betavoltaic development program is to investigate the betavoltaic effect with various metal-semiconductor Schottky barrier devices in conjunction with various beta decay radioisotopes. The final goal is to produce a small-size, light-weight, long-lived microwatt battery capable of operating 5 to 10 years with high reliability. This dissertation is the necessary first step of the overall betavoltaic program.

2.2 Specifications

There are many potential applications of nuclear microwatt batteries. The most important one at present is as a power source for artificial pacemakers. In the following paragraphs, the specifications will be discussed based on such an application. For other applications, the specifications and constraints should be developed based on the specific requirements for each application.

For pacemaker batteries, the design specifications can be stated as follows:

(1) Useful Life — Longevity of a battery is of prime interest to the pacemaker manufacturers. The useful life of a pacemaker battery should be at least 5 years, preferably 10 years. The economic advantage

will be much greater for batteries with longer useful life as shown in Fig. 1.3.

(2) Reliability — For mercury cell powered pacemakers, experience gained by Medtronic, Inc., shows the critical failure rate of the power source is about 0.2% for a 2-year operational period. The criterion for "failure" is not well defined. In general, two kinds of failure rate were reported. The first one is a failure of one mercury cell in a 5-cell battery package. This failure rate is approximately 1 to 2% per one-year operation. This failure would not constitute an immediate hazard to the patient. The patient would be able to sense the failure by realizing that his heart was beating at a slower rate. The second failure is a critical failure of the entire battery package. In this case, the patient would require the immediate attention of a physician. However, his heart would probably continue to beat by its own rhythm but at a much slower rate. The failure of the electronic circuitry is approximately 0.05% for a 2-year period. For a nuclear battery, the reliability criterion should be set at 0.5% failure for a 5-year operational period. The design goal should be set at 0.2% failure for five year's operation.

(3) Power Output and Output Voltage — The required power output of a pacemaker battery depends on the type of pacemaker: it is on the order of 50 μwatts for asynchronous pacemakers and 200 μwatts for synchronous pacemakers. The output voltage of the battery should be 5 to 7 volts to match the input voltage required for the pacemaker electronic circuit. A dc-to-dc converter may be used to achieve the output voltage. The conversion efficiency of a dc-to-dc converter depends on the input voltage and is about 80% for conversion from 3 volts to 6 volts.

(4) Size, Shape, and Weight — The size should be less than 15 cm^3 and the weight should be less than 60 grams. A "design goal" has arbitrarily been set at 5 cm^3 and 30 grams. A flat disk shape is preferred for convenient implantation.

(5) Maintenance — No maintenance should be required for the entire operational period.

(6) Environmental Conditions — The battery operation should not be affected by external electromagnetic fields, x-rays, vibrations, falls, and other accidents which may occur to the patient during his normal life.

(7) Economics — The cost of the nuclear battery should be competitive with the cost of mercury cells, including the cost involved for the operations required for battery replacements.

(8) Safety — Safety against radiation and radioactive materials is a problem unique to the nuclear batteries. A large fraction of the cost of the nuclear battery is due to the handling, control, and containment of radioactive materials. In addition, a large fraction of the total weight and size is due to the shielding materials required to reduce the radiation dose rate and the requirement that capsules be strong enough to contain radioactivity under maximum credible accidents. The safety problem of nuclear devices is a significant problem by itself. No nuclear devices can be used commercially until these problems are definitely solved and an adequate set of standards is issued by regulatory authorities. At the present time, no standards have been set in the United States for nuclear pacemaker batteries, and therefore, only several nuclear pacemakers (French made ^{238}Pu thermoelectric battery) were implanted in patients for experimentation. In Europe, the European Nuclear Energy Agency (ENEA)

has issued a set of safety guides for nuclear batteries which recommends maximum radiation emission of 2.5 mrem/hr at the surface of the pacemaker. Further discussion on nuclear safety will be presented in Chapter 12. For the purpose of battery design, it is assumed that the radiation dose rate absorbed by the tissue as a result of the nuclear battery should be less than 2.5 mrem/hr (this is about the same dose rate produced by a wrist-watch with a radium luminous dial). There should not be any radioactive contamination as a result of a severe accident to the patient.

It may be impossible to satisfy all of the design goals discussed above. Therefore, compromise and selection procedures, based on overall performance, would have to be used in order to optimize the battery. However, the specifications dealing with safety are true constraints which cannot be compromised.

2.3 Design Parameters

The parameters which a designer can manipulate are outlined below:

(1) Output Voltage of the Battery — Most batteries consist of a number of cells or elements. The method of interconnection between the cells allows one to select the output current and voltage. Recent technical advances in the electronic industry have presently made available miniaturized dc-to-dc converters at high conversion efficiencies, about 80% from 3 volts to 6 volts. Therefore, one has more freedom to adapt to different output voltage and current characteristics of the battery. For pacemaker batteries, an output voltage of 5 to 7 volts is required. Conventional pacemakers have 4 or 5 mercury cells connected in series. For betavoltaic nuclear batteries, the highest output voltage may be obtained if all the Schottky cells are connected in series. Since each

cell would generate ∿0.2 volt, a voltage of ∿3 volts would be generated for a 17-cell battery in all series configurations. A dc-to-dc converter must be used to increase the voltage to 6 volts.

(2) Energy Sources — Chemical, nuclear energy, etc., can be selected as the energy source of the battery. For pacemaker applications, a radioisotope power source offers better characteristics than other energy sources because the radioisotope has much higher energy density as compared to chemical systems. For a 200-μwatt, 5-year battery, the weight of a nuclear system would be 30 grams while that of a mercury cell would be about 100 grams.

(3) Conversion Methods — Based on the selected energy source, a conversion device is required to convert the energy into a useful form, namely, electrical energy. Different conversion systems have different optimized ranges of operation. In the microwatt region, thermoelectric, betavoltaic conversion, and chemical batteries have better performances than do other systems. For pacemaker applications, in particular, a betavoltaic conversion system offers higher conversion efficiency and perhaps lower cost than a thermoelectric system, and longer useful life compared to the chemical batteries. Therefore, the betavoltaic system was selected for study. Chapters 4 and 5 present detailed discussions on conversion methods and their comparisons.

(4) Selection of Semiconductor Materials — For betavoltaic application, the selection of the semiconductor material and the metal-semiconductor junction is vital to the performance of the battery. The important parameters in the performance of a betavoltaic cell are functions of band gap, resistivity, barrier height, p or n type, and thicknesses of the

metal layer and the semiconductor wafer. For this study, n-type silicon was selected because it is the best understood and most readily available among all other semiconductors.

(5) Selection of Radioisotopes — The selection of radioisotopes in a nuclear battery depends on the desired half-life and the selection of conversion methods. In general, the radioisotope should have a half-life matched to the mission life. The radiation level should be low enough to be tolerable for the specific application considered. Availability and cost of the radioisotope should also be considered. The selection of ^{147}Pm as the radioisotopic source will be discussed in detail in Section 7.1.

2.4 Contribution of the Present Work

At this point it may be worthwhile to summarize the contribution of this thesis in matching the above design specifications, by comparing the final design of the Schottky barrier nuclear battery (see Chapter 14) with the design goals discussed in this chapter.

(1) Useful Life — The design life of the battery should be 5 years based on energy content, radioactive half-life, and known material damage. However, the design has not been life tested and cannot be guaranteed in the absence of definite experimental evidence.

(2) Reliability — It is difficult to estimate the reliability at this stage. It is expected that this device after full development will be more reliable than a mercury cell.

(3) Power Output and Output Voltage — Based on prototype tests, it is clear that the battery is capable of meeting the power requirements. To obtain the desired voltage a dc-to-dc converter is needed.

(4) Size, **Shape, and Weight** — The final design has a disk shape with a volume of 3 cm^3 and a weight of 30 grams which meets the specifications.

(5) Maintenance — No maintenance is required.

(6) Environmental Conditions — The device is designed to be unaffected by external conditions. This should be confirmed experimentally in the future.

(7) Economics — The cost analysis (Chapter 13) shows that there is a cost advantage of Schottky barrier nuclear battery over mercury cells for pacemaker application.

(8) Safety — The battery was designed to withstand accident conditions as required by the Department of Transportation (DOT) and USAEC transportation regulations (see Chapter 12). The radiation dose **rate** at the surface of the battery would be less than 2.5 mrem/hr as recommended by ENEA.

3. APPLICATIONS AND MARKET ANALYSIS

At the present time, the most important practical application for the microwatt nuclear battery is as a power source for cardiac pacemakers. Approximately 50,000 pacemakers were sold throughout the world in 1970. Heart block disease, which requires pacemaker implantation, is a disease of the elderly; about 70% of the patients are above the age of 60, and the mean age is about 70 years. The ratio between males and females is 2:1. The incidence of chronic heart block has been estimated at 6.3 patients per 100,000 population per year,[8] a figure that indicates an approximate incidence of about 13,000 new cases a year in the United States. Because of the continuing increase in longevity of the population and the greater diagnostic awareness of the problem, a greater incidence of the disorder is to be expected in the future.

In the field of medicine, microwatt nuclear batteries may also be used to power many implantable prosthetic devices which are in the development stage. The possibility of applying the microwatt nuclear battery to the problem of amplifying the electrical signals in a prosthetic stump and of transmiting these signals to the motor that drives a prosthetic device is also being investigated. Electrical stimulators for other organs have been tried. For example, electrical pacers can stimulate organs such as a neurogenically paralyzed bladder or the intestinal tract.

In the future, undoubtedly there will be other branches of medicine where the microwatt nuclear battery may be applied, e.g., pacers may be adapted to stimulate paralyzed muscles, or an artificial neuron system powered by a microwatt nuclear battery might transmit signals from the eyes to the brain. Other potential applications include implantation within the body as a power source for biomedical telemetry devices.

Microwatt batteries also find their application in miniaturized electronic and mechanical industries. Most of the logic and linear microcircuits now available have a power consumption of about 1 milliwatt. It can be foreseen that further technical improvements may allow the minimum power consumption of many microcircuits to be reduced by a factor of 10 to 100. Some laboratories already have integrated counting and amplifying circuits working at a power of 1 microwatt or less at very low frequencies. A low-power flip-flop circuit has been tested at Sandia Corporation.[9] This report shows a power consumption of less than 1 microwatt per stage of the flip-flop circuit. It suggests that a number of transistor circuits could be designed for operation using a microwatt nuclear battery as the power source for remote applications.

In summary, the microwatt nuclear battery should have a potential market of at least 50,000 units per year throughout the world for pacemaker applications. The demand will be increased if the battery is proven to be beneficial in other applications. Detail discussions on the specifications of a pacemaker battery were presented in Chapter 2. An economic analysis of pacemaker batteries will be presented in Chapter 13.

4. ALTERNATIVE DEVICES

4.1 Chemical Battery

Among all chemical batteries, mercury cells best meet the requirements of small volume, light weight, high capacity and voltage, and are capable of producing a reasonable current-drain over a long period of time.

The mercury cell uses mercuric oxide mixed with 5% graphite as the cathode, and zinc amalgamated with about 10% mercury as the anode. A 45% solution of potassium hydroxide saturated with zinc oxide is the electrolyte. Each cell gives 1.35 V. These cells have good voltage-current characteristics with only 0.5% drop in voltage after 1000 hours of operation with 1 mA drain. Each mercury cell (Mallory RM-1) has a volume of 3 cm^3 and a weight of 12 grams. Most power sources for the present artificial pacemakers consist of 4 or 5 such cells connected in series.

In storage, mercury cells have slow internal chemical reactions which reduce the quantity of available oxygen and the amount of zinc oxide in the system. Therefore, there is a fundamental limitation on the shelf life of the cell. As reported in Eveready Battery Applications and Engineering Data, the service capacity after one year of storage at 70°F is approximately 90% of the fresh capacity.

For most applications, mercury cells are ideal. They have 18 to 24 months of useful life, are not very expensive, and are readily available. However, for certain special applications where the battery is extremely inaccessible and if long service life is required, they become less satisfactory. For example, in the case of artificial pacemakers,

one would like to have a power source capable of operating at least 5 years. The fundamental limitation is the relatively low energy content of the mercury system when compared to the nuclear system. Within the weight specification of a pacemaker battery, the mercury cell may be operated at a power level of 200 microwatts for a maximum of 3 years as shown in Fig. 1.1. This is shorter than the desired useful life of 5 years. However, it is possible that improvement in mercury cells and decrease in power requirements of pacemakers might improve the competitive position of the mercury cells.

Although mercury cells are used for almost all the commercial pacemakers available today, a new type of battery with higher energy density and therefore longer life is needed to reduce the number of operations for battery replacement.

4.2 Thermoelectric Power Generation

When two dissimilar conductors are connected in a single loop and if the two junctions between the materials are at different temperatures, electrical current will flow in the circuit. This is the Seebeck effect. The system which converts heat energy into electrical energy by this method is called a thermoelectric conversion system.

Semiconductor materials, such as lead telluride, bismuth telluride, or silicon germanium have been used as thermoelectric elements. Figure 4.1 shows a sketch of a thermoelectric generator. Semiconductor materials of the p and n type are connected thermally in parallel and electrically in series to produce a current through an external load.

The efficiency of this conversion system is primarily determined by the temperature differential across the thermopile for a given

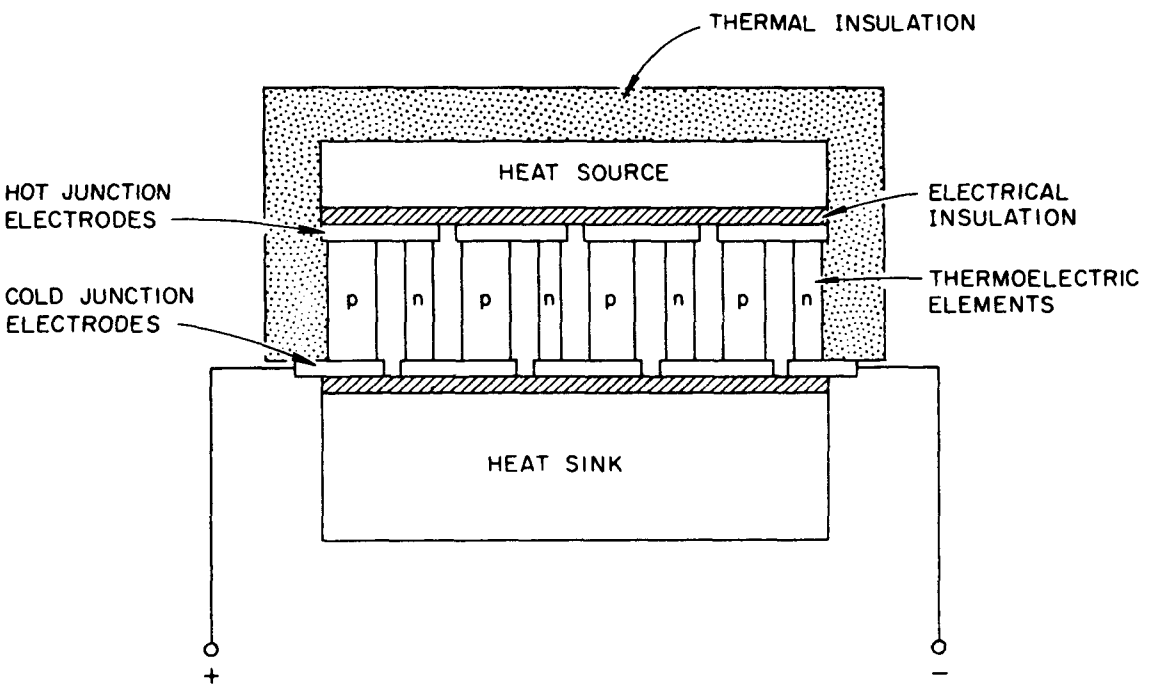

Fig. 4.1. Schematic of a Thermoelectric Conversion System.

thermocouple material. The efficiency, η, of a thermoelectric battery can be expressed by the following equation:[10]

$$\eta = \eta_c \eta_{th} (1 - V) \tag{4.1}$$

where

η_c = pure Carnot efficiency

η_{th} = thermoelectric material efficiency

V = heat losses due to thermal shunts and imperfect heat transfer

The Carnot efficiency is

$$\eta_c = (T_h - T_c)/T_h \tag{4.2}$$

where

T_h = the temperature of the hot junction

T_c = the temperature of the cold junction

The thermoelectric material efficiency is dependent on the physical properties of the thermocouple materials. This efficiency is given by

$$\eta_{th} = \frac{\sqrt{1 + ZT} - 1}{\sqrt{1 + ZT} + 1} \tag{4.3}$$

where

$Z = \alpha^2/\rho k$

α = thermoelectric power

ρ = thermal conductivity

k = electrical resistivity

T = mean temperature = $(T_h + T_c)/2$

The last factor, V, in Eq. 4.1 depends on the design of a particular generator.

Radioisotope heat sources have been used in conjunction with thermoelectric elements. Absorption of the emitted particles of electromagnetic radiation by the radioisotope and its container converts the decay energy into heat. With thermal insulation surrounding the heat source and the hot junctions of the thermoelectric elements, the temperature of the hot junction rises to more than 500°F. Heat is propagated from hot junction to cold junction and dissipated through the environment. If radioisotopes of 2- to 10-year half-life can be selected, then the useful life for the radioisotope powered thermoelectric generator is expected to exceed 5 years.

To date most thermoelectric radioisotope generators have a power level of one to hundreds of watts electrical. The conversion efficiency[11] is about 5% with a hot junction temperature between 500 to 600°F and a cold junction temperature of about 200°F. For a miniaturized microwatt generator, however, this efficiency reduces to about 0.3 to 0.5%. The

loss in efficiency in miniaturization is mainly for reasons of geometric configuration. In general, when the size of the battery is reduced, the ratio of surface-area-to-volume increases. Since the heat generation is proportional to the volume and the heat losses through conduction and radiation are proportional to the surface area, the increase in area-to-volume ratio means an increase in percent heat loss. The smaller the battery size, the higher the percent heat loss. Therefore, the hot junction temperature is lowered, which in turn, reduces the conversion efficiency as indicated by Eq. 4.1 to 4.3. However, even with low efficiency, the thermoelectric device still meets the specifications for a pacemaker battery. As a matter of fact, the French-made ^{238}Pu thermoelectric batteries have been successfully implanted in patients.

The disadvantages of miniaturized thermoelectric devices are potentially high cost and perhaps low reliability. Due to the large number (hundreds) of thermoelements connected in series electrically and in parallel thermally, thermal stress and contact resistance may present problems in miniaturized thermopiles.

4.3 Betavoltaic Power Generation — pn Junction Devices

The betavoltaic effect can be defined as the generation of power through an external load when beta radiation is incident on a semiconductor system. This is analogous to the photovoltaic effect except that electrons are used instead of photons. When electrons are incident on the semiconductor, electron-hole pairs are generated by an ionization process. The number of these carriers generated is in excess of the thermal equilibrium value and they diffuse randomly through the semiconductor. If they are generated within a diffusion length from an

internal potential barrier, they will be collected by the field and caused to flow across the barrier. This flow constitutes an electric current. The current produced is proportional to the number of electrons absorbed in the semiconductor and the voltage is dependent on the height of the internal potential barrier. An internal potential barrier can be generated by either pn junction or Schottky barrier devices.

The process of betavoltaic effect can best be illustrated by using an energy band diagram. When two pieces of semiconductor material, one n-type and the other p-type, are joined together, a pn junction is formed as shown in Fig. 4.2(a). Before they are joined, the fermi level of the n-type is near the top of the forbidden gap and that of the p-type is near the bottom of the gap. Figure 4.2(b) shows the energy levels when p and n are separate.

There is a large concentration of electrons on the n side and a large concentration of holes on the p side. As they come in contact with each other, the large concentration gradients at the interface will force the electrons to diffuse from the n region into the p region and vice versa until both electrons and holes are in a new equilibrium. A continuity condition requires the fermi levels to be the same throughout both materials; this causes the fermi levels to shift until they are at the same level. The energy bands, since they are tied to the fermi level, shift accordingly. Figure 4.2(c) illustrates such an equilibrium condition. As the holes diffuse from the p region, they leave behind negatively charged centers. Likewise, the electrons leave positively charged centers in the n region. Thus, an internal electric field is built up near the interface. This interface region and its built-in potential

barrier comprise the pn junction. Under beta bombardment, electron-hole pairs are created by an ionization process. They are collected by the internal field and cause current to flow. Figure 4.2(d) illustrates the flow of electrons and holes under bombardment.

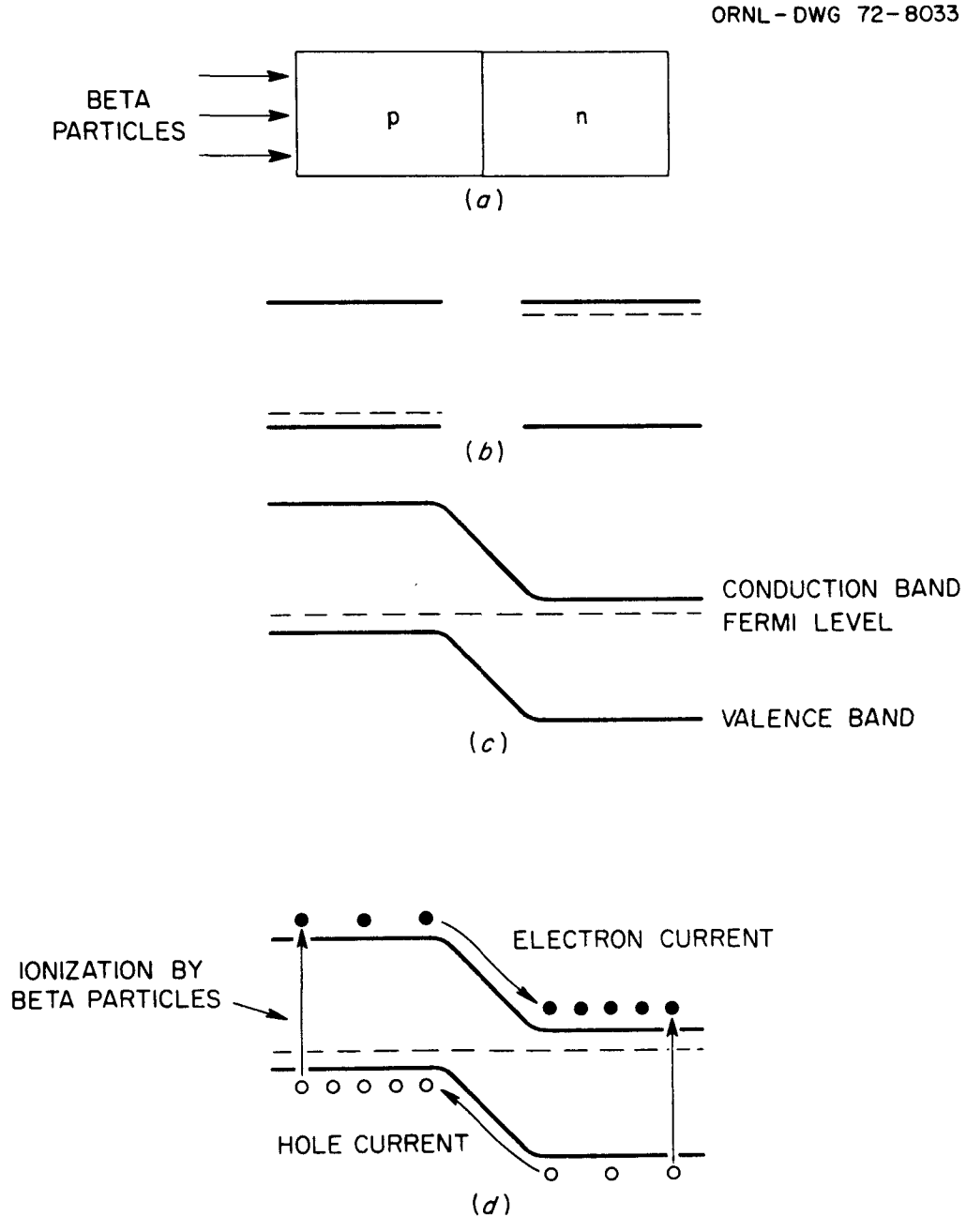

Fig. 4.2. Electron Energy-Band Diagram of p-n Junction Cells.

The betavoltaic effect can best be utilized in batteries of small power level, milliwatt or less. When the power level increases, the temperature of the system rises. As will be discussed in Section 6.1, Eq. 6.2 shows that the leakage current (I_s) of the semiconductor device increases as the temperature rises. Equations 6.6 and 6.7 show that when I_s increases, both V_{mp} and $(-I_{mp})$ decrease. Since the maximum power output is equal to the product of V_{mp} and $(-I_{mp})$, the maximum power output decreases rapidly with increase in the temperature of the system.

The betavoltaic effect on silicon pn junction devices has been studied by many investigators.[12-17] Conversion efficiencies of 0.7% to 1% were reported.

4.4 Betavoltaic Power Generation — Schottky Barrier Devices

Schottky cells have many applications in electronic industry: used as mixers, detectors, and in integrated circuits to perform various gating and clamping functions. However, they have not been investigated in the content of betavoltaic power generation. In this section, the principle of Schottky barrier and its behavior under electron bombardment will be discussed.

When a metal is brought into contact with a semiconductor, it forms two types of junctions according to the relative energy level of the metal and the semiconductor. In n-type semiconductors, if the electron affinity of the semiconductor is greater than the work function of the metal, the electrons flow to the semiconductor and make it more strongly n-type. This is called an ohmic contact. The voltage and current characteristic of ohmic contacts exhibit linear relationships. On the other hand, if the work function of the metal is greater than the electron

affinity of the n-type semiconductor, then a barrier is formed. It is called a Schottky barrier. The height of the barrier depends on the difference in the energy levels of the semiconductor and the metal. The Schottky barrier gives nonlinear rectifying current voltage characteristics similar to that of a pn junction. This potential barrier causes current to flow when excited with photons or electrons. Theoretical evaluations of the maximum power output from a Schottky barrier will be discussed in Section 6.1. Figure 4.3 is a schematic to show the basic configuration of a Schottky cell betavoltaic energy conversion system.

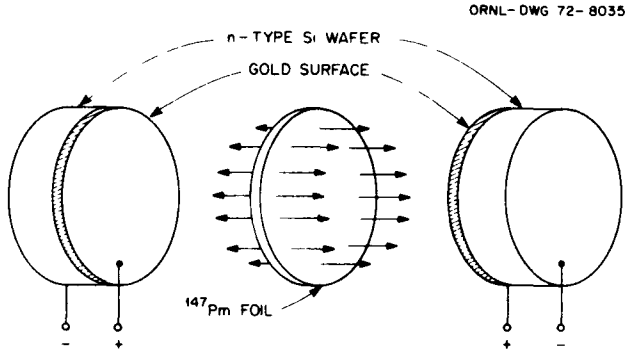

Fig. 4.3. Basic Configuration of a Betavoltaic Battery.

The Schottky barrier is a relatively old device, but fabrication techniques that permit Schottky diodes to perform close to the ideal case have only recently become possible.[18] It was shown that Schottky barriers can be made on silicon with an extremely simple process. It is now feasible to manufacture reliable Schottky barriers with excellent performance at a cost even lower than that of pn junctions.

A sketch of the physical structure of a Schottky barrier is shown in Fig. 4.4(a). Figure 4.4(b) shows the energy levels of the metal and semiconductor before contact and when the system is not in equilibrium.

As the two materials are brought into intimate contact, the fermi level must be the same throughout both materials. Figure 4.4(c) illustrates such an equilibrium condition. Under bombardment of electrons, the electron-hole pairs created by the incoming high energy electrons will diffuse across the built-in potential and will be collected, which causes current to flow. Figure 4.4(d) shows the flow of current under electron excitation.

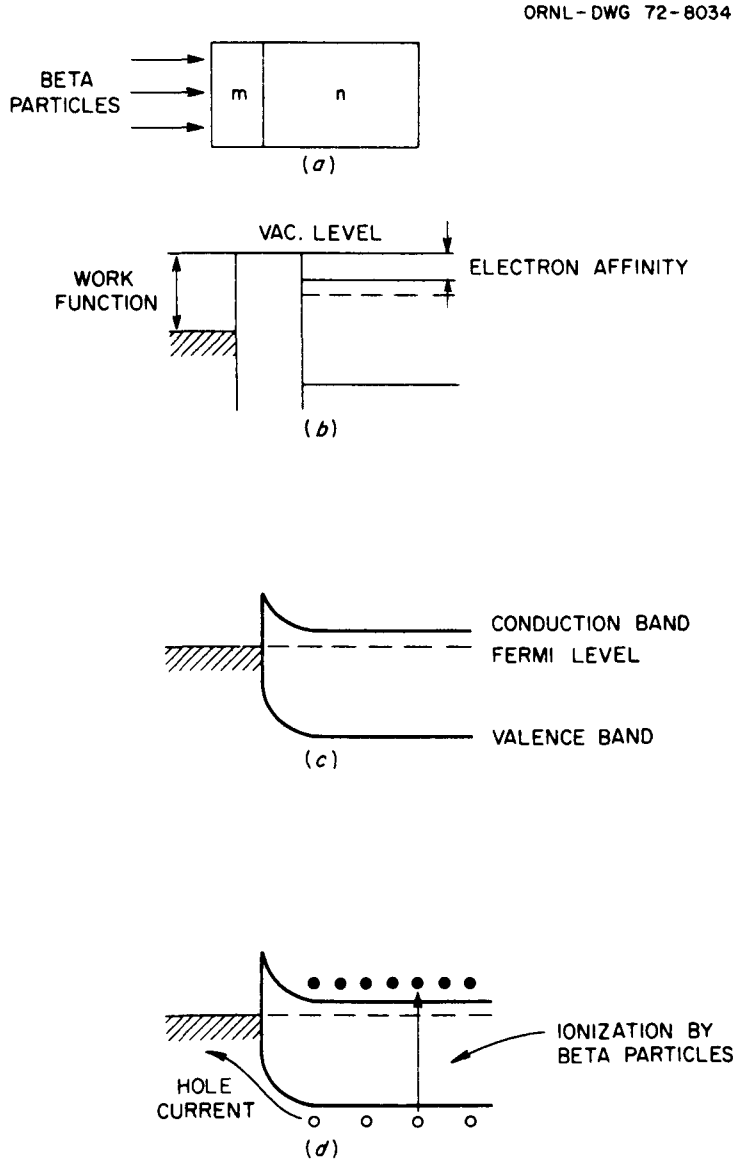

Fig. 4.4. Electron Energy-Band Diagram of Schottky Cells.

Use of Schottky barrier devices makes possible a considerably wider choice of materials than is possible with pn junctions, since virtually any metal-semiconductor combination can be fabricated. Thus, the selection of material is not limited by the relatively stringent requirements necessary for pn junction fabrication. The requirements of barrier height, diffusion length, mobility, and radiation-damage resistance can be optimized using a much wider selection of materials. Table 4.1 lists the Schottky barrier cells with large barrier heights and which, therefore, are possible candidates for betavoltaic applications.[19,20]

Schottky barrier devices have conversion efficiencies comparable to pn junction devices. From comparison between Figs. 4.2 and 4.4, it is obvious that the barrier height is generally larger in pn junction devices than it is in Schottky barriers. The depletion layer is also wider in

Table 4.1 Band Gap and Barrier Height of Schottky Barriers

Semiconductor	Band Gap (eV)	Metal	Barrier Height[a] (V)
n-Si	1.12	Au	0.78
		PtSi	0.85
p-Si	1.12	Hf	0.90
n-GaAs	1.43	Au	0.90
		Pt	0.86
n-GaP	2.24	Au	1.3
n-CdS	2.42	Au	0.78
		Pt	1.1
n-ZnO	3.2	Pt	0.75
n-ZnS	3.6	Au	2.0
		Pt	1.84

[a]Determined by photoelectric measurement.

pn junctions. However, there are at least two factors which increase the efficiency of Schottky diodes, and the net result makes the conversion efficiency of Schottky diodes comparable to or better than that of pn junctions. The first factor relates to the curvature of the V-I characteristic. The curve for pn junctions in practice tends to follow an $e^{qV/AkT}$ law, with $A \approx 2$ and dependent primarily on the doping profile at the junction. Schottky barrier devices can be fabricated which follow an $e^{qV/kT}$ law almost exactly.[18] At low illumination levels this results in increased efficiency due to the sharper corner. Second, in a Schottky barrier device, recombination lengths are typically at least twice as large as in comparable semiconductor pn junction devices. This effect is the result of the fabrication process. Metal can generally be deposited on a semiconductor at much lower temperatures and with much less surface damage than can another layer of semiconductor. Both high temperature fabrication and surface damage act to shorten the recombination length.

Recent experimental work has indicated that these effects are in fact operative. Pinkham[21] reported efficiencies on the order of 0.02% for silicon junction solar cells and 0.5% for silicon gold Schottky barrier cells for electron energies between 0.1 and 1 MeV. Kalibjian and Mayeda[22] have reported comparable efficiencies of about 1.5% for both pn junctions and Schottky barriers on GaAs for electron energies of 3 keV. However, no experimental work has been done on Schottky barrier power generation. This work is therefore performed to determine the feasibility of the Schottky barrier–radioisotope power generation system.

4.5 Other Devices

4.5.1 Thermionic Conversion

Thermionic energy conversion is a method of converting heat energy into electrical energy by thermionic emission. In this process, electrons are thermionically emitted from the surface of a metal by heating the metal to high temperature. Some of the electrons, which become part of the working fluid, overcome retarding forces and migrate to a cold electrode (the collector) where a fraction of their energy is lost in the form of heat and the remainder drives the electrons through an external load back to the emitter. The working fluid, usually cesium gas, is required to prevent the buildup of a space charge cloud near the emitter. Figure 4.5 illustrates a typical thermionic energy converter. For high-pressure gaseous converters, the space between the two electrodes is typically about 0.003 in. This distance should be less than the mean free path of the emitted electrons. The emitter temperature should be 1800°F or higher.

The energy distribution of electrons in the metal follows the Fermi-Dirac law.[23] For temperatures below 3000°K, the distribution is given by

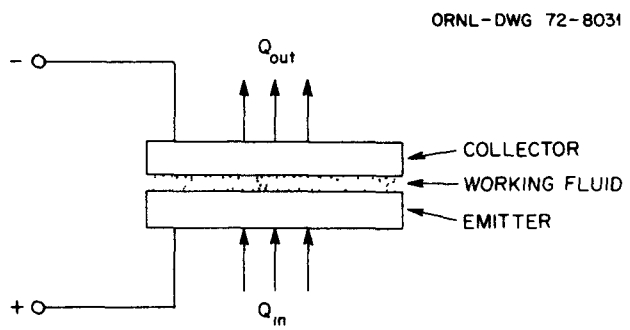

Fig. 4.5. Schematic of a Thermionic Conversion System.

$$f(E)\,dE = (4\pi/h^3)(2qm)^{3/2}\left[\frac{E^{1/2}\,dE}{1 + \exp[(E - E_F)/kT]}\right] \tag{4.4}$$

where

$f(E)\,dE$ = number of electrons per unit volume in energy interval dE

m = electron mass

q = electron charge

h = Planck constant

k = Boltzmann constant

T = absolute temperature of the emitter

E_F = Fermi energy

The electrons which possess energies in excess of the internal potential energy ($E_i = E_W + E_F$) will escape from the metal, where E_W is the work function of the metal.

The emission current density can be expressed by integrating the above distribution in momentum space. The result is known as the Richardson-Dushman equation:

$$J = -AT^2\, e^{-E_W/kT} \tag{4.5}$$

where

J = emission current density

A = Richardson constant = $(4\pi em/h^3)k^2$

For a large system and with high emitter temperature, the theoretical efficiency of a thermionic converter can be as high as 20%. There is no fundamental limitation why a small thermionic battery cannot be efficient, except that there is a practical difficulty to reduce the thermal leakage with a miniaturized thermal insulation system. From Eq. 4.5, the emission current is exponentially dependent on the emitter temperature. For small,

microwatt size conversion systems, the emitter temperature decreases as the surface-area-to-volume ratio increases, which causes the emission current to decrease. Therefore, for small size batteries, the thermionic conversion system would yield a very low conversion efficiency. For example, thermionic devices with microwatt to milliwatt power range have been assembled and tested by Donald W. Douglas Laboratories.[24] The efficiency for a 100-microwatt unit is about 0.01%.[11] For the same power output, low efficiency means more radioisotope fuel and therefore requires heavier shielding. Another practical problem for a thermionic converter is that thermal stresses due to temperature gradients may cause distortion of the gap between electrodes which affects the operation and causes failure of the electrode. Compared to the betavoltaic and thermoelectric systems, the thermionic system is less favorable in the microwatt range.

4.5.2 Photoelectric Nuclear Battery

The photoelectric nuclear battery is a two-stage conversion system. The first stage is to convert electrons from the decay of the radioisotope to light. This is accomplished by mixing the radioisotope with a luminescent powder. A photovoltaic cell is then used to convert light into electrical energy. By sandwiching a number of such luminescent material-radioisotope-photocell combinations, the required power level is obtained. Figure 4.6 shows the basic arrangement of a photoelectric nuclear battery.

Several such devices have been assembled and tested.[25] Zinc sulfide and ^{147}Pm were used as the light-generating materials. Since the efficiency of the photocells decreases very rapidly with decreasing illumination intensity, the overall efficiency of the device was about 0.05% and is therefore less favorable when compared to the betavoltaic and the thermoelectric systems. Another major disadvantage for this system is the

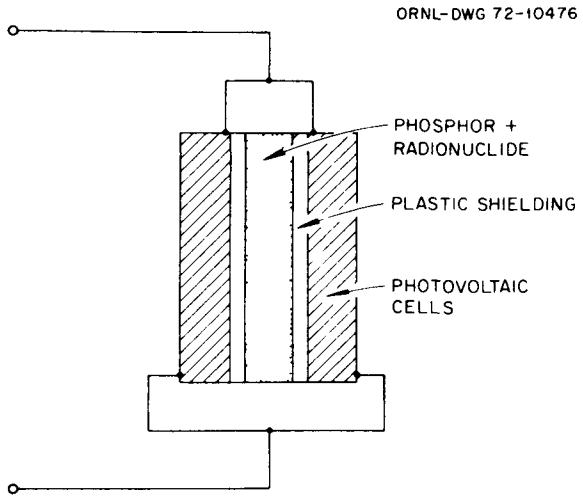

Fig. 4.6. Photovoltaic Radioisotope Battery.

rapid damage of luminescent material by ionizing radiation which would limit the life of the system to about one year.

4.5.3 Direct Charge Collection

The direct charge collection method has the characteristic feature in that the charged particles emitted by the radionuclide are converted directly into electricity in a simple process. Figure 4.7 shows a sketch of a charge collection device. An alpha or beta emitter is placed at the center of a large evacuated metallic container. The charged particles emitted by the radioisotope travel through the vacuum or an insulating layer and are collected on the metal container. A voltage is then built up between the source and the container.

The efficiency of the device is about 2% for parallel plates and about 10% for concentric spherical configurations. The major disadvantage is that this device has a very high voltage and very low current. Typically, the voltage is on the order of tens of kilovolts while the current is about 10^{-8} ampere.[26] This device resembles a capacitor; any external resistance which is less than 10^{10} ohms would essentially

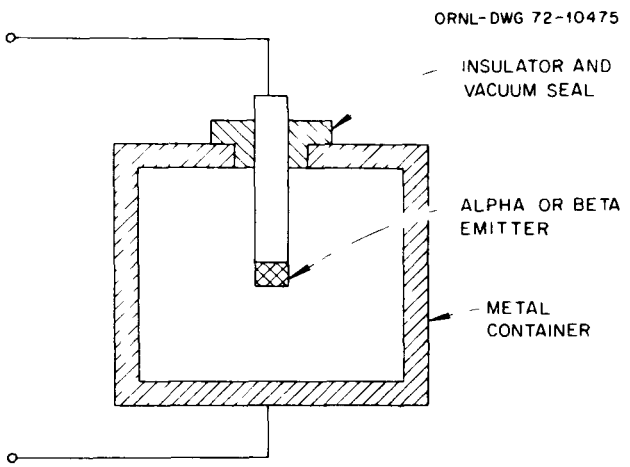

Fig. 4.7. Charge Collection Device.

short the circuit. Since the resistance of a pacemaker is about 10^3 ohms, the collection device cannot be used as a pacemaker battery because of the unmatched impedance. Another practical problem is the electrical insulation layer between electrodes. It cannot be too thick to stop alpha or beta particles from reaching the other electrode. On the other hand, it cannot be too thin to cause discharge under the high voltage. Therefore, this device is probably impractical for use as a power source.

4.6 Summary

In this chapter, seven alternatives were presented and their basic physical principles, advantages, problems, and other main features were discussed. A comparison between various alternatives will be made in the following chapter. Due to the lack of quantitative information for most alternatives, the comparison will be based on the discussions presented in this chapter.

5. COMPARISON OF THE ALTERNATIVES

The selection of alternatives should depend on the requirements specified for a particular application. Since the current need is a pacemaker battery, the comparison of alternatives will be based on such an application. In this chapter, major advantages and disadvantages will be summarized. Detailed discussions of various alternatives are found in Chapter 4.

Mercury cells with energy content of 360 joules/gram will not meet the weight specification for 200-μwatt, 5-year operation of a pacemaker battery. For other applications with shorter operational periods or less power output, mercury batteries are more economical and convenient than nuclear batteries.

The thermionic conversion system has a very low conversion efficiency (∿0.01%) in the microwatt power range. Since this system would be operated at high emitter temperature, thermal leakage and thermal stress would be a problem for a small-size battery. Compared to the betavoltaic and thermoelectric systems, the thermionic system would be less favorable in the microwatt region.

The photovoltaic nuclear conversion system suffers from two disadvantages. The major disadvantage is the short life due to the radiation damage to the luminescent materials. The second disadvantage is the low conversion efficiency of ∿0.05%.

The direct charge collection device has many good characteristics. It has high conversion efficiency, long life, and is a simple process. The main disadvantage of the device is the very high internal impedance. This system can generate extremely high voltage (30 kV), but with only

a very low current (10^{-8} ampere). Electrical insulation between two electrodes also presents a problem. Therefore, it is less favorable to be used as a power source for pacemakers.

The thermoelectric conversion system has better characteristics when compared to the previous systems. A microwatt battery has a conversion efficiency of about 0.3 to 0.5%. The hot junction temperature would be much lower than the emitter temperature of the thermionic system. However, as compared to the betavoltaic system, the thermoelectric microwatt battery may suffer potentially both from high cost and low reliability because there are a large number of thermoelectric elements in a thermoelectric battery. These elements are connected in series electrically and in parallel thermally. The complexity of the interconnections between the thermoelectric elements in miniaturized form makes the battery more costly and less reliable.

As discussed in Sections 4.3 and 4.4, Schottky barrier cells seem to have more potential advantages than pn junction cells in betavoltaic applications. Schottky barrier devices should have much wider choice of usable materials than is possible with pn junctions. Metal can be deposited on a semiconductor using a simpler process than that requiring the growing of another layer of semiconductor. On a mass production basis, the manufacturing cost of Schottky barrier cells should be much lower than that of pn junctions because Schottky barriers can be made on silicon with an extremely simple process. In addition, since the metal thickness of the Schottky barrier cell is only about 100 Å, the Schottky barrier battery will have higher power density ($\mu W/cm^3$) than that of pn junction batteries.

Based on the above discussions, the betavoltaic effect with Schottky barrier cells as conversion devices was selected for further investigation. Table 5.1 summarizes the conversion efficiencies and useful lifes, as well as the advantages and disadvantages for various alternatives, based on the requirements of a pacemaker battery.

Table 5.1 Comparison of Alternatives in Microwatt Power Range for Pacemaker Applications

System[a]	Efficiency (%)	Useful Life (years)	Advantages	Problems
Mercury cell		2	Economical, readily available, and less environmental safety problems	Useful life not long enough
Thermoelectric	0.3	10	Well established technique, proven performance in higher power levels, and long life	High cost, less reliable, relatively low efficiency, and complicated manufacturing process
Betavoltaic pn Junction	1	5	Long life, high reliability, and simple process	Limited choice of semiconductor materials and some radiation damage problem
Schottky Barrier	1	5	Long life, high reliability, simple process, wider choice of semiconductor material, less radiation damage if a proper material is selected, less expensive than pn junction, and higher power density than pn junction	Less understood and less developed
Thermionic	0.01	10	Simple process	Less understood and very low efficiency
Photoelectric	0.05	2		Low efficiency, radiation damage to phosphor, and short life
Charge Collector	10	10	High efficiency, simple process, and reliable	Very high internal impedance and not useful for power source

[a]All systems except mercury cell use radioisotope energy sources.

6. SCHOTTKY BARRIER CELLS — Si-Au

6.1 Principle of Betavoltaic Effect on Schottky Cells

The Schottky barrier betavoltaic power conversion may best be described by considering the case of an ideal Schottky barrier diode with a constant-current source in parallel with the junction. The constant-current source results from the excitation of excess carriers by electron irradiation. Figure 6.1(a) shows the idealized equivalent circuit of a betavoltaic cell. The internal series and shunt resistances are neglected. Electron ionization causes a current, I, to flow in the load. The magnitude of this current is the difference between the generated short-circuit current and the current flowing in the diode.[19] Thus,

$$I = I_s(e^{qV/kT} - 1) - I_L \tag{6.1}$$

where

I = current flow in the load

I_s = reverse saturation current in the diode

V = voltage across the diode

q = the electronic charge

k = Boltzmann constant

T = absolute temperature

I_L = current generated by electrons

For Schottky diodes

$$I_s = AA^*T^2 \exp(-q\phi_B/kT) \tag{6.2}$$

where

A = cross-sectional area of the junction

A^* = effective Richardson constant

ϕ_B = barrier height of the Schottky diode

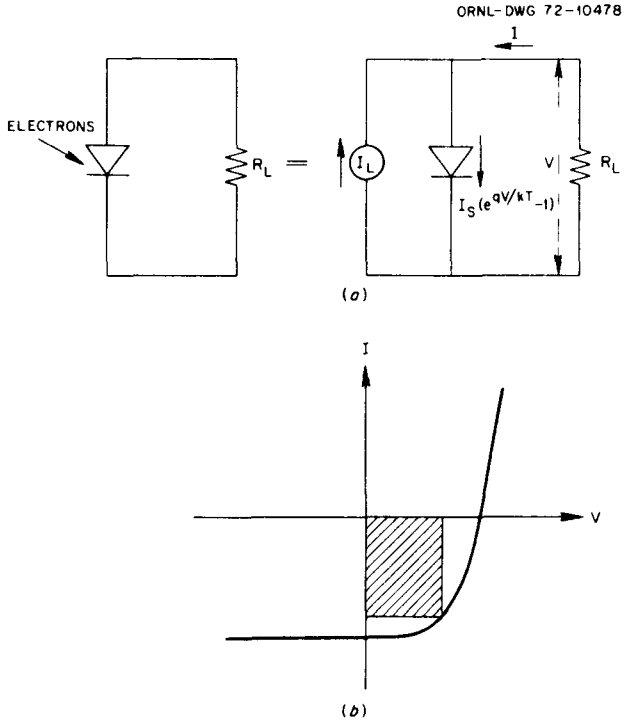

Fig. 6.1. Equivalent Circuit and V-I Characteristic of a Betavoltaic Cell.

A plot of equation (6.1) is given in Fig. 6.1(b). It is seen that the curve passes through the fourth quadrant and, therefore, power can be extracted from the device. The maximum power delivered is represented by the largest rectangle that can be fitted into the area in the fourth quadrant. Therefore, the more rectangular the current-voltage characteristic curve, the higher the conversion efficiency.

The short-circuit current, open-circuit voltage and the maximum power output can be calculated from Eq. 6.1 as follows.

The short-circuit current, I_{sc}, can be obtained by setting V = 0, thus

$$I_{sc} = -I_L \tag{6.3}$$

Similarly, the open-circuit voltage, V_{oc}, can be obtained by setting I = 0,

$$V_{oc} = (kT/q)\ \ell n[(I_L/I_s) + 1] \tag{6.4}$$

The power output, P, is the product of the voltage and the current at a particular operating point. Thus

$$P = VI = VI_s(e^{qV/kT} - 1) - VI_L \tag{6.5}$$

The voltage corresponding to maximum power output, V_{mp}, can be calculated by setting $(\partial P/\partial V) = 0$:

$$e^{qV_{mp}/kT} = \frac{(I_L/I_s) + 1}{1 + \frac{q}{kT} V_{mp}} \tag{6.6}$$

The current at maximum power output is

$$I_{mp} = I_s(e^{qV_{mp}/kT} - 1) - I_L \tag{6.7}$$

Finally, the maximum power output, P_{max}, is equal to the product of V_{mp} and I_{mp}:

$$P_{max} = V_{mp}I_{mp} = I_sV_{mp}(e^{qV_{mp}/kT} - 1) - V_{mp}I_L \tag{6.8}$$

Since the power output is negative in sign, this relationship states that the maximum power output increases as the reverse saturation current (I_s) decreases. Substituting Eq. 6.6 into Eq. 6.8, we have

$$P_{max} = -\frac{I_s \frac{q}{kT} V_{mp}^2}{1 + \frac{q}{kT} V_{mp}} [(I_L/I_s) + 1] \tag{6.9}$$

The detailed theoretical evaluations of the betavoltaic effect on Schottky barriers was a thesis topic of Peter Roitman of Dartmouth College.[27]

6.2 Production of Schottky Cells

Schottky cells can be produced by simpler processes than can the pn junction devices. Raw silicon with desirable resistivity is first obtained from silicon suppliers. The silicon is cut into wafers (about

0.012-in.-thick) and treated by special cleaning cycles; one side of the silicon wafer is then made n^+ by diffusion and nickel-plated to form the back electrode. The front side of the wafer is chemically etched to about 0.008-in. thick. A phenolic mask (0.016-in.-thick ring with 0.050-in. wide) is mounted on the silicon by insulating epoxy. The masked silicon wafer is then loaded into a vacuum chamber and gold is evaporated onto the wafer to a thickness of between 100 to 200 Å. In the final step leads are attached to the gold and nickel surfaces. Figure 6.2 shows a sketch of the Schottky cell for battery assembly.

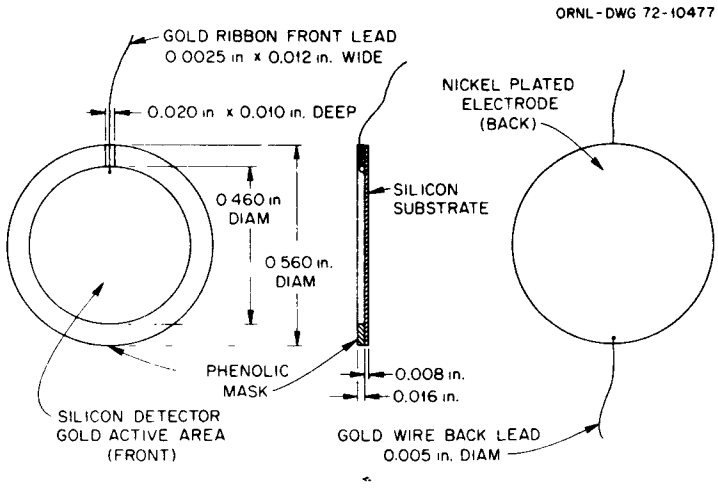

Fig. 6.2. Construction of Schottky Cells for Battery Assembly.

There are two main reasons for using a phenolic mask. The first function of the mask is to reduce the leakage current. However, it also reduces the effective area for power production because it shields the electrons from reaching the silicon. In addition, the presence of the mask increases the thickness of the Schottky cell by almost a factor of three. Hence, the power density ($\mu W/cm^3$) is reduced much more than the

increase in conversion efficiency (about 30%) due to leakage current reduction. On the basis of optimized power density, the presence of the mask is disadvantageous for Schottky cells when used in betavoltaic power conversion systems. The second function of the mask is to provide a tunnel for the front lead such that the front surface of the Schottky cell is flat and the sensitive gold surface is recessed under the mask. This arrangement protects the sensitive gold surface from being scratched during assembly.

6.3 Schottky Cells for Optimization Tests

Silicon resistivity is the first quantity which should be optimized because power output is a function of resistivity. Since the current flowing inside the silicon consists of both electrons and holes, the current density can be expressed as follows:

$$J = nqv_n + pqv_p \tag{6.10}$$

Since

$$v = \mu\varepsilon \tag{6.11}$$

then

$$J = (nq\mu_n + pq\mu_p)\varepsilon \tag{6.12}$$

where

n,p = charge density of electrons and holes

q = electron charge

v_n, v_p = electron or hole velocity

μ_n, μ_p = electron or hole mobility

ε = electric field

Since electrical conductivity is defined as

$$J = \sigma\varepsilon \tag{6.13}$$

therefore

$$\sigma = nq\mu_n + pq\mu_p \tag{6.14}$$

The resistivity is

$$\rho = 1/\sigma = 1/(nq\mu_n + pq\mu_p) \tag{6.15}$$

For n-type silicon, $n \approx N_d$ = density of donor atoms. Therefore,

$$\rho = (1/N_d q\mu_n) \propto (1/N_d) \tag{6.16}$$

Thus, light doping must be used for high resistivity silicon. For intrinsic silicon, the resistivity is about 50,000 Ω-cm, and it is impurity limited. For an intrinsic material, there is very little potential barrier; therefore, no voltage and current can be generated. For heavily doped material, on the other hand, the carrier diffusion length becomes very small and the tunneling effect will increase the leakage current. Therefore, between these two extreme conditions, there is a resistivity which will yield a maximum power output.

Due to the complexity of the beta spectrum of the ^{147}Pm metal and the interaction between electrons and the Schottky barriers, it was decided to perform irradiation experiments to determine the optimum silicon resistivity.

The thickness of the silicon wafer is another quantity which should be optimized. To obtain this value, the depletion width of a Si-Au Schottky barrier device was calculated as follows:[19]

$$W = \sqrt{(2\varepsilon_s/qN_d)[V_{bi} - V - (kT/q)]} \tag{6.17}$$

where

W = depletion width

ε_s = permittivity of Au-Si system = $12\ \varepsilon_o$

N_d = donor concentraction = 10^{17} per cm^3

q = electron charge

V_{bi} = barrier height $\cong$ 0.5 V

V = bias voltage $\cong$ 0

k = Boltzmann constant

T = absolute temperature

The result of the calculation showed that the depletion layer at zero bias volt is about 10^{-4} cm thick.

The diffusion length can be expressed as

$$L_d = v_d \tau = \sqrt{D\tau} \tag{6.18}$$

where

L_d = diffusion length

v_d = drift velocity

τ = carrier life-time $\approx 10^{-6}$ sec

D = diffusion coefficient $\approx$ 35 cm^2/sec

Substituting values into Eq. 6.18, one obtains

$$L_d = 6 \times 10^{-3}\ cm = 0.0025\ in.$$

Therefore 0.002 to 0.003 in. is the optimum thickness of the silicon wafer. However, after a wide search, it was found that Schottky cell manufacturers were unable to supply such a thin cell. The cells provided by UDT were 0.008-in. thick, which is the thinnest they can make, without investing a large amount of research and development effort.

Five Schottky cells with different resistivities were obtained from United Detector Technology, Inc., of Santa Monica, California, and two cells from ORTEC, Inc., of Oak Ridge, Tennessee, for evaluation. They were all mounted on BNC connectors for easy handling. Figure 6.3 shows typical UDT cells, two with phenolic masks and one without mask. A 0.002-in.-diam gold wire was used as a lead for the front connection. The silicon wafers are 0.840 in. in diameter and 0.015 in. thick. Two 0.016-in.-thick phenolic masks were mounted on both the front and back

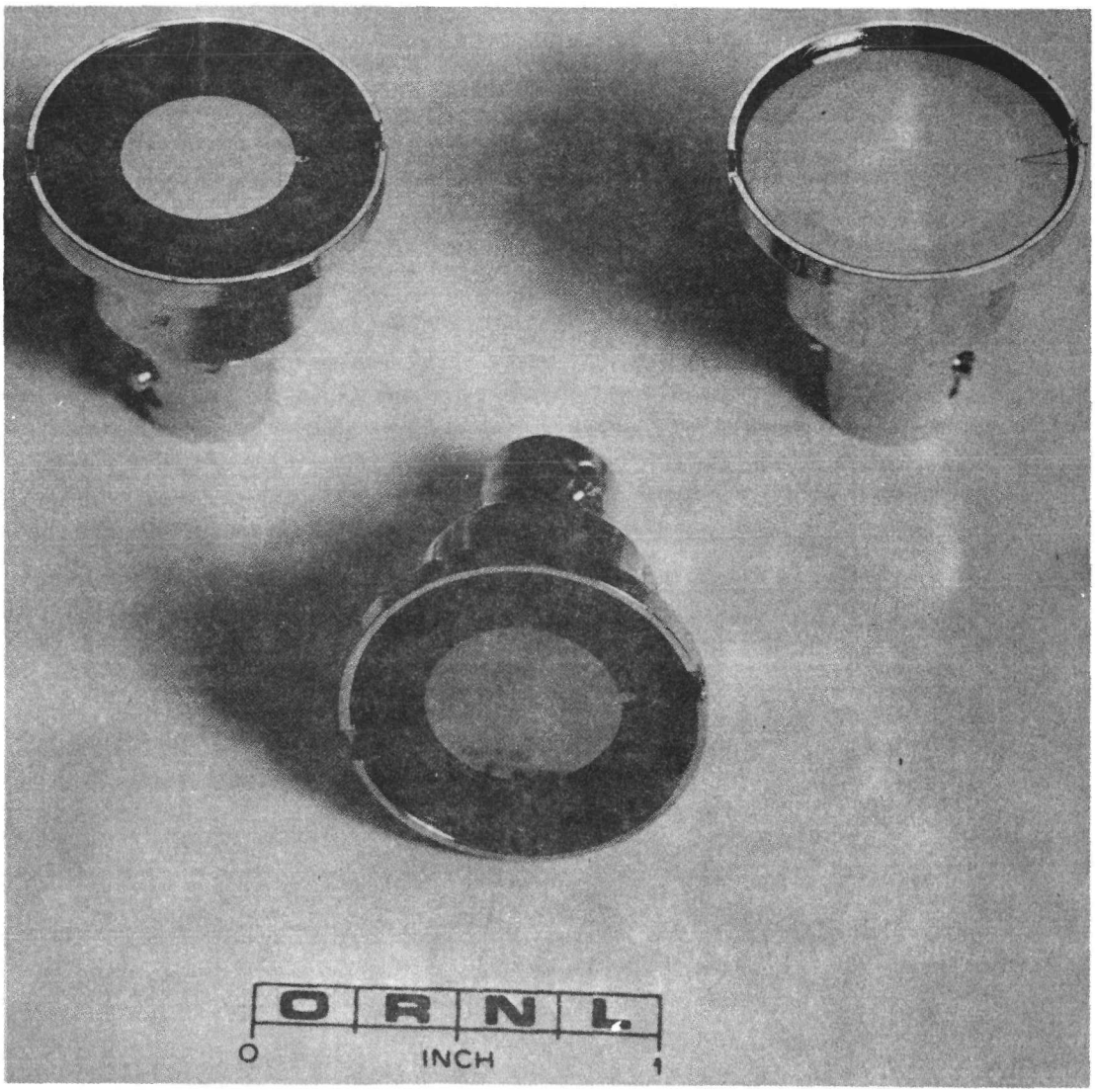

Fig. 6.3. Schottky Cells for Optimization Tests.

sides of the silicon wafer. The resistivities of the silicon wafers varied from 8 to 10,000 Ω-cm. All five cells were processed together such that they had identical properties except for the resistivity.

The ORTEC cells are surface barrier detectors for radiation detection. They are normally used under large bias voltage. The silicon wafer is mounted in a ceramic ring whose front and back surfaces are metallized. The front surface of this ceramic ring is grounded to the metal case and the back surface is connected to the center electrode of the BNC connector.

The resistivities and the sensitive surface areas for all test cells are tabulated in Table 6.1. These cells were used for tests to determine the optimized silicon resistivity and thickness of the promethium radiation source and to perform life tests.

Table 6.1 Physical Characteristics of Schottky Cells for Optimization Tests

No.	Company	Active Area (cm^2)	Resistivity (Ω-cm)
1B	UDT	1.25	10,000
2A	UDT	1.98	520[a]
2C	UDT	1.25	520
3A	UDT	1.25	1,800
4A	UDT	1.00	8
5A	ORTEC	1.00	5,000
5B	ORTEC	1.00	1,250

[a]Without mask.

6.4 Battery Cells

After the optimization tests, which will be discussed in Chapter 9, UDT cells with resistivity of about 500 Ω-cm were selected for battery cells because they gave higher power output than cells with other resistivities. The battery cells differed slightly from test cells. The silicon wafer for the battery cell had a diameter of 0.560 in. and a thickness of 0.008 in. A phenolic mask was used on the front surface, and the mask on the back side was eliminated. The phenolic mask had a thickness of 0.016 in. and a width of 0.050 in. A groove of 0.020 in. wide by 0.010 in. deep was cut in the mask for the front lead. Thus, the front surface of the cell was flat. The diameter of the sensitive area was 0.460 in., yielding an area of $\sim$1 cm^2. In order to increase the strength of the front lead, the 0.002-in.-diam gold wire was replaced by a 0.0025-in. by 0.012-in. gold ribbon. The ribbons were rolled from 0.005-in.-diam gold wire by a small rolling machine.

A total of twenty cells were obtained from UDT for battery assembly. Figure 6.4 shows the battery cells and Fig. 6.2 is a sketch to illustrate the construction of the battery cells.

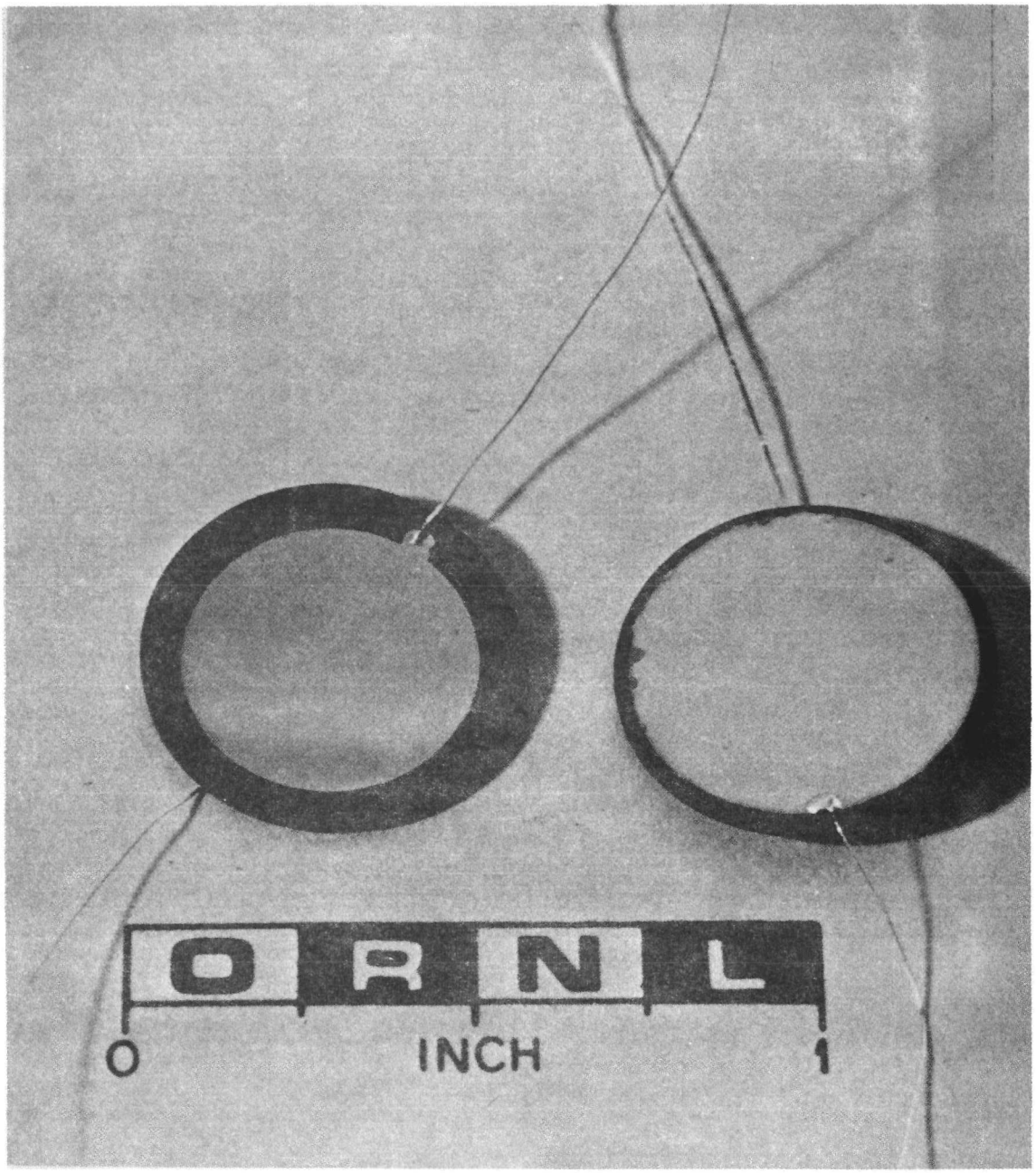

Fig. 6.4. Schottky Cells for Battery Assembly.

7. RADIOISOTOPE SOURCES — ^{147}Pm

7.1 Selection of Radiation Source

The selection of a radionuclide for betavoltaic applications is based on the types of radiation, energy, specific activity, cost, and half-life. Alpha particles can be used to create electron-hole pairs in semiconductors, but they cause severe damage to the lattice. Gamma-ray-emitting radionuclides require considerable external shielding to reduce the radiation dose rate. Pure beta emitters are best suited for our application. They are strongly absorbed by silicon, they do not cause lattice damage if their energy is lower than the damage threshold energy of the particular semiconductor material, and there is no need for heavy external shielding.

Among beta emitters, one selection criterion is maximum beta energy. High-energy beta particles can cause radiation damage in the lattice, limiting the life of betavoltaic devices to a much shorter period than the half-life of the radionuclide. Experiments with monoenergetic electrons show that for n-type silicon the electron damage threshold energy is 145 keV;[28,29] therefore, for n-type silicon devices, the maximum beta energy should be limited to the vicinity of 145 keV. Half-life of the radionuclide is also a major criterion. It is desirable to have an isotope long-lived compared to the life of the battery. However, if the half-life becomes too long, the specific activity becomes too low, thus reducing power output. A half-life of a few years to ten years seems more desirable.

Based on the above criteria, ^{171}Tm, ^{147}Pm, and ^{3}H were selected as potential power sources for a betavoltaic battery. Their major characteristics are shown in Table 7.1. Thulium-171 presents a major problem:

Table 7.1 Potential Power Source for Betavoltaic Applications

Radionuclide	Half-life (years)	Maximum beta energy (MeV)	Maximum power density (W/g)
Tritium	12	0.018	0.35
Promethium-147	2.6	0.225	0.33
Thulium-171	1.9	0.098	0.2

it must be separated from ^{170}Tm. Thulium-170 has a maximum beta energy of about 1 MeV which will cause radiation damage to the lattice and its bremsstrahlung will require considerable external shielding. If an isotopic separation method can be found within reasonable cost, ^{171}Tm could be a very attractive power source. Tritium is an ideal source for betavoltaic application because of its low beta energy and ideal half-life. However, it is difficult to obtain a source with high specific activity. Until these questions can be resolved, ^{147}Pm appears as the best pure beta source suitable for silicon betavoltaic conversion. As the maximum beta energy of ^{147}Pm (225 keV) exceeds the damage threshold for n-type silicon (145 keV), degradation in output could result but at a very slow rate because the number of betas per unit energy decreases as energy increases. Flicker *et al.*[13] report that the radiation damage to np silicon cells by ^{147}Pm beta particles would lead to a 12% drop in efficiency in one half-life (2.6 years). Assuming the damage rate of np cells is limited by n silicon, the degradation rate would be tolerable for this demonstration unit.

Both promethium oxide and promethium metal can be used as a power source for the battery. Metal was selected for this project because (1)

the metal has a higher specific activity than the oxide, (2) metallic foil can be made more uniform in a thin radiation source than can the oxide, (3) oxides are more hazardous to work with than metallic foil, and (4) metal has not been previously investigated. However, in working with promethium metal, argon must be provided to prevent oxidation of promethium metal for source preparation and battery assembly.

7.2 General Characteristics of ^{147}Pm

Promethium is a rare-earth metal. It does not occur in nature because promethium does not have stable and long-lived isotopes. The principal source of promethium is from fission of uranium and of plutonium in nuclear reactors. Figure 7.1 shows the mass yield in the low-energy fission of ^{235}U by thermal neutrons. Note that ^{147}Pm with a mass number of 147 falls in the yield peak near mass number 140. The fission process yields mostly ^{147}Pm (2.6%) with only trace amounts of other promethium isotopes. Through chemical processing of the spent reactor fuel elements, relatively pure ^{147}Pm can be recovered. At present, the availability of ^{147}Pm is estimated at about 10 kW per year. The production rate is projected at 30 kW per year in 1980 and 150 kW per year in 1990.[30] Promethium is currently available at about $560 per watt, and the cost could be reduced by a factor of 2 by large-scale recovery if demands were sufficiently great.

Promethium-147 decays by beta emission to ^{147}Sm which is essentially stable (with half-life of 10^{11} years). The decay scheme and the beta energy spectrum[31] of ^{147}Pm are shown in Figs. 7.2 and 7.3. The major characteristics of ^{147}Pm metal are tabulated in Table 7.2. The density of promethium metal has been determined as 7.22 g/cm^3.[32]

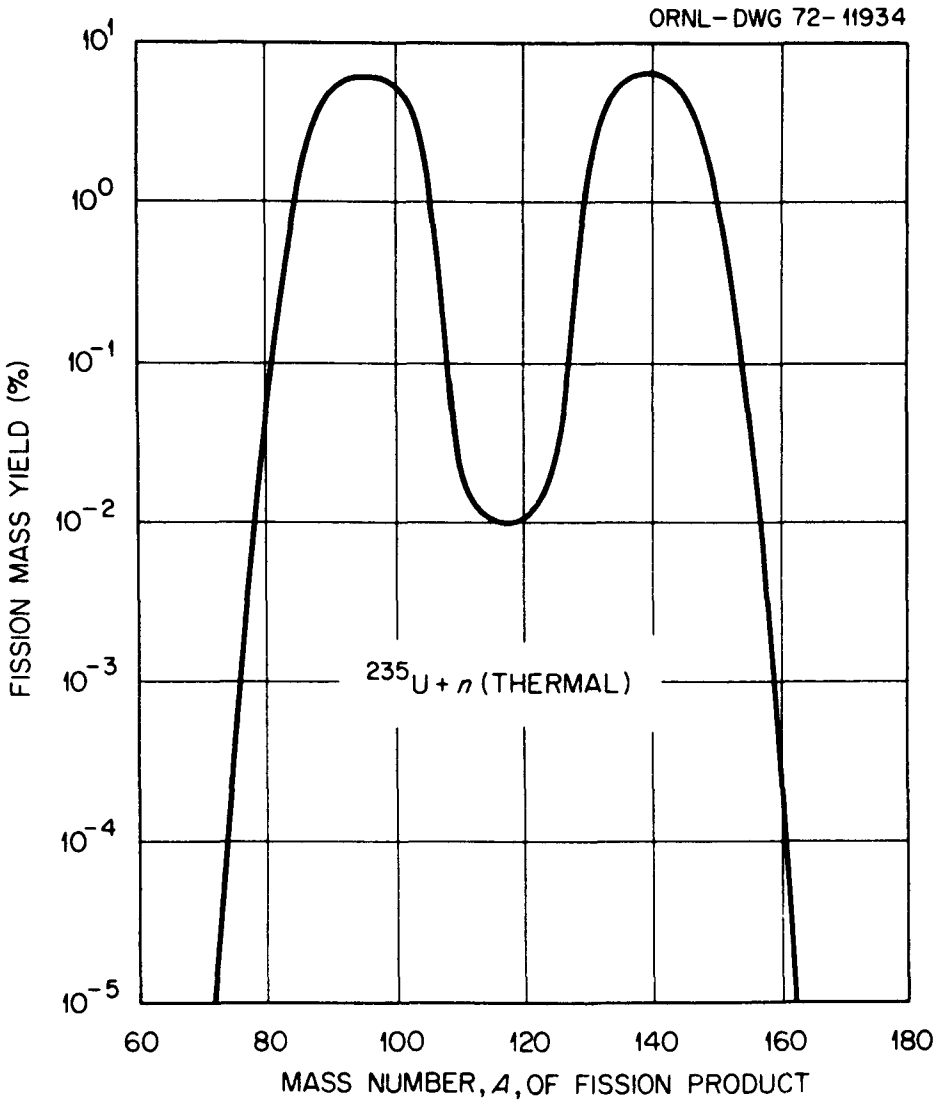

Fig. 7.1. Mass Yield in Fission of ^{235}U by Thermal Neutrons.

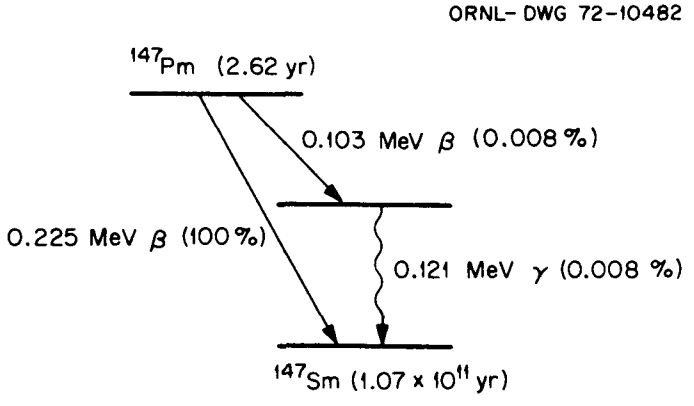

Fig. 7.2. Decay Scheme of Promethium-147.

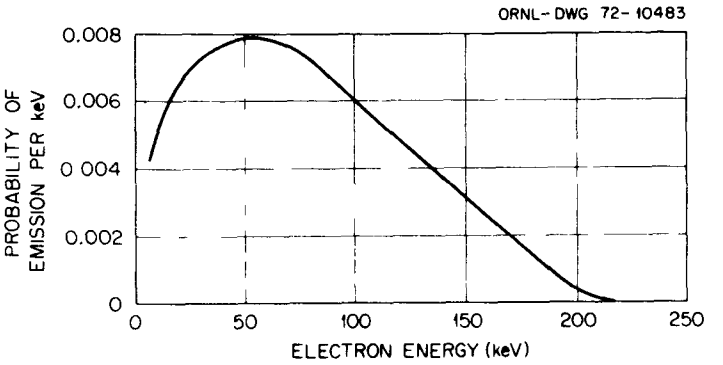

Fig. 7.3. Beta Spectrum of Promethium-147.

Table 7.2 Characteristics of Promethium-147 Metal

Half-life	2.62 years
Density	7.22 g/cm^3
Specific activity	927 Ci/g^a
Activity per watt	2786 Ci/W
Specific power	0.33 W/g
Maximum beta energy	0.225 MeV
Average beta energy	0.062 MeV
Range in aluminum	
Maximum beta energy	55 mg/cm^2
Average beta energy	6 mg/cm^2
Availability	
Present	10 kW/year
1980	30 kW/year
1990	150 kW/year
Cost	$560/W

[a]100%.

7.3 Preparation of ^{147}Pm Metallic Foils

The ^{147}Pm separated from spent reactor fuel elements was obtained from Pacific Northwest Laboratories in the form of oxide. Metallic promethium was prepared at Oak Ridge National Laboratory. To reduce promethium oxide to metallic form, reduction-distillation technique was used.[33] This method employs thorium as the reductant metal. Thorium, whose vapor pressure is much lower than that of promethium at the temperature of chemical reaction, captures oxygen from promethium oxide to

form thorium oxide. Promethium metal was subsequently vaporized from the reaction mixture. The general chemical reaction is

$$2Pm_2O_3 + 3Th \rightleftarrows 4Pm + 3ThO_2 \ .$$

Heating was provided by a radiofrequency induction heating coil. The mixture was heated to a temperature of about 1500°C to 1700°C to initiate the chemical reaction. A vacuum of less than 2×10^{-5} **torr** was maintained during the operation. In order to avoid radioactive contamination, the whole system, including the vacuum system, was enclosed in a glove box operating at a negative pressure with respect to the atmospheric pressure of the room.

Promethium metal was continuously removed from the system. This was done by distilling promethium metal into a quartz dome collector located over the top of the still. Bright metallic promethium collected in the shape of the dome.

The fresh distilled metal was then removed from the dome and transported to another glove box which contained the rolling equipment. Argon was used in all procedures to avoid reoxidation of the metal. Sandwiched between two stainless steel sheets of about 0.02 in. thickness, promethium metal was then rolled into a foil of the desired thickness. An arch punch was used to punch the foil into the appropriate size disks.

This technique also removes the daughter product, ^{147}Sm, from the promethium source material. The reaction temperature for samarium distillation is about 1300°C to 1350°C, which is much lower than that of promethium, permitting separation of the samarium from promethium by the distillation method.

One advantage of using promethium metal instead of promethium oxide was the fact that the metal can be rolled into a uniform foil. To check the uniformity, an autoradiograph technique was used. Polaroid films were exposed by a promethium metal foil; the results showed that the radiation dose was quite uniform across the entire foil.

7.4 Specific Characteristics of Radiation Sources

7.4.1 The Impurity Levels of Promethium Metal

The promethium oxide used for the reduction-distillation process was chemically purified on October 13, 1971. The radioactive contaminants and chemical impurities in the promethium oxide were measured by Pacific Northwest Laboratories and are given in Table 7.3. After the reduction-distillation process, the chemical impurities of the promethium metal were determined at Oak Ridge National Laboratory by mass spectrometer on April 7, 1972. Table 7.4 tabulates the result of the spectrographic analysis which shows that the metal is clean enough for this application. The alpha contamination level and the gamma spectrum of ^{147}Pm metal are discussed in Sections 9.8 and 9.11.

Table 7.3 Impurity Levels of Promethium Oxide

Gamma Impurities	
^{146}Pm	3.1×10^{-7} Ci per Ci ^{147}Pm
^{148}Pm	$<1.1 \times 10^{-11}$ Ci per Ci ^{147}Pm
^{144}Ce	$<4 \times 10^{-9}$ Ci per Ci ^{147}Pm
^{154}Eu	5.1×10^{-10} Ci per Ci ^{147}Pm
Alpha Impurities	
	$<2.5 \times 10^{5}$ dis/min.Ci ^{147}Pm or $<1.1 \times 10^{-7}$ α Ci per Ci ^{147}Pm
Chemical Impurities	
	Trace amounts of Ca, Cu, Fe, Mg, Si, and Nd (trace means less than 0.01%)

Table 7.4 Chemical Impurity Levels of Promethium Metal

Elements	ppm	Elements	ppm
Al	10	Si	20
Ba	0.2	Ta	0.7
Ca	200	Th	9
Co	<0.1	Ti	<0.2
Cr	7	V	<0.1
Cu	4	Zn	3
Fe	100	Cl	700
K	20	S	<0.3
Mn	0.7	Nd	20
Ni	4	Sm	2
P	<0.1	Other	
Pb	50	rare earths	<1

7.4.2 The Power Density of Promethium Metal

The ^{147}Pm metal was distilled again on June 5, 1972, to remove samarium. The specific activity and power density reached 100% of the theoretical values, that is, 927 Ci/g and 0.33 W/g, respectively. This value will decay according to the exponential law with a half-life of 2.62 years starting with the date of distillation.

$$A = A_0 \, e^{-(0.693/T_{1/2})t} \qquad (7.1)$$

where

A = activity at time t

A_0 = initial activity at t = 0

$T_{1/2}$ = half-life of the radionuclide

t = decay time

Figure 7.4 shows the specific activity of ^{147}Pm in metal form as a function of time.

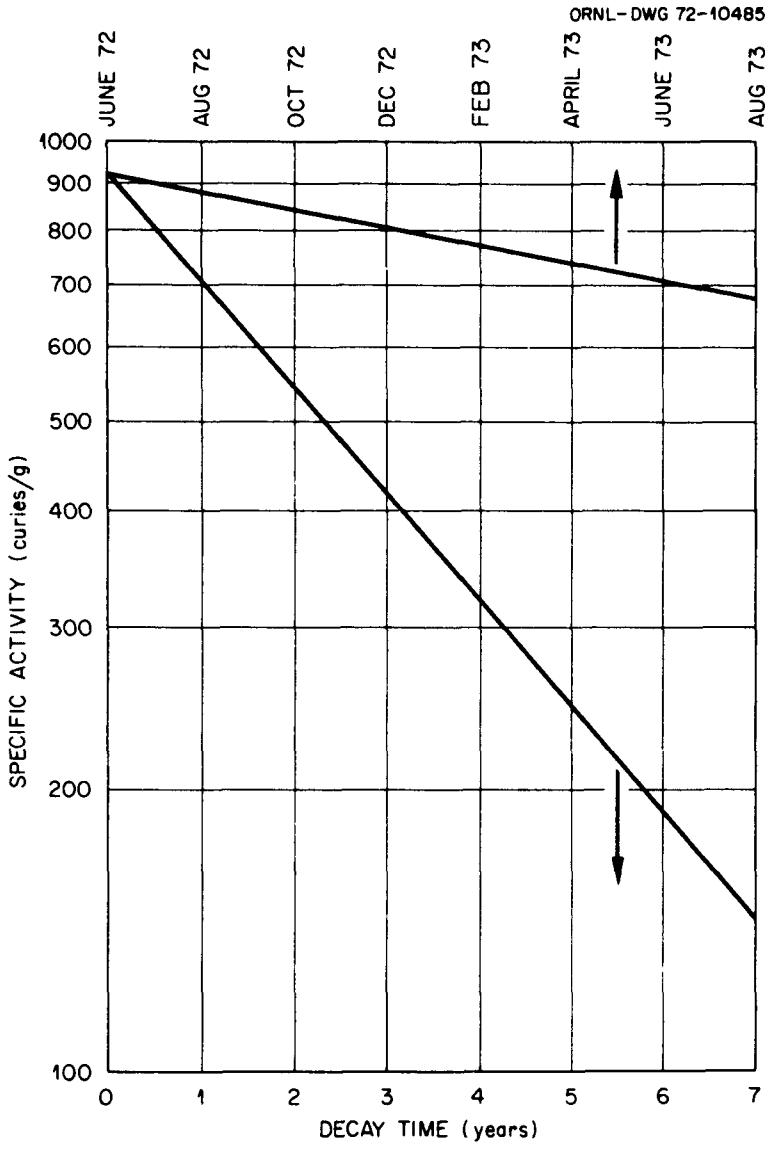

Fig. 7.4. Decay of Promethium-147 Versus Time.

7.4.3 Configuration of the Sealed Source

The construction of the sealed source is shown in Fig. 7.5(a). The promethium metal foil is 5/8 in. in diameter with a thickness of 5.55 mg/cm^2 (about 0.0003 in.) and a total activity of about 10 Ci. To prevent oxidation of the foil and to eliminate the use of argon, the foil is sealed with an aluminum foil window of 0.001 in. thickness. The external

contamination level at the surface of the sealed source was wipe tested, and the results showed 194 counts/min.

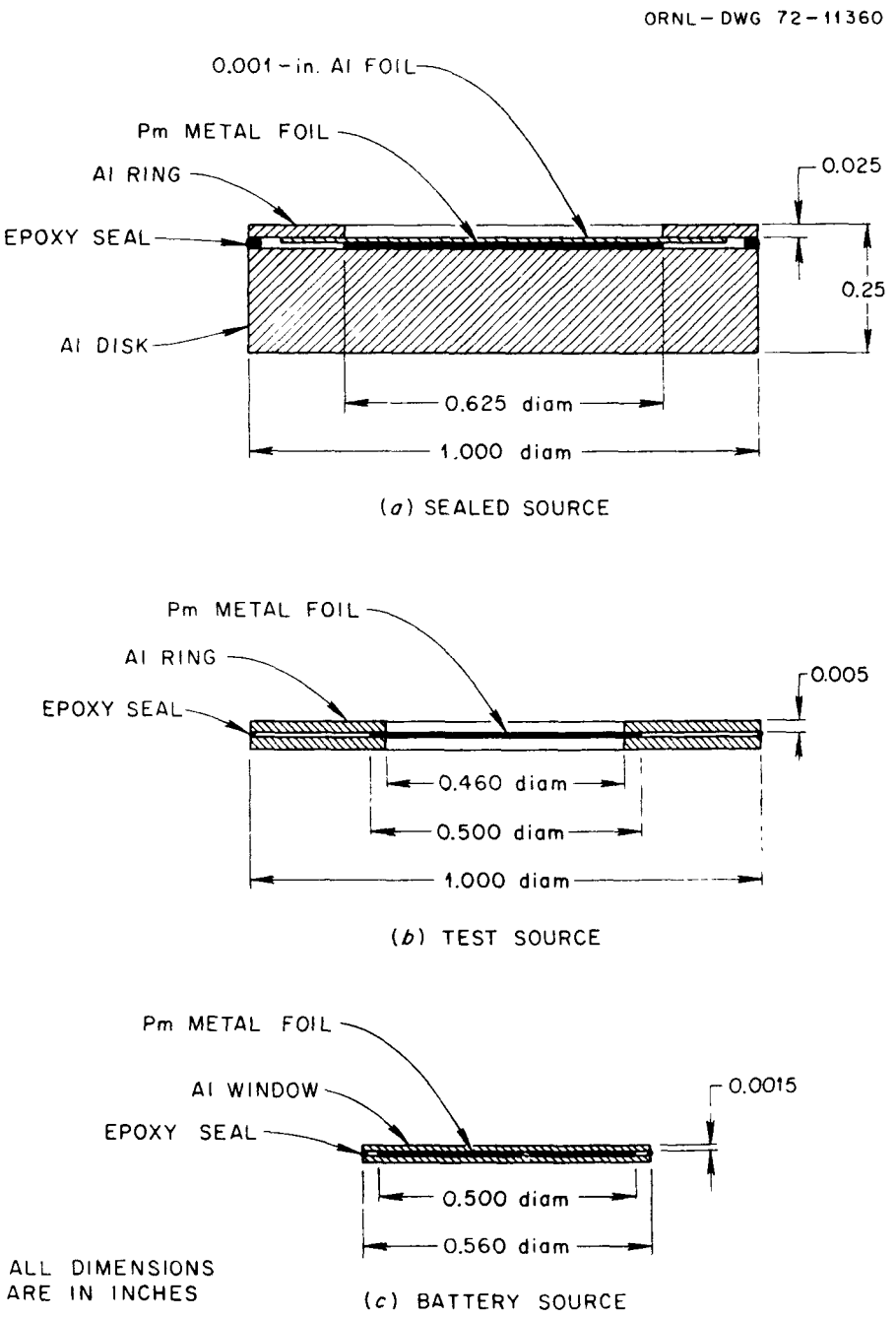

Fig. 7.5. Construction of Promethium-147 Sources.

This source was used for the following experiments:

1. to test the uniformity of the promethium foil
2. to optimize the Schottky cells with respect to silicon resistivity
3. to perform radiation shielding studies, and
4. to perform life tests.

This sealed source was later determined to be contaminated with alpha emitters on the surface of the source (see Sections 9.7 and 9.8). A second sealed source was constructed in exactly the same fashion as the first one except that a 2.52 mg/cm^2 thick promethium foil was used. The second sealed source was assembled in a clean glove box. A smear test showed no alpha contamination on the surface of the second sealed source. This source was used to continue the life test.

7.4.4 Bare Sources for Promethium Thickness Optimization

Four bare sources of different thicknesses were made to test the relationship between source thickness and the power output. The foils were 1/2 in. in diameter and 11.1, 5.55, 4.56, and 2.52 mg/cm^2 in thickness. In order to conserve the promethium metal, two 5.55 mg/cm^2 foils were loaded together to obtain the 11.1 mg/cm^2 source. All foils were sandwiched into two aluminum foil rings with a 0.005 in. thickness. Figure 7.5(b) shows the construction of these sources. The use of aluminum rings provided spaces for handling and makes the source outside diameter the same as the Schottky cells so that the sources could be aligned. For all bare sources the active source area was 1 cm^2.

These sources were not sealed and therefore argon was used during the experiments. They were used for the following experiments:

1. With the 5.55 mg/cm^2 bare source, power output was measured for every Schottky cell.
2. Using the best cell as determined in Step 1, power output was measured for each of the four bare sources.

7.4.5 Battery Sources

Two foils were made for battery sources. These were 1/2 in. in diameter and 5.55 mg/cm^2 in thickness and had an activity of 6.6 Ci per foil. The foil thickness was selected based on experiments as will be discussed in Section 9.5. Due to the limited quantity of promethium metal available, the three promethium foils with 5.55 mg/cm^2 as described in Section 7.4.4 were to be used as battery sources after the experiments were completed. In addition, it was expected that the promethium foil in the sealed source could be punched into a 1/2-in.-diam foil which was to be used as a battery source if it had not oxidized after the life test. However, among possible six battery sources, only four sources were made for battery assembly while two promethium metals were oxidized and they could not be mounted as battery sources. These promethium metal foils were sandwiched in aluminum foils of 0.0015-in. thickness. The aluminum foils were used to stop the alpha particles from reaching the Schottky cells (see Section 9.8). Figure 7.5(c) shows the construction of the sources.

Until ready for use, all battery sources were stored under vacuum in a vacuum jar which was under argon.

8. EXPERIMENTAL INSTRUMENTATION AND APPARATUS

8.1 Electronic Measurement System

To obtain V-I characteristics of the Schottky cells, an ammeter and a voltmeter were required to measure current and voltage, respectively. An x-y plotter was used to display, on rectilinear paper, the V-I characteristics. Two E-H model 202 electrometers were used: one electrometer measured current, and the other electrometer, with a series resistance of 10^8 ohms, measured the voltage. An electrometer was used to measure voltage instead of a voltmeter because the Schottky cell had a very high internal impedance — on the order of thousands of ohms. A regular voltmeter does not have very high impedance so that it would drain current. When 10^8 ohms was connected in series with the electrometer, the current passing through this electrometer could be interpreted as voltage across the terminal. The conversion was 10^{-9} amp, equivalent to 0.1 volt. The arrangement of the measurement system is shown in Fig. 8.1. Both electrometers had the necessary output voltage of 10 mV full scale needed to drive the x-y plotter.

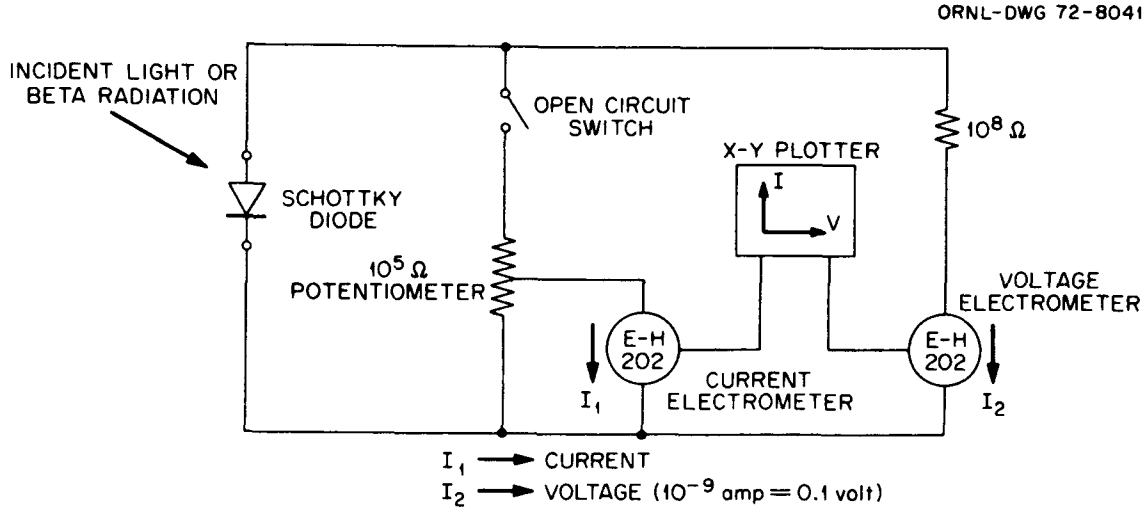

Fig. 8.1. V-I Characteristic Measurement System.

A 10^5-ohm, ten-turn potentiometer was connected across the Schottky cell as the load resistance. When light or beta radiation was incident on the cell, the V-I characteristic curve could be plotted by varying the resistance of this potentiometer. An open-circuit switch was mounted on the instrument panel to give a true open-circuit voltage. The short-circuit current was obtained with the potentiometer set to zero resistance, but with about 200 ohms resistance in the electrometer circuitry.

A calibration box was assembled to provide the calibration of the electrometers and the x-y plotter. This box consisted of a 1.5-volt battery, a 10^4-ohm, ten-turn potentiometer, and a switch. The calibration procedure was as follows. The output of the calibration box was connected to the input of the measurement system. Both electrometers were zeroed accurately. The ten-turn 10^4-ohm potentiometer (on the calibration box) was set at 2.0, giving a voltage output of 0.3 volt. The ten-turn 10^5-ohm potentiometer (on the measurement system) was set at 3.0, giving a current flow of 10^{-5} amp. With ranges of the voltage electrometer and current electrometer set at 0.3 volt full scale and 10×10^{-6} amp full scale, respectively, both electrometers gave full deflections. With the x-y plotter set to zero and full scale at both x (voltage) and y (current) directions, any value in between zero and full scale could be interpolated linearly.

Reverse leakage current of the Schottky cells was first measured by a Tektronix Transistor Curve Tracer Type 575. Low leakage current would mean higher power output as indicated by Eq. (6.8). However, the curve tracer would not give a satisfactory result because the reverse leakage current was so small that it was practically zero on a 50-microampere-per-division scale. To measure the reverse leakage current more

accurately, the calibration box and two electrometers were used. The calibration box supplied the dc bias voltage to the cell. The voltage and current were measured by two electrometers and then the voltage was plotted against the reverse leakage current on the x-y plotter. Figure 8.2 shows the system for reverse leakage current measurement.

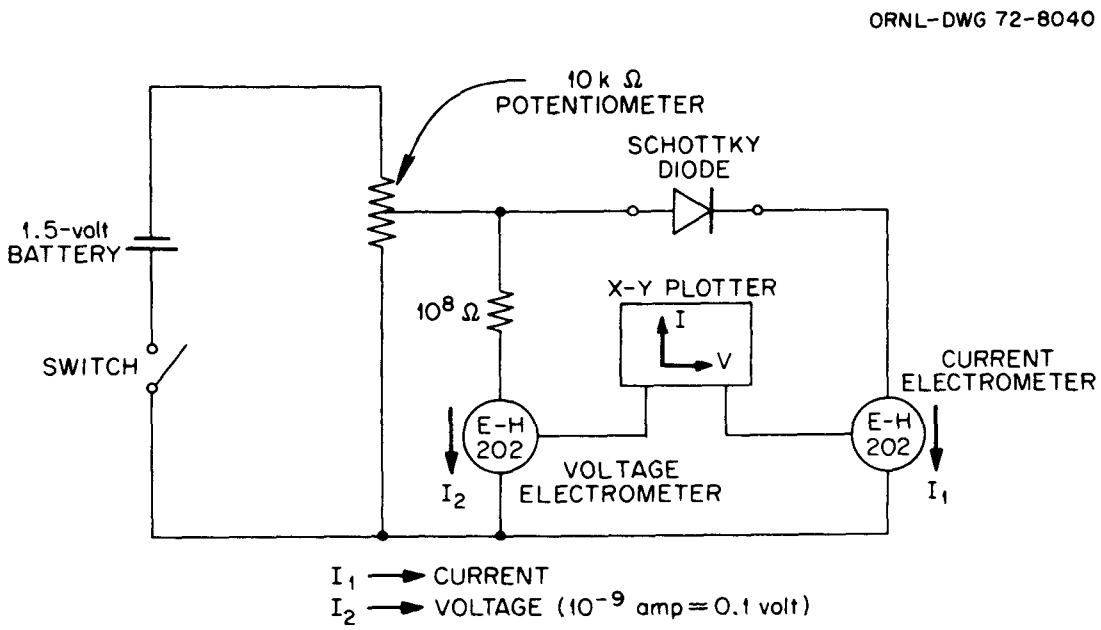

Fig. 8.2. Reverse Leakage Current Measurement System.

8.2 Glove Box

To avoid contamination of radioactive material, all operations involving radioactive material were done in a glove box. For additional protection, this glove box was located in a hood. The hood had an exhaust system which would draw the air through the hood and into a set of absolute filters before discharge through a stack.

The glove box was made of plastic. It served two purposes: (1) to contain the radioactive material and (2) to provide an air-tight container for working with promethium metal foils under argon. Two rubber gloves

were mounted in the front for manipulating objects inside the box. Two transport ports were provided on the opposite side of the glove box to transport material in and out of the box without contaminating the laboratory. A gas connector and an exhaust filter were mounted on the glove box for the argon supply. A leaktight electrical lead feedthrough was installed in order to transmit signals through the glove box. Figure 8.3 shows a sketch of the glove box.

8.3 Health Physics Instrumentation

With all the precautions taken, there was always the possibility that some radioactive materials would leak out of the glove box. Standard health physics instruments were used in the laboratory to check radioactivity or contaminants.

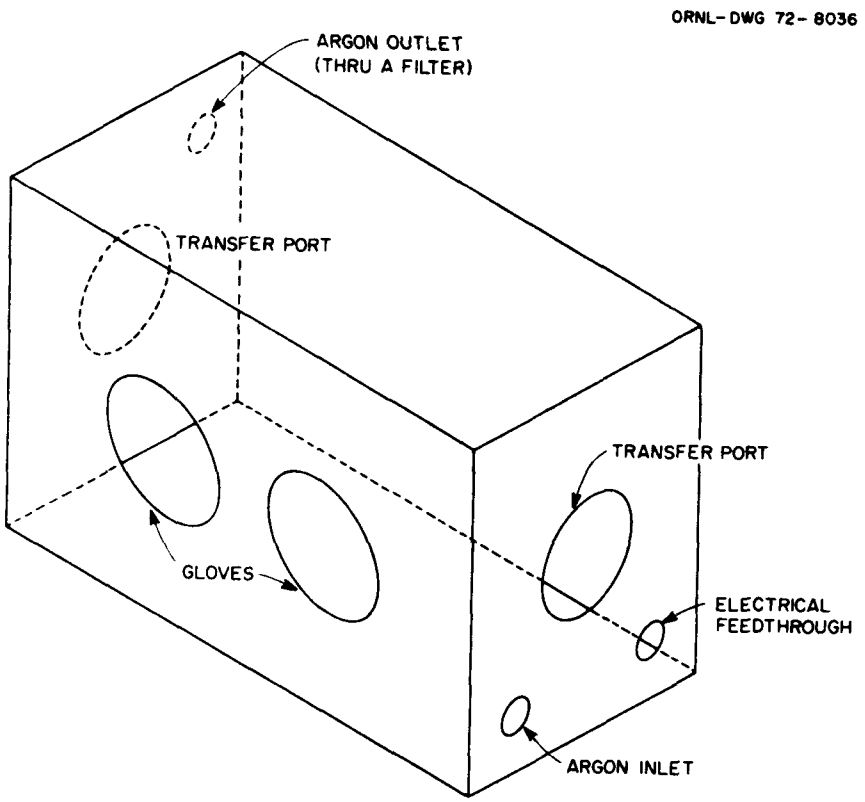

Fig. 8.3. Glove Box.

An air monitor system with an alarm was used to check the radioactivity in the air. An alarm was sounded if the airborne activity exceeded the safety level. A thin-window Geiger-Müeller (GM) tube, capable of detecting promethium betas, was installed near the entrance of the laboratory. Before any personnel left the area, both hands and feet were carefully examined with this instrument. Smear tests in the hood area were performed routinely. The smear test filter paper disks were counted in a sensitive gas flow proportional detector. Low-level contamination could be detected with this instrument.

Two pencil dosimeters were worn when radiation experiments were performed. They were read every day to give the radiation dose rate received. Finger dosimeters were worn to check the dose rate received on the fingers when promethium foils were handled at close range.

9. CHARACTERIZATION EXPERIMENTS

9.1 Diode Characteristics and Reverse Leakage Current

The diode characteristics of all UDT Schottky cells were measured by Tektronix Transistor Curve Tracer Type 575. Figure 9.1 shows the curves obtained with a Polaroid camera. The pictures show that for most cells, except cell 4A (with resistivity 8 Ω-cm), the leakage current was lower than this instrument could resolve. A second set of reverse leakage currents was taken with the dc power supply and the measurement system. This measurement system was described in Section 8.1. The results are shown in Fig. 9.2. Cell 4A (8 Ω-cm) had high leakage current. Cell 2A (520 Ω-cm), without the insulating mask, also showed a large reverse leakage current. The rest of the cells demonstrated a reverse leakage current of less than 10^{-7} ampere. Cells with low leakage current should be used because this means high power output as indicated by Eq. 6.8.

9.2 Photovoltaic Response

Schottky cells are sensitive to visible light. The incident photons ionize an atom to create an electron-hole pair through the photoelectric effect. After the electron-hole pairs are generated, the holes are diffused through n-type silicon and are collected by the junction. With the light source, it is much easier to compare the output of Schottky cells with various parameters than with the beta radiation because of the radiation source handling procedures. Thus, every Schottky cell was tested by light. The light intensity was set to 1 mW/cm^2 which was comparable to the energy output of a promethium foil.

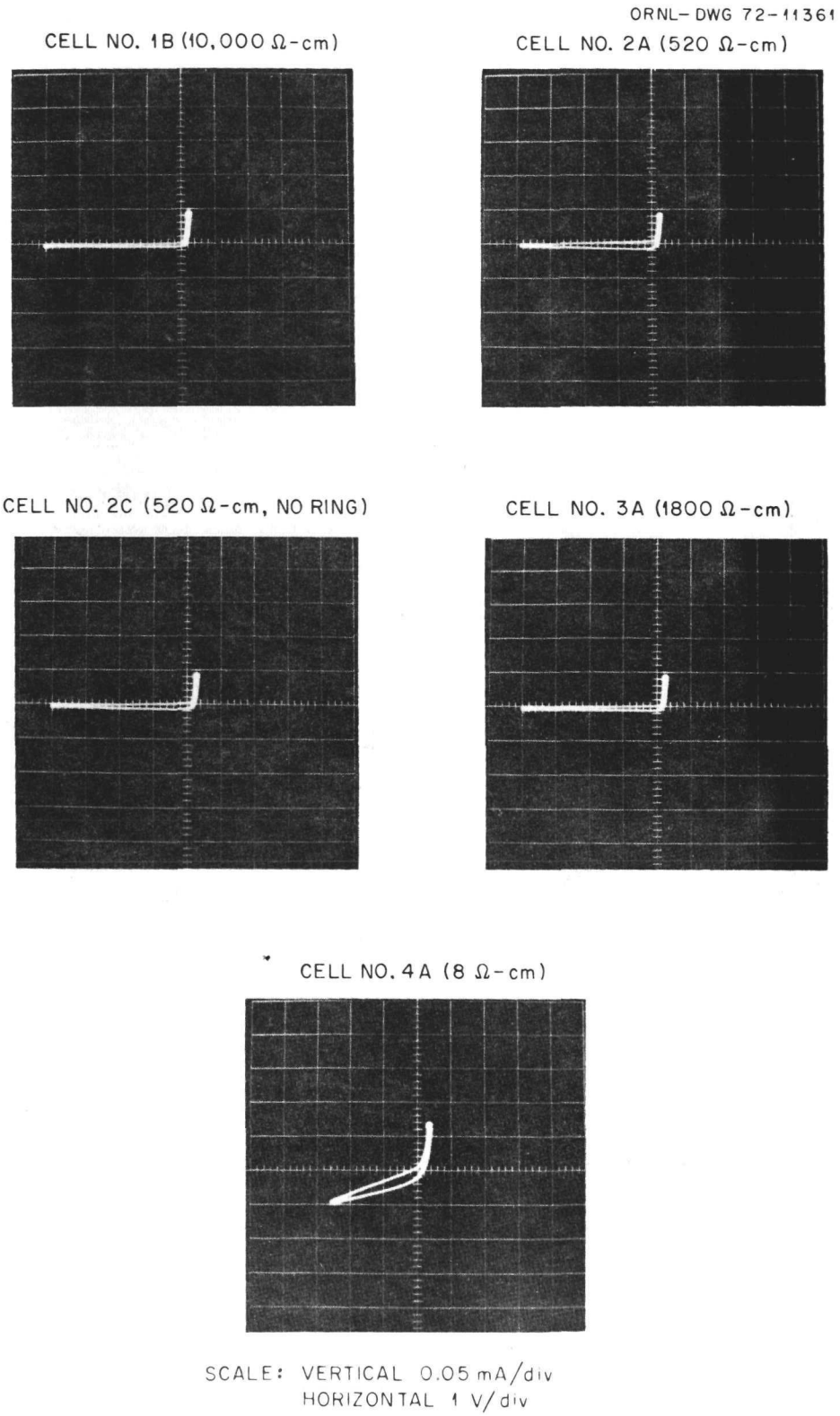

Fig. 9.1. Diode Characteristics of Schottky Cells.

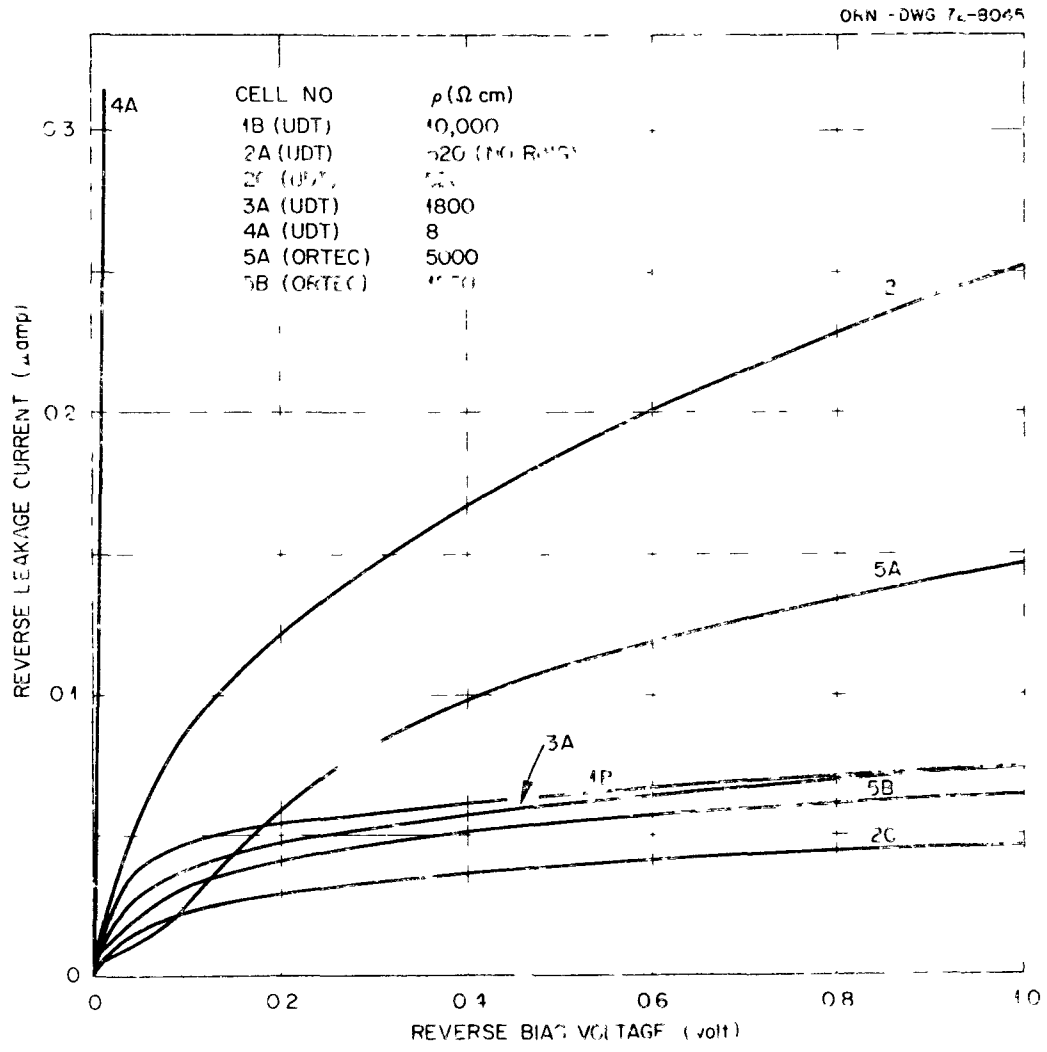

Fig. 9.2. Reverse Leakage Current of Schottky Cells.

An optical bench was set up in a dark room. A General Electric 200-W standard light source (6.6A/T4/1CL) was used and the distance between the light source and the Schottky cell was set at 127 cm, which yields an intensity of 1 mW/cm^2. An ac power supply and an ammeter were used to monitor the power output of the standard light source.

The V-I characteristics of all Schottky cells were measured by the measurement system consisting of two electrometers and an x-y plotter as described in Section 8.1. Five cells from UDT and two cells from ORTEC

were measured. Figures 9.3 and 9.4 show the V-I characteristics of the photovoltaic response. The power outputs were calculated by multiplying the current and the voltage at a particular operating point. The ORTEC cells showed a negligible response when compared to UDT cells. Figure 9.5 summarizes the results of power output, short-circuit current and open-circuit voltage as a function of silicon resistivity and shows that cells with resistivity around 520 Ω-cm yield the maximum power output. In Fig. 9.5, short circuit current and maximum power output of cell No. 4A have been multiplied by 1.25 to take into account the differential in effective cell area. Table 9.1 lists the results of the optical test.

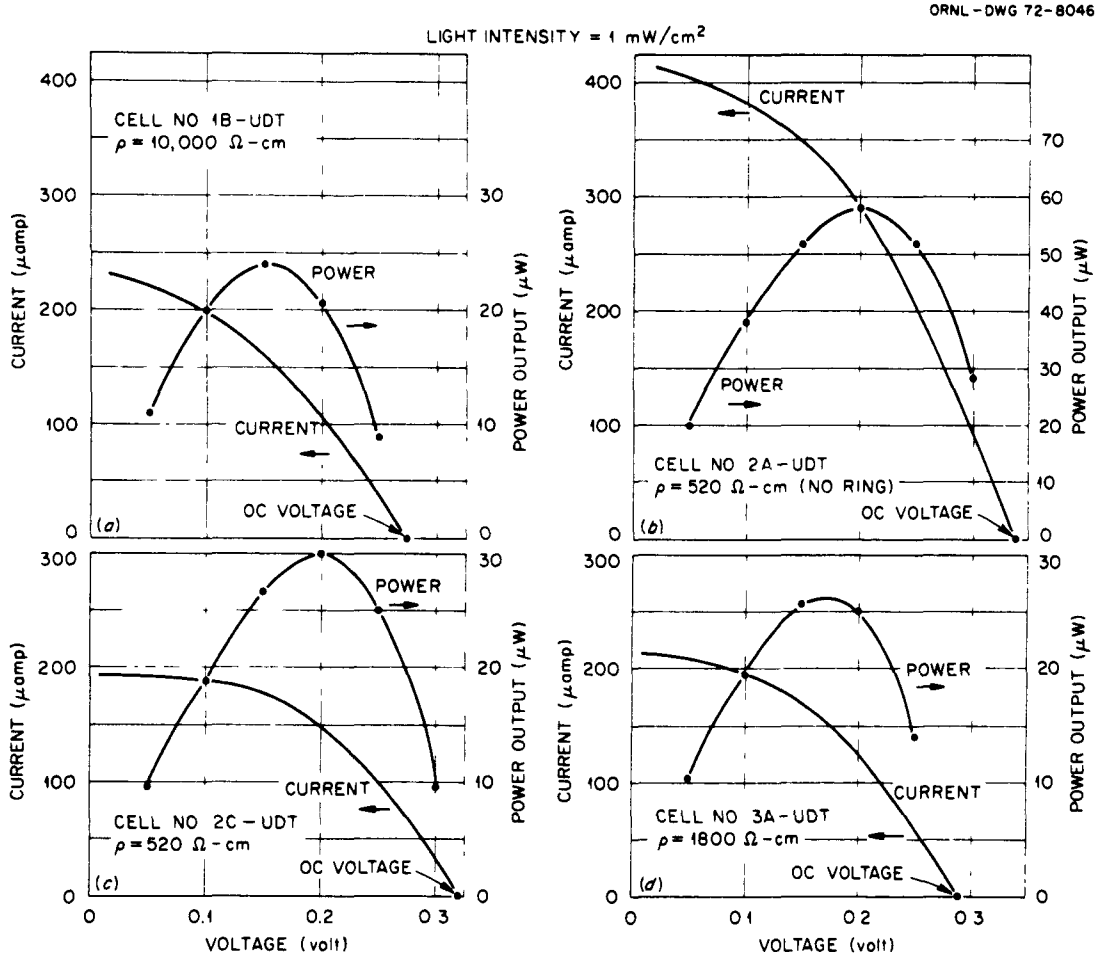

Fig. 9.3. V-I Characteristics of Optical Response (Cells 1B, 2A, 2C, and 3A).

It was anticipated that in the final battery assembly, cells would be connected either in parallel or in series or by a combination of these. Since they are neither pure voltage sources nor pure current sources, they have to be optimized in series-parallel arrangement to yield maximum overall power output, i.e., the cells would be matched. However, after the parallel and series experiment as described in Section 11.2, it became clear that the total power output is equal to the sum of the power output of individual cells, regardless of how the cells are connected. Therefore, the matching process became unnecessary.

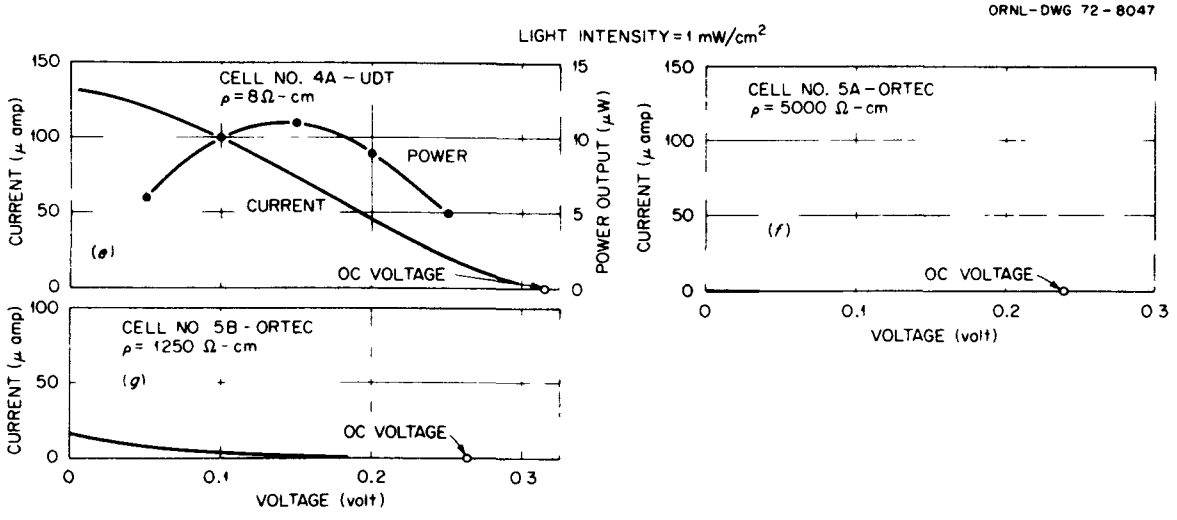

Fig. 9.4. V-I Characteristics of Optical Response (Cells 4A, 5A, and 5B).

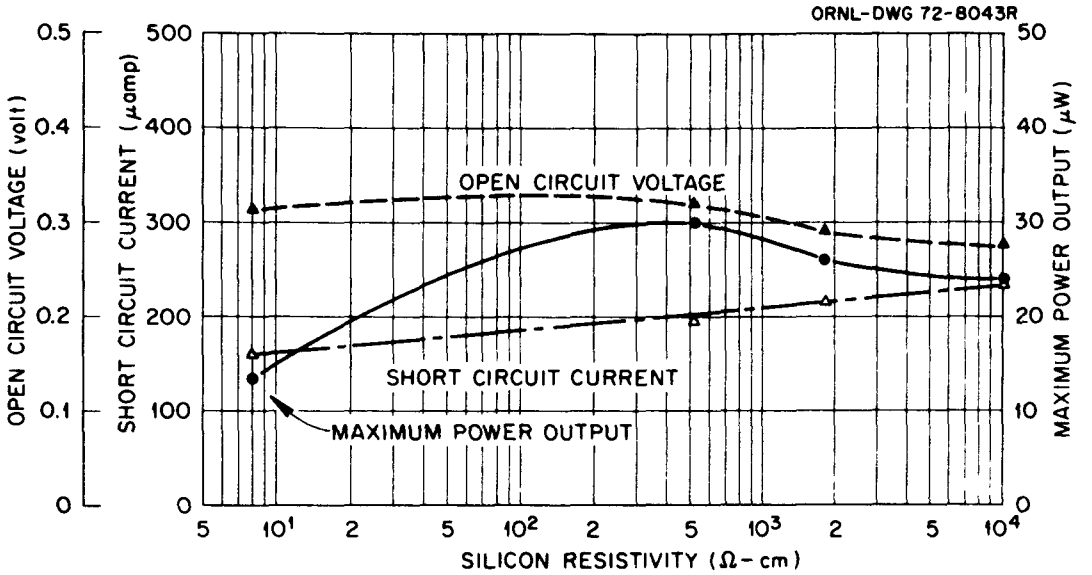

Fig. 9.5. Silicon Resistivity Versus Output Characteristics With Light Source.

Table 9.1 Characteristics of Cells — Photovoltaic Response

Light Intensity = 1 mW/cm^2

Cell No.	Resistivity (Ω-cm)	Active Cell Area (cm^2)	Maximum Power Output (μW)	V_{oc} (V)	I_{sc} (μA)
4A	8	1.00	11	0.315	130
2C[a]	520	1.25	30	0.32	195
2A[a]	520	1.98	58	0.34	440
3A	1,800	1.25	26	0.29	215
1B[b]	10,000	1.25	24	0.275	235
5A[b]	5,000	1.00	Negligible response		
5B[b]	1,250	1.00	Negligible response		

[a]No mask.

[b]ORTEC cells.

9.3 Betavoltaic Response with Sealed Promethium Source

This measurement was similar to that of photovoltaic response except the sealed promethium source was used instead of light. The Schottky cells and the radiation source were transported into the glove box. A stand and two clamps were used to move the cells up and down. Electrical signals were taken out through the electrical feedthrough. Section 8.2 gives a brief description of the glove box. The measurement instruments were placed on a stand next to the hood.

The V-I characteristics of all Schottky cells were measured and the power outputs were calculated. Figures 9.6 and 9.7 show the betavoltaic response and Fig. 9.8 summarizes the result as functions of silicon resistivity (in Fig. 9.8, P_{max} and I_{sc} of cell No. 4A have been multiplied

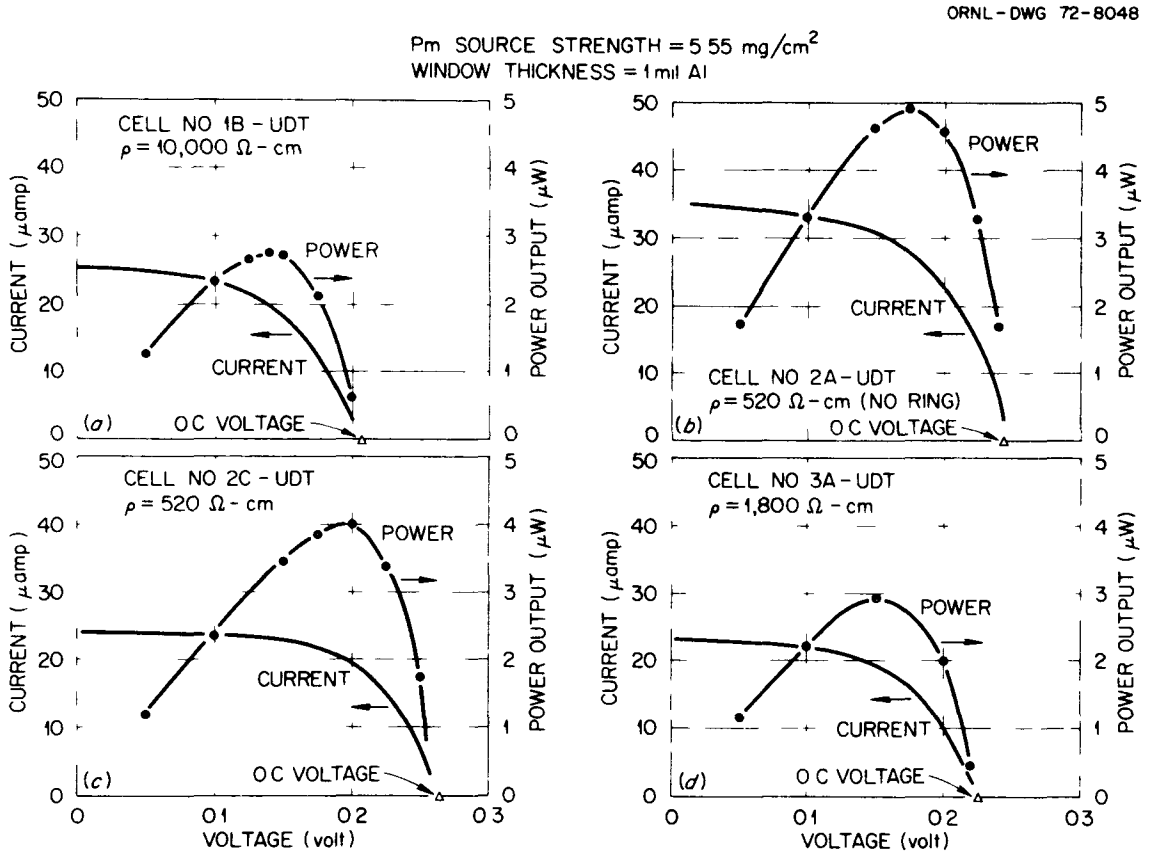

Fig 9.6. V-I Characteristics of Betavoltaic Response — Sealed Promethium Source (Cells 1B, 2A, 2C, and 3A).

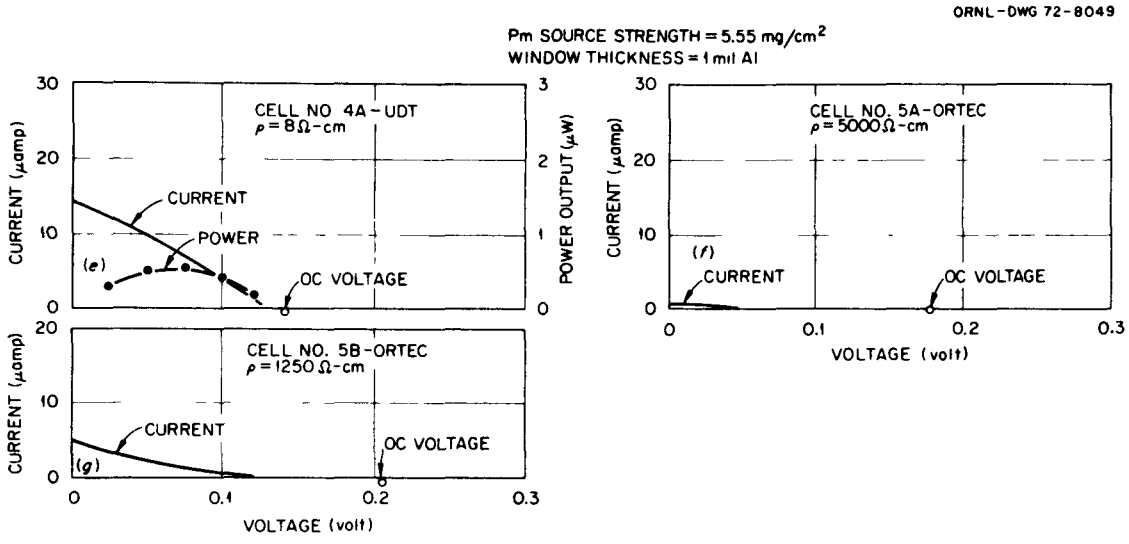

Fig. 9.7. V-I Characteristics of Betavoltaic Response — Sealed Promethium Source (Cells 4A, 5A, and 5B).

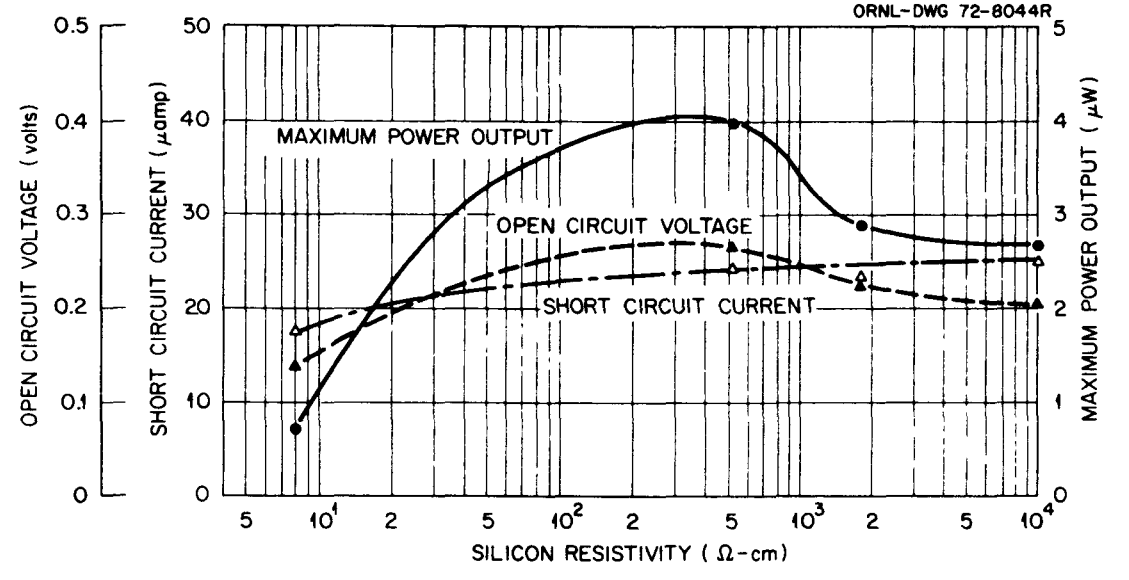

Fig. 9.8. Silicon Resistivity Versus Output Characteristics With Sealed Promethium Source.

by 1.25). ORTEC cells, again, showed negligible response compared to UDT cells.

By comparing the results obtained from the light source (Fig. 9.5) and from the beta radiation source (Fig. 9.8), one finds that the Schottky cell with 300 to 400 Ω-cm resistivity yields maximum power output under both light and electron irradiations. Table 9.2 shows the results of the betavoltaic test with the sealed source.

Table 9.2 Characteristics of Cells — Betavoltaic Response With Sealed Promethium Source

Promethium Source Strength	5.55 mg/cm^2
Active Source Area	2 cm^2
Window Thickness	0.001 in. Al

Cell No.	Resistivity (Ω-cm)	Active Cell Area (cm^2)	Maximum Power Output (μW)	V_{oc} (V)	I_{sc} (μA)
4A	8	1.00	0.55	0.14	14
2C[a]	520	1.25	4	0.265	24
2A[a]	520	1.98	4.9	0.245	35
3A	1,800	1.25	2.9	0.225	23
1B[b]	10,000	1.25	2.7	0.206	25
5A[b]	5,000	1.00	Negligible response		
5B[b]	1,250	1.00	Negligible response		

[a] No mask.

[b] ORTEC cells.

9.4 Betavoltaic Response with Bare Promethium Source

In this measurement, argon was connected the day prior to the experiment and the glove box was continuously flushed overnight. Promethium foil with a thickness of 5.55 mg/cm^2 (same as the sealed source) was used to irradiate all UDT Schottky cells. Figure 9.9 shows the V-I characteristics and Fig. 9.10 summarizes the result as a function of silicon

resistivity. These data show (1) the use of 1-mil aluminum foil reduced the power output by a factor of about 4 and (2) for an optimized cell (520 Ω-cm), the maximum power output was about 15 μW/cm^2 of effective area. Although most cells had an active area of 1.25 cm^2, the radiation

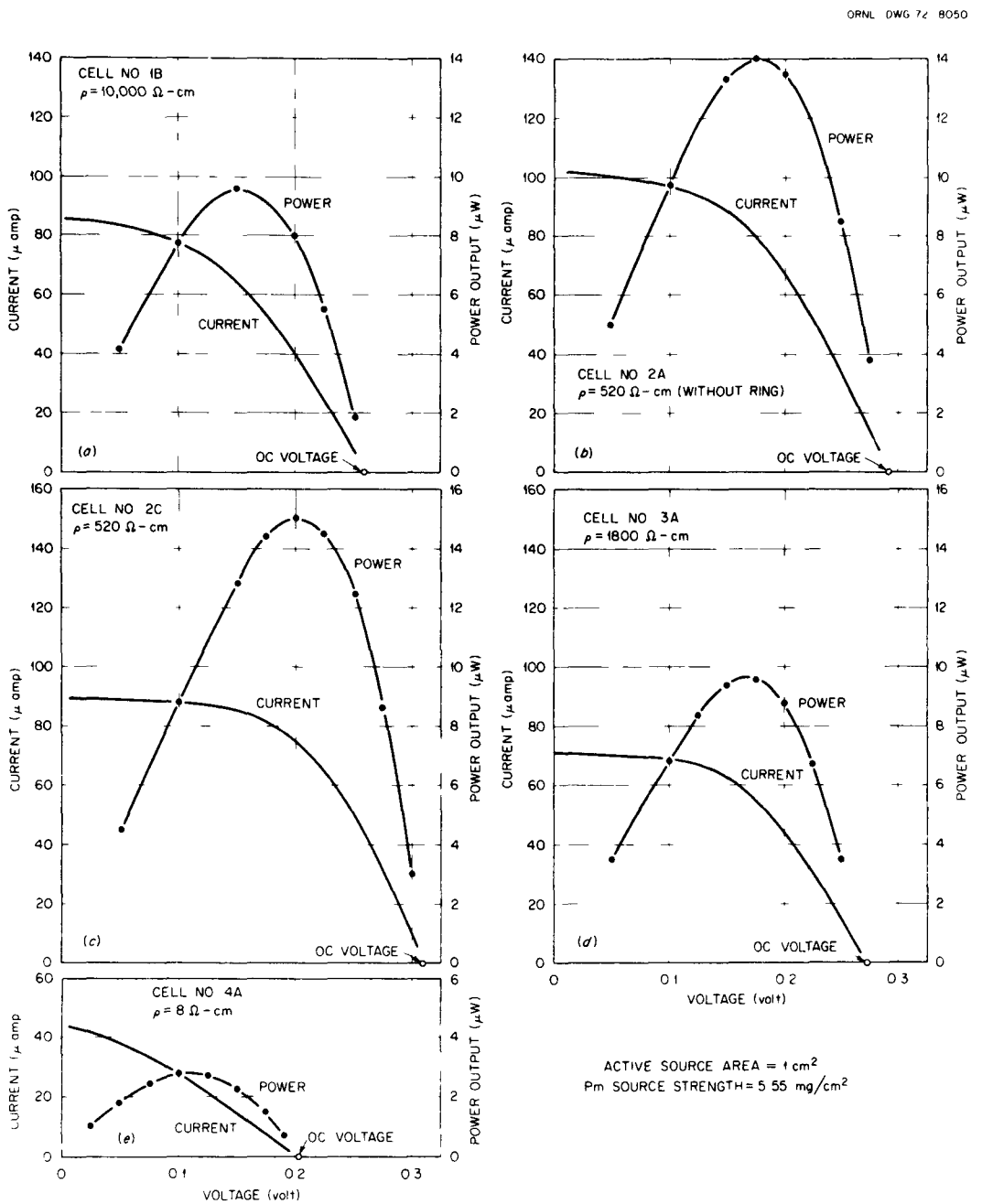

Fig. 9.9. V-I Characteristics of Betavoltaic Response — Bare Promethium Source.

source had only 1 cm^2 of active area. Therefore, one should consider the power output to be generated by 1 cm^2 effective area. Table 9.3 gives the results of the betavoltaic test with a bare source.

Comparing Fig. 9.10 with Figs. 9.5 and 9.8, one finds that the Schottky cells with ∿400 Ω-cm resistivity yields maximum power output for all three types of measurement.

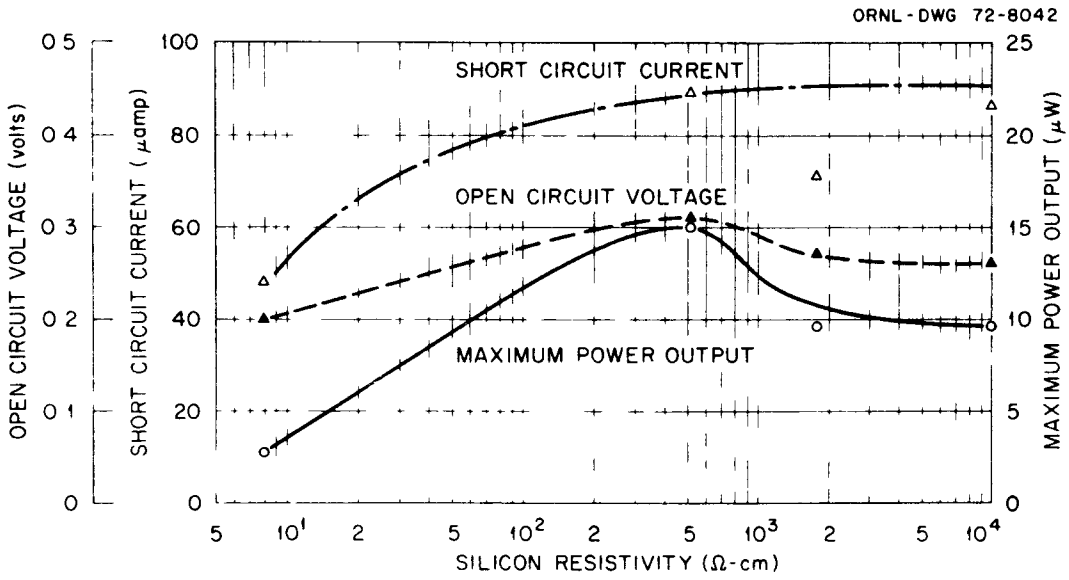

Fig. 9.10. Silicon Resistivity Versus Output Characteristics — Bare Promethium Source.

Table 9.3 Characteristics of Cells — Betavoltaic Response With Bare Promethium Source

Promethium Source Strength	5.55 mg/cm^2
Active Source Area	1 cm^2

Cell No.	Resistivity (Ω-cm)	Maximum Power Output (μW)	V_{oc} (V)	I_{sc} (μA)
4A	8	2.8	0.2	48
2C[a]	520	15	0.31	89
2A[a]	520	14	0.29	102
3A	1,800	9.6	0.27	71
1B	10,000	9.6	0.26	86

[a] No ~~k.

9.5 Conversion Efficiency, Power Output Versus Promethium Metal Foil Thickness

The self absorption of beta energy in the promethium source decreases the power output of the radiation source and, therefore, reduces the conversion efficiency. The self absorption can be calculated by using the equations developed for beta-ray attenuation (see Section 9.9). However, since the main interests here are the power output and the conversion efficiency of the Schottky barrier cells, calculations would need to be extended to the generation, diffusion, recombination, and collection of carriers in a metal–semiconductor system for which a theory has not yet been developed. Therefore, experimental determination of the effect of the promethium foil thickness was made.

To determine the optimum thickness of promethium foil, four foils with thicknesses of 11.1, 5.55, 4.56, and 2.52 mg/cm^2 were used to irradiate cell 2C (520 Ω-cm, with mask). The V-I characteristics of cell 2C as irradiated by promethium foils of different thicknesses are shown in Fig. 9.11. Figure 9.12 shows the maximum power output, conversion efficiency, short-circuit current, and open-circuit voltage versus foil thickness. Table 9.4 gives the results of the thickness optimization tests.

The conversion efficiencies were calculated by the following equation

$$\varepsilon = P_{out}/P_{in} \tag{9.1}$$

where

ε = conversion efficiency

P_{out} = maximum electrical power output

P_{in} = power input of the promethium metal foil

Power input per 1 mg/cm^2 promethium foil is estimated as

$$P_{in} = 1/2(1 \text{ mg/cm}^2)(1.25 \text{ cm}^2)(0.927 \text{ Ci/mg})(1/2786 \text{ W/Ci})$$

$$= 0.209 \text{ mW}$$

Here, the total area of the promethium foil has to be used because the loss of energy through the aluminum rings should be considered as a part of the total efficiency.

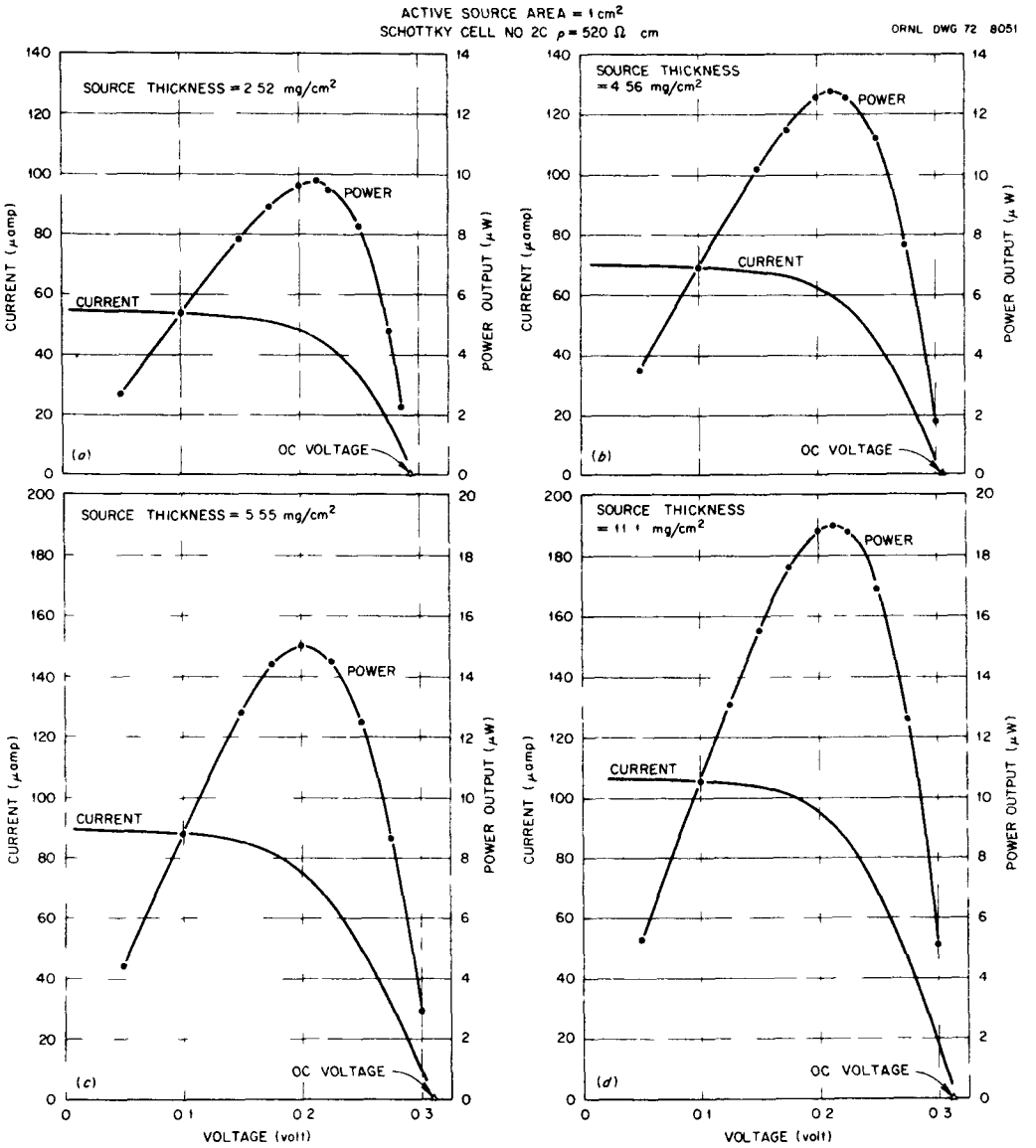

Fig. 9.11. V-I Characteristics of Cell 2C With Various Promethium Metal Foil Thicknesses.

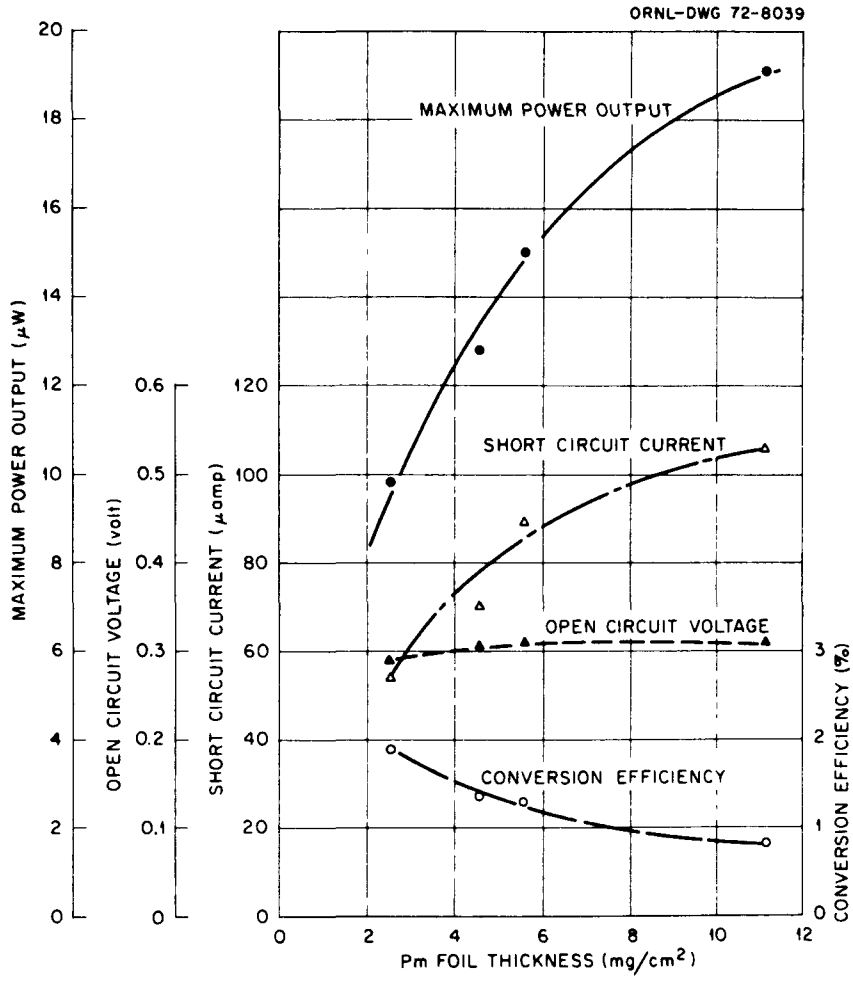

Fig. 9.12. Conversion Efficiency and Power Output Versus Promethium Foil Thickness.

Table 9.4 Characteristics of Cell 2C Versus Promethium Metal Foil Thickness

Active Source Area = 1 cm^2
No window

Source Thickness		Maximum Power	V_{oc}	I_{sc}
mg/cm^2	mils	Output (μW)	(V)	(μA)
2.52	0.14	9.8	0.29	54
4.56	0.25	12.8	0.305	70
5.55	0.3	15	0.31	89
11.1	0.6	19.1	0.31	106

The factor of one-half is used in the last equation because of 2π geometry, i.e., one-half of the radiation is directed toward the Schottky cell. Since the power input is linearly proportional to the thickness of the foil, the power input can be easily obtained for foils whose thickness is other than 1 mg/cm^2. Table 9.5 shows the results of this calculation.

Table 9.5 Conversion Efficiency Versus Promethium Metal Foil Thickness

Active Source Area = 1 cm^2
No Window

Source Thickness (mg/cm^2)	Maximum Power Output (μW)	Power Input (μW)	Efficiency (%)
2.52	9.8	522	1.88
4.56	12.8	950	1.35
5.55	15	1150	1.31
11.1	19.1	2300	0.83

From this experiment, the optimum promethium foil thickness can be selected. As shown in Fig. 9.12, the curves of power output and conversion efficiency are functions which change slowly. Therefore, there is no clear-cut advantage to selection of any particular thickness. The conversion efficiency of a very thin promethium foil is high, but the power output is very low. On the other hand, with thicker foils the power is increased but radiation dose rates are also increased. However, a range of thicknesses can be selected to satisfy both the power output and radiation dose rate considerations. For this project, a thickness of between 5 to 6 mg/cm^2 was selected and foils of 5.55 mg/cm^2 were prepared.

9.6 Radiation Damage

Many investigators have studied the damage of silicon under electron bombardment. Flicker *et al.*[34] reported a damage threshold of about 200 keV for p silicon and 145 keV for n silicon. As the maximum beta energy of ^{147}Pm (225 keV) is above the damage threshold for silicon, cell degradation could result from the ^{147}Pm betas penetrating the silicon semiconductor. Flicker *et al.*[13] also reported that radiation damage to pn junction cells by the ^{147}Pm betas would lead to a 12% drop in efficiency during one half-life (2.62 years). Donald W. Douglas Laboratories has tested their ^{147}Pm silicon pn junction betavoltaic battery for more than one year and reported the maximum power output reduced by a factor of 2 in 1.7 year.[17] Since the gold atoms are much heavier than silicon atoms, the damage threshold energy for gold is about a factor of 3 higher than that of silicon.[35] It is therefore anticipated that Si-Au Schottky barrier cells would be at least as radiation resistant as the silicon pn junction cells.

If an alpha emitter is present in the radiation source, however, the situation would be very different. Since alpha particles have large masses (∿8000 times heavier than electrons) and high energies (∿5 to 6 MeV), they will damage silicon devices very rapidly. Flicker *et al.*[13] have shown experimentally that the ^{147}Pm source would have to emit less than 3000 alphas/min.Ci of ^{147}Pm if the damage caused by these particles were to be neglected during one ^{147}Pm half-life.

Therefore, if the alpha activity of the ^{147}Pm source is less than 3000 alphas/min.Ci, the radiation damage to silicon should be tolerable for this prototype battery.

9.7 Life Test

The purpose of the life test is to observe the degradation of the performance of the Schottky cells under irradiation by promethium sources. Cell 2C and the sealed source (with 0.001-in. aluminum window) were used, and V-I characteristic curves were measured. The power output decreased very rapidly. After a one-hour irradiation, the power decreased by a factor of two. By the end of three hours, it reduced by more than a factor of five compared to the initial output. Figure 9.13(a) shows the V-I characteristics versus time for cell 2C. As discussed in the last

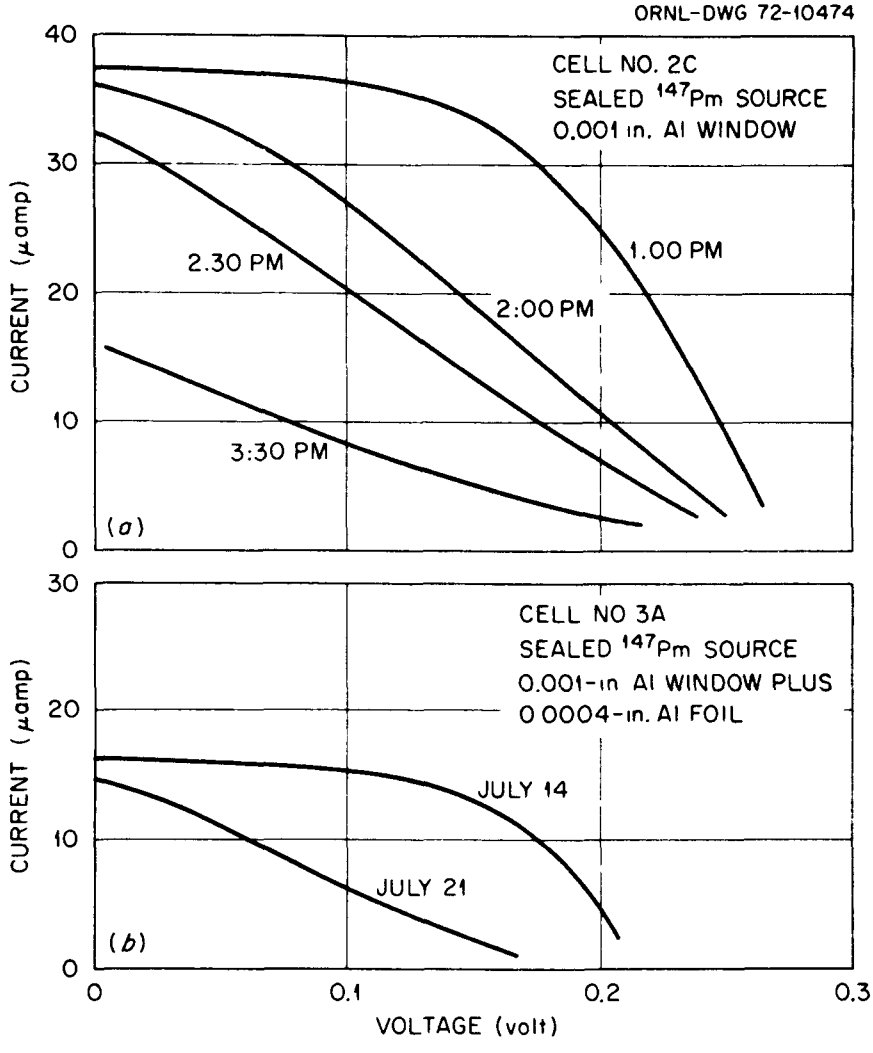

Fig. 9.13. Life Test With Alpha Contaminated Sealed Promethium Source.

Section, alpha contamination was suspected to be responsible for such a large damage rate. An additional 0.0004-in.-thick aluminum foil was used between the sealed source and cell 3A. The power output was still decreased with time but at a much slower rate, a factor of two in seven days. Figure 9.13(b) shows the measured curves. The 0.0004-in.-thick aluminum foil was then removed; further irradiation of cell 3A showed a much faster degradation, similar to cell 2C. It was obvious that the 0.0004-in.-thick aluminum foil was responsible for the reduction in power degradation, not the difference between cells 2C and 3A.

This power degradation of the cells is due to two levels of alpha contamination. Detailed discussions of alpha contamination will be presented in the next section.

Since the promethium foils, outside surface of the sealed source, glove box, Schottky cells, and all apparatus inside the glove box were contaminated with alpha-emitting radioisotopes, a new set of material was required to perform a life test against electron bombardment. A new glove box, new Schottky cells, and a new sealed source were set up for measurement. The second sealed source was assembled in a glove box without alpha contamination, and a clean source was assembled. The promethium metal foil, however, was still heavily contaminated with alpha. The life test was continued with the second sealed source. A total of 0.0015 in. of aluminum foil was used to stop the alpha particles from reaching the Schottky cell. The result of the test is shown in Fig. 9.14. It shows no significant change in V-I characteristics versus time.

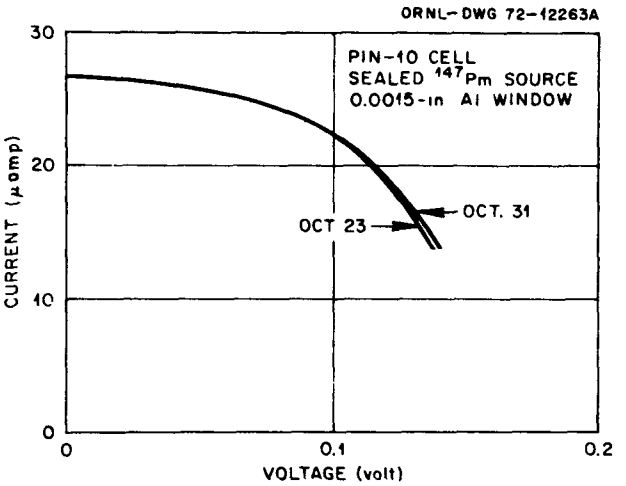

Fig. 9.14. Life Test With Second Sealed Source.

9.8 Alpha Contamination

The initial life test showed that the power output decreased rapidly with time, which immediately suggested severe radiation damage. Electrons, due to their light mass and low energy (0.225 MeV maximum), were not likely to produce such a degradation rate. As discussed in Section 7.1, one of the major reasons to select ^{147}Pm as the radiation source was the fact that the radiation damage to silicon was tolerable. However, if alpha emitters were present in the radiation source, the heavy mass and high energy (5 to 6 MeV) of alpha particles would indeed cause severe damage in the materials.

After the test of cell 2C, the first step was to stop the alpha particles from reaching the Schottky cell. From the alpha energy-range curve,[36] Fig. 9.15, it can be seen that an aluminum foil of 0.001-in. thickness (6.7 mg/cm^2) was insufficient to stop alpha particles in an energy range of about 6 MeV, but 0.0014-in. (9.5 mg/cm^2) aluminum foil would stop alpha particles completely. Cell 3A was tested with a total of 0.0014-in.-thick aluminum foils. The result still showed a

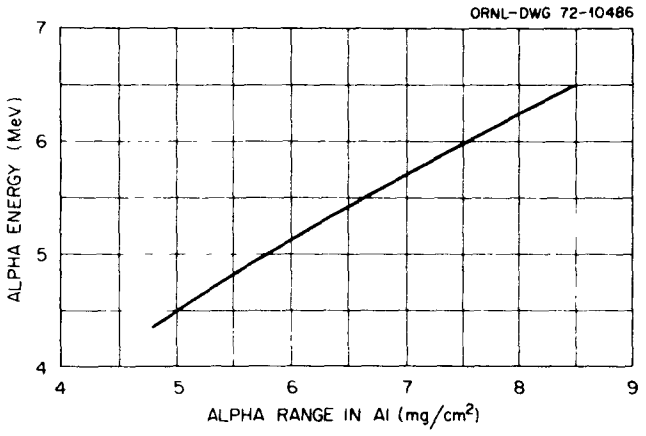

Fig. 9.15. Alpha Range in Aluminum.

degradation of power output but with a much slower rate. It was suspected that there might be two levels of alpha contamination: a heavy contamination with the promethium metal foil and a light contamination on the outside surface of the sealed source. When an 0.001-in. aluminum window was used, both sources of alpha were causing the damage. After 0.0004-in.-thick aluminum was added, only the alpha particles from the outside surface of the sealed source caused the damage while the alpha particles from promethium metal foil were stopped completely by 0.0014-in.-thick aluminum. Since the outside surface of the sealed source had much less contamination, the damage was at a much slower rate.

If this was true, the glove box for the source assembly must be alpha contaminated. A wipe test of the glove box containing the rolling equipment (also used as the source assembly) showed the box was grossly contaminated with alpha emitters. An aluminum plate was brought inside the box and the same procedures were followed as with the 0.001-in. aluminum window in the sealed source. After the aluminum plate was removed from the glove box, a wipe test showed 20,000 dpm alpha. This test showed clearly that the glove box was heavily contaminated with alpha emitters.

To make certain that there was no alpha contamination in the promethium prior to the rolling process, a small promethium metal sample obtained right after the distillation process was dissolved in 1 *M* nitric acid. The metal had been oxidized. The weight of promethium oxide is 18.5 mg which corresponds to about 14 Ci of activity after correction for 100 days' decay. The sample was subsequently diluted to 0.83 mCi/ml in 0.3 *M* nitric acid solution. One milliliter of the solution was pipetted onto a stainless steel planchet, evaporated, and alpha counted. A 2π geometry, gas-flow proportional counter was used to count the alpha particles. The counting efficiency was 52% with some contribution from backscattering. The self-absorption is neglected because the thickness is less than 2 $\mu g/cm^2$. The alpha particle count was <1 dpm per milliliter of solution, i.e., <1200 dpm per curie of ^{147}Pm. This was the lower limit of the counting system in the presence of approximately 2×10^9 dpm beta particles per milliliter of solution.

From the above measurements, it is clear that the alpha contamination was picked up inside the glove box which contains the rolling equipment. Compared to the criterion, <3000 alpha/min.Ci, discussed in Section 9.6, the promethium metal prior to the rolling process would be satisfactory for battery assembly.

9.9 Absorption of Beta Energy in Aluminum

In the final battery assembly, one cannot tolerate such a large alpha contamination on the promethium metal foil. One technique to avoid the alpha radiation damage is to use aluminum foil to stop the alphas. Two 0.0015-in.-thick aluminum foils were used for the battery source assembly as described in Section 7.4. This arrangement stopped the alpha particles

from reaching the Schottky cells, but also stopped a large fraction of beta particles.

The absorption of beta energy in an absorber from a point source can be calculated by Laevinger's empirical formula:[37]

$$R(r) = (CK/r^2)\{[c - re^{1 - (r/c)}] + re^{1 - r}\} \tag{9.2}$$

For $r \geq c$, the quantity inside the square bracket is set equal to zero where

$R(r)$ = energy absorbed at a distance r in an absorbing medium from a point source

C = activity of the point source

The quantities K, r, and c can be expressed as

$$K = \frac{\bar{E}}{4\pi[c^2(3 - e) + e]} \tag{9.3}$$

$$r = \nu x \tag{9.4}$$

$$\nu = \mu/\rho = \frac{16}{(E_m - 0.036)^{1.4}} [2 - (\bar{E}/\bar{E}^*)] \tag{9.5}$$

$$c = 3.11\ e^{-0.55E_m} \tag{9.6}$$

where

x = thickness of absorber in terms of g/cm^2

ν = mass absorption coefficient, cm^2/g

E_m = maximum energy of the beta spectrum

$\bar{E}$ = average energy per disintegration

$\bar{E}^*$ = average energy per disintegration for an allowed spectrum of the same energy

The point source formula can be applied to an infinitesimally thin infinite plane source by integrating over the entire plane. Thus, the energy absorbed at distance Z from the thin plane source is

$$R(Z) = \int_Z^\infty SR(r)\, dA$$

$$= \int_Z^\infty 2\pi r R(r)\, dr$$

$$= 2\pi kS\left\{[c(1 - \ell n\ Z/c - e^{1 - (Z/c)})] + e^{1} - Z\right\} \qquad (9.7)$$

For $Z \geq c$, the quantity inside the square bracket is set equal to zero. Here S is the surface activity of the plane source.

To obtain the dose rate for a slab source with finite thickness, the last equation can be integrated over the thickness. Assume y is the distance from a differential source dy to the dose point (at y = 0). Let x equal the distance between the surface of the source to the dose point. Then the dose at dose point from a semi-infinitely thick slab source is:

$$D(x,\infty) = \int_x^\infty R(y)\, dy$$

$$= 2\pi kT\left\{[c^2(3 - e^{1 - (x/c)}) - cx(2 - \ell n\ x/c)] + e^{1 - x}\right\} \qquad (9.8)$$

Again, the quantity inside the square bracket is set equal to zero for $x \geq c$. T is the volume activity of the slab source.

For a slab source of finite thickness h, the dose can be obtained by simple subtraction:

$$D(x,h) = D(x,\infty) - D(x + h,\infty) \qquad (9.9)$$

where

$D(x,h)$ = dose rate at a perpendicular distance x from a slab source of thickness h

$D(x,\infty)$ = dose rate at same point with source of semi-infinite thickness

$D(x + h,\infty)$ = dose rate of same dose point at a distance x + h from a plane source of semi-infinite thickness

The total energy per unit area dissipated up to a distance x from the surface of the semi-infinite thick slab source is the integration of Eq. 9.8 over x. Thus,

$$E(x,\infty) = \int_0^x D(x,\infty)\, dx$$

$$= 2\pi kT\{[3c^2x + c^3e(e^{-x/c} - 1) - (cx^2/2)(2.5 - \ln x/c)]$$

$$+ e(1 - e^{-x})\} \qquad (9.10)$$

Again, the square bracket is set equal to zero when $x \geq c$.

The total energy per unit area dissipated in the absorber up to a distance x from the surface of a slab source with finite thickness h can be obtained by subtraction:

$$D(x,h) = E(x,\infty) - [E(x + h,\infty) - E(h,\infty)] \qquad (9.11)$$

The fraction beta energy absorbed at a distance x from the surface of a slab source with thickness h is:

$$F(x) = [E(x,h)]/[E(\infty,h)] \qquad (9.12)$$

For promethium source and aluminum absorber, the values for various parameters are as follows:

E_m = 0.225 MeV

$\bar{E} = \bar{E}^*$ = 0.062 MeV

c = 3.5

ν = 163 cm^2/g

K = 0.766

h = 5.55 mg/cm^2

T = 927 Ci/g

The results of substitution of these values into Eq. 9.12 are plotted in Fig. 9.16. Note that although all the equations are developed for an infinitely large slab source, they can be applied to a finite source with dimensions greater than several times the range of electrons with maximum energy.

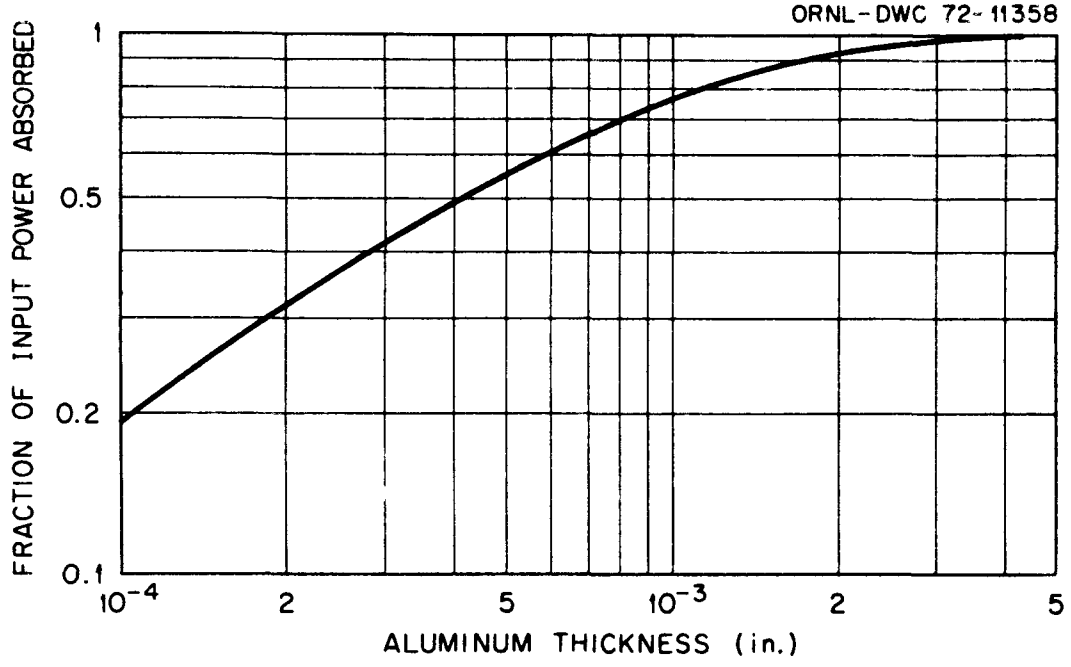

Fig. 9.16. Fraction of Promethium-147 Beta Power Absorbed in Aluminum.

The experimental power output of Schottky cells for light source, sealed promethium source, and bare promethium sources and their ratios are tabulated in Table 9.6. The data are in agreement with Fig. 9.16 except for cell 4A. This is probably due to the very low resistivity (8 Ω-cm) of the cell. From Fig. 9.16, the fraction of beta energy absorbed in 0.0015-in. aluminum foil is 0.87. Therefore, the power output would be reduced by a factor of $1/(1 - 0.87) \approx 8$ compared to that of a bare promethium foil.

To estimate the betavoltaic power output from optical response, the ratios of Table 9.6 can be used. The power ratio between optical response

Table 9.6 Power Ratio Between Light, Sealed, and Bare Promethium Sources

Cell No.	Cell Active Area (cm^2)	Power Output (μW)			
		Light (1 mW/cm^2)	Sealed Source (5.55 mg/cm^2)		
			1 mil Al	1.4 mils Al	Bare
4A	1.00	11	0.55	—	2.8
2C	1.25	30	4	—	18.7[a]
3A	1.25	26	2.9	2	12[a]
1B	1.25	24	2.7	—	12[a]

	Power Ratio			
	Light/1 mil Al	Light/Bare	Bare/1 mil Al	Bare/1.4 mils Al
4A	20	4	5.1	—
2C	7.5	1.6	4.6	—
3A	9	2.2	4.2	6
1B	8.9	2	4.4	—

[a]The active area of the bare promethium source is 1 cm^2. The power indicated here has been multiplied by 1.25 to increase the area to 1.25 cm^2.

and betavoltaic response with bare source is about 2. Therefore, the power ratio between optical response and promethium source with 1.5-mil aluminum foil would be approximately $2 \times 8 \approx 16$.

9.10 Radiation Shielding Experiment

To reduce the radiation dose rate of the battery to an acceptable level, a radiation shielding study is necessary to determine the thickness of the primary shielding. This section presents a theoretical and experimental evaluation of radiation dose rates through tantalum and stainless steel.

The radiation dose rate from a shielded pure beta emitter such as promethium is primarily a result of bremsstrahlung radiation. When electrons are being slowed down in an absorbing medium, a fraction of

the electron energy is transformed into x-rays, which is called the bremsstrahlung radiation. The maximum photon energy of the x-rays is equal to the maximum electron energy, but the intensity falls rapidly as the photon energy increases. Before the radiation dose rate can be calculated, a bremsstrahlung spectrum should be obtained.

For continuous spectrum beta radiation, the fermi beta-energy distribution function N(W) should be used.[38]

$$N(W) = CF(Z,W)(W^2 - 1)^{1/2}(W_{max} - W)^2 W \qquad (9.13)$$

where

$N(W)$ = the probability that the radiation source will emit an electron with a total energy of W

$W = \varepsilon/m_o c^2 = 1 + (T/m_o c^2)$

ε = total energy of the electron

m_o = electron rest mass

C = constant

c = speed of light

T = kinetic energy of electron

W_{max} = W corresponding to maximum energy ε_{max}

$F(Z,W)$ = coulomb correction term

Z = atomic number of the medium in which the electron is slowing down

The bremsstrahlung intensity dI (number of photons x photon energy) in the energy band dE at photon energy E is given by the sum over all electrons whose kinetic energy exceeds T, thus

$$\frac{dI}{dE} = 2kZ \frac{\int_{W_1}^{W_{max}} (T - E)N(W)\, dW}{\int_{1}^{W_{max}} N(W)\, dW} \text{ per beta disintegration} \qquad (9.14)$$

where

E = energy of the bremsstrahlung photon

$W_1 = (E/m_o c^2) + 1$

k = constant

The bremsstrahlung radiation spectrum per radiation source can then be evaluated from Eq. 9.14 by multiplying this equation by the total number of beta disintegrations per source.

With the bremsstrahlung spectrum known, one can then calculate the radiation dose rate after attenuation by shielding materials.

The absorption of gamma rays (or x rays) with energy E and flux $I_o(h,E)$ at any point h can be expressed as[37]

$$R(h) = K \int \mu_a(E) I_o(h,E)\, dE \tag{9.15}$$

where

R(h) = absorbed dose rate at h

$\mu_a(E)$ = absorption coefficient for photons at energy E

$I_o(h,E)$ = gamma-energy flux at h

K = constant

For a point source, the gamma-energy flux $I_o(h,E)$ can be calculated from the following equation

$$I_o(h,E) = [I(E)/4\pi h^2]\, e^{-\mu(E)t} \tag{9.16}$$

where

I(E) = gamma-energy intensity of the point source

h = distance between the source and the dose point

$\mu(E)$ = linear attenuation coefficient of the shielding material

t = thickness of the shielding material

For a plane disk source, the gamma flux on the disk axis can be obtained by integrating over the entire area,

$$I_o(h,E) = \frac{I_s(E)}{4\pi} \int_0^R \frac{e^{-\mu(E)t\sec\theta}}{r^2 + h^2} 2\pi r \, dr \qquad (9.17)$$

where

$I_s(E)$ = surface gamma-energy intensity

h = distance between plane source and the dose point on the disk axis

R = radius of the plane source

If Eq. 9.17 is substituted into Eq. 9.15, the dose rate at point h, from a plane source with gamma spectrum $I_s(E)$, attenuated by a shielding material with thickness t and attenuation coefficient $\mu(E)$, can be calculated. For shielding configuration with multiple layers, the above equations are applicable except for the use of $\sum_i \mu_i(E)t_i$ instead of $\mu(E)t$, where i indicates different shielding materials.

Because of the uncertainty due to the complexity involved in the calculation of the bremsstrahlung spectrum and the attenuation of x-rays in various capsules, the radiation dose rate was experimentally determined.

To estimate the shielding required to reduce the radiation dose rate to an acceptable level, a shielding experiment was performed to determine the radiation dose rate through two absorbers, stainless steel 304L and tantalum. The selection of these materials was based on many factors. Both stainless steel 304L and tantalum are compatible with promethium metal. It has been shown[39] that there is less than 0.001 in. of penetration for both metals at 400°C for 1000 hr. Tantalum has a high absorption coefficient against gamma and bremsstrahlung radiation.[40] Tantalum has a

very low thermal expansion coefficient[41] which will have a better chance to match that of the Al_2O_3 (ref. 42) used in bonding. Stainless steel 304L is needed to shield against the x-rays generated by the interaction of tantalum and the gamma radiation. Stainless steel 304L is also a good barrier against corrosion in water.[41]

Three 1-in.-diam disks with various thicknesses of each material were obtained. The promethium sealed source was loaded into a lead pig to reduce the scattered radiation. One absorber and a plastic spacer were placed on top of the sealed source. The plastic spacer was used to keep a constant distance between the promethium source and the dose point. A plastic bottle containing TLD (thermoluminescence dosimeter) powder was placed on top of the spacer. Figure 9.17 shows the arrangement of the radiation shielding experiment.

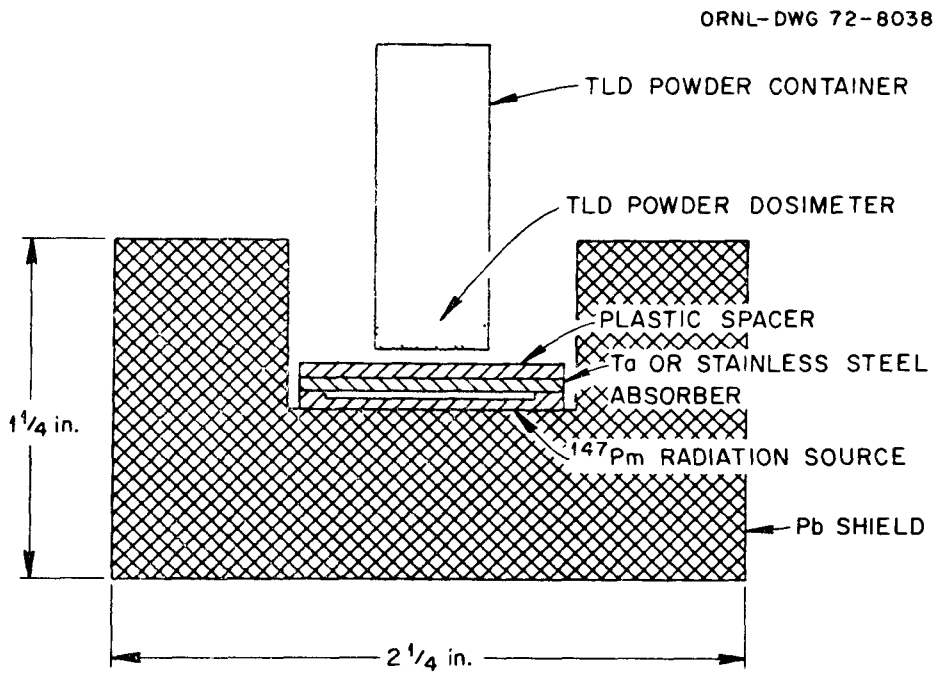

Fig. 9.17. Arrangement of Radiation Shielding Experiment.

Lithium fluoride powder was used as a phosphor. When radiation is incident on phosphor, the electrons of the phosphor will be excited to higher energy states and will remain excited. Upon heating, the electrons are de-excited.[43] Photons are emitted as the electrons drop to the lower energy level. The number of photons emitted are proportional to the radiation dose received by the phosphor. A photomultiplier picks up the light and converts it into electrons. This electrical signal can then be amplified and counted.

A National Bureau of Standard's calibrated standard ^{60}Co source was used to irradiate TLD powder to several dose levels. A calibration curve, dose versus counts, was obtained. Unknown doses were interpolated from the calibration curve.

The results of the measurement are summarized in Fig. 9.18, and it can be seen that tantalum was very effective in reducing the radiation dose rate. Half value layers (HVL) for both stainless steel 304L and tantalum are indicated in the figure. The HVL is the thickness of the absorber required to reduce the radiation dose rate by a factor of 2.

9.11 Gamma Spectra

In order to determine the content of radioactive impurities, gamma spectrum analysis was used. The decay energies of gamma rays and their intensity are characteristics of a particular radioisotope. By measuring the gamma-ray spectrum,one can identify and calculate the amount of impurities present in the sample.

The gamma-spectrum obtained from the diluted promethium sample (also used for the alpha particle determination work) is shown in Fig. 9.19. A 50-cm^3 Ge(Li) detector was coupled to a 4096 channel 2200 Nuclear Data System.

The major gamma peaks observed were 0.121 MeV from ^{147}Pm and 0.453, 0.633, 0.736, and 0.747 MeV from ^{146}Pm. The ^{146}Pm activity level was determined to be 2.2×10^{3} dpm per milliliter of solution based on relative branching obtained from coincidence spectrometer measurements.[44] The ^{146}Pm content, after correction for decay, was 1.2×10^{-6} Ci per curie of ^{147}Pm. No other impurities were observed in the spectrum.

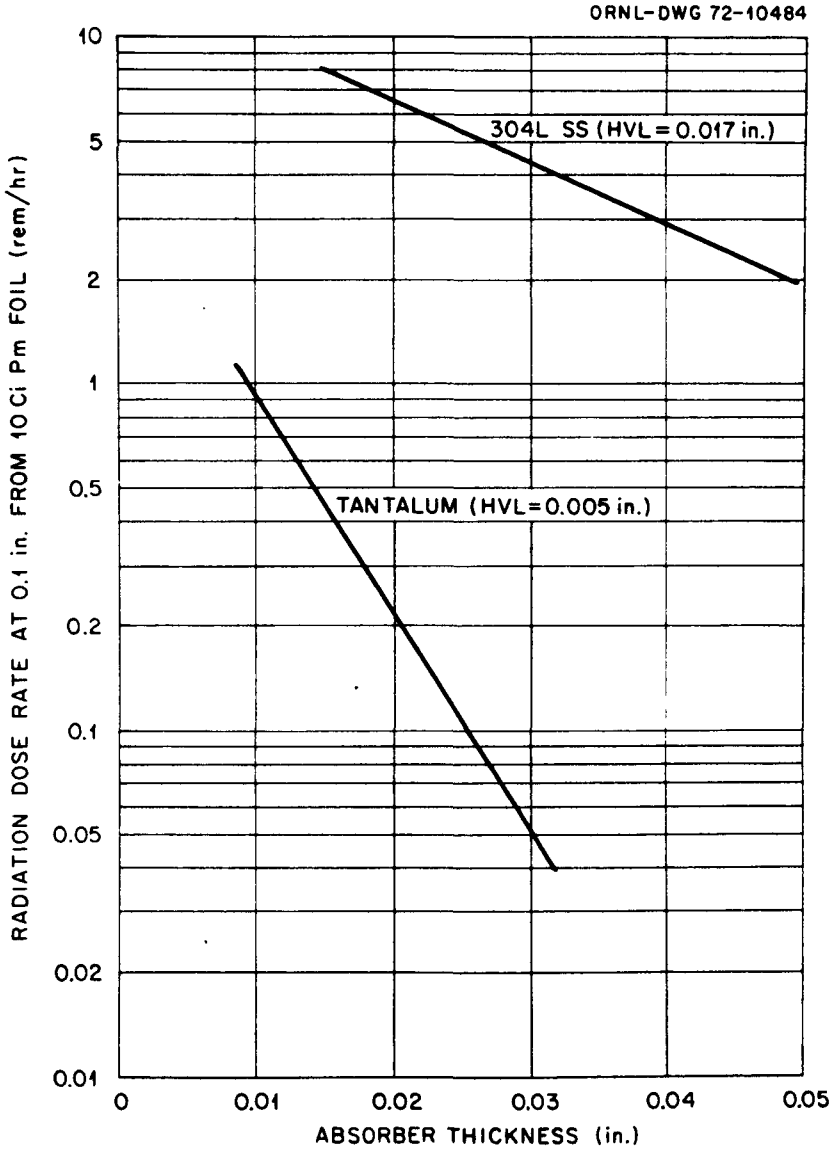

Fig. 9.18. Radiation Dose Rate Versus Absorber Thickness.

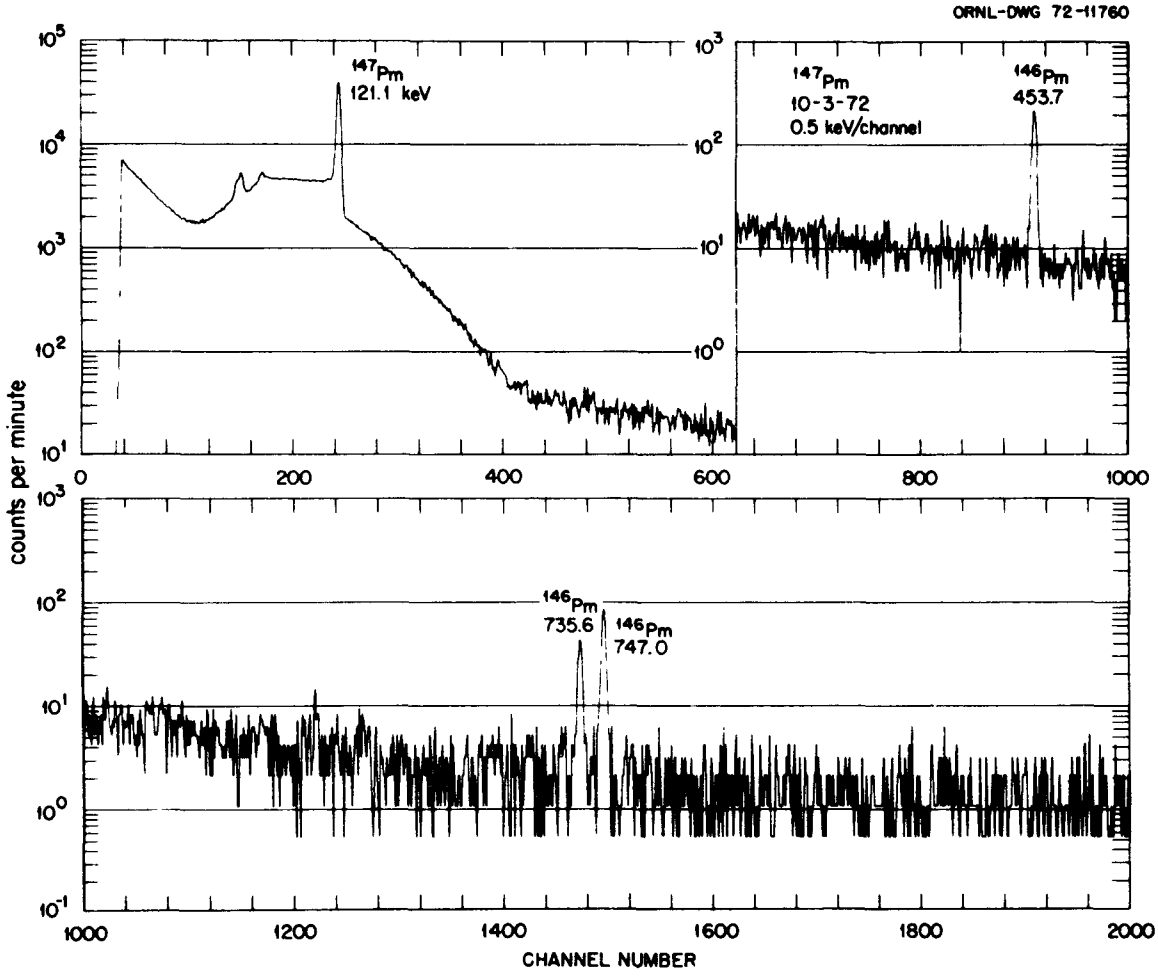

Fig. 9.19. Gamma-Ray Spectra.

10. BATTERY DESIGN AND CONSTRUCTION

10.1 Basic Capsule Design

The capsule design is based on three major factors: (1) to provide an electrical path from which the power is delivered to the load, (2) to reduce the radiation dose rate to an acceptable level, and (3) to provide structural integrity which will contain the radioactivity inside the capsule in the event of a maximum credible accident. This section will give an overall design of the capsule and the following sections will discuss specific designs for major components of the capsule.

Figure 10.1 shows a schematic of the battery assembly. The electrical path consists of the connections between the cells, the lavite insulation can, and the feedthrough. The negative terminal is grounded to the capsule

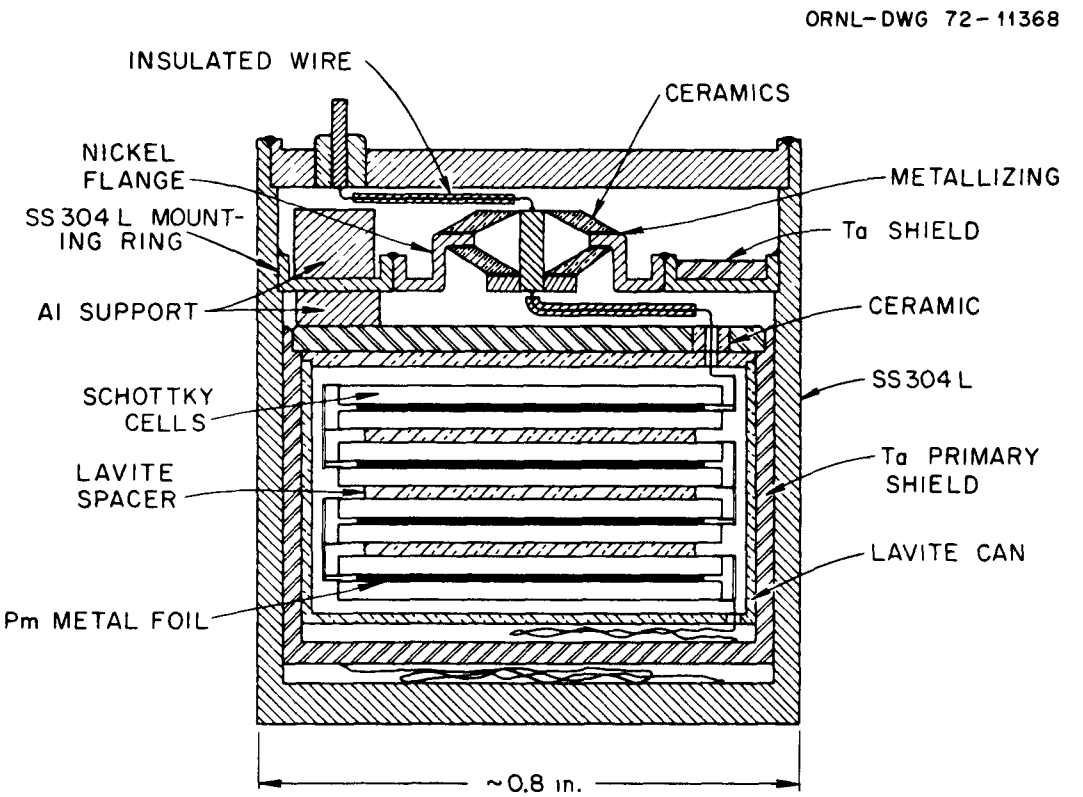

Fig. 10.1. Schematic of the Battery.

and the positive terminal is insulated from the capsule. The primary radiation shielding is provided by the tantalum container. The dose rate is further reduced by the outer stainless steel capsule. The structural integrity is provided by the outer stainless steel capsule. It is designed to be able to survive accidental conditions specified by the Department of Transportation (DOT) and Atomic Energy Commission (AEC) transportation regulations. The feedthrough provides an absolute containment of radioactivity during a fire. This feedthrough will remain vacuum tight after a 1475°F fire as required by DOT and AEC regulations.

A small tantalum shield is mounted on top of the feedthrough mounting ring to stop radiation streaming through the opening of the tantalum cover. Two aluminum support rings are required to protect the feedthrough mounting ring from rupture if the external positive terminal drops during a puncture accident.

Figure 10.2 shows detailed drawings for the tantalum and stainless steel capsules and the feedthrough mounting ring. Figure 10.3 is a photograph showing the actual components used in the battery assembly.

10.2 Cell-Source Assembly

The cell-source assembly was arranged in such a way that optimization of performance (power density) was obtained. Two cells were connected in parallel with the radiation source between the cells. This arrangement eliminated insulation material required if they were connected in series.

To be of any practical usefulness, a minimum voltage of greater than 0.6 V was required. This is the minimum voltage to operate a transistor. Although a solid-state dc-to-dc converter can be used to increase the voltage, the conversion efficiency decreases rapidly with decreasing

input voltage. Therefore, all pairs of Schottky cells were connected in series to supply a higher output voltage. Figure 10.4 shows the cell-source assembly and the interconnections between the cells.

Lavite disks, 0.020 in. thick, were used as insulation spacers between each pair of cells. Two holes were cut at the opposite sides of each spacer to accomodate the contact point of the gold wire to the nickel-plated silicon wafer. Figure 10.5(a) gives the dimension of the spacer.

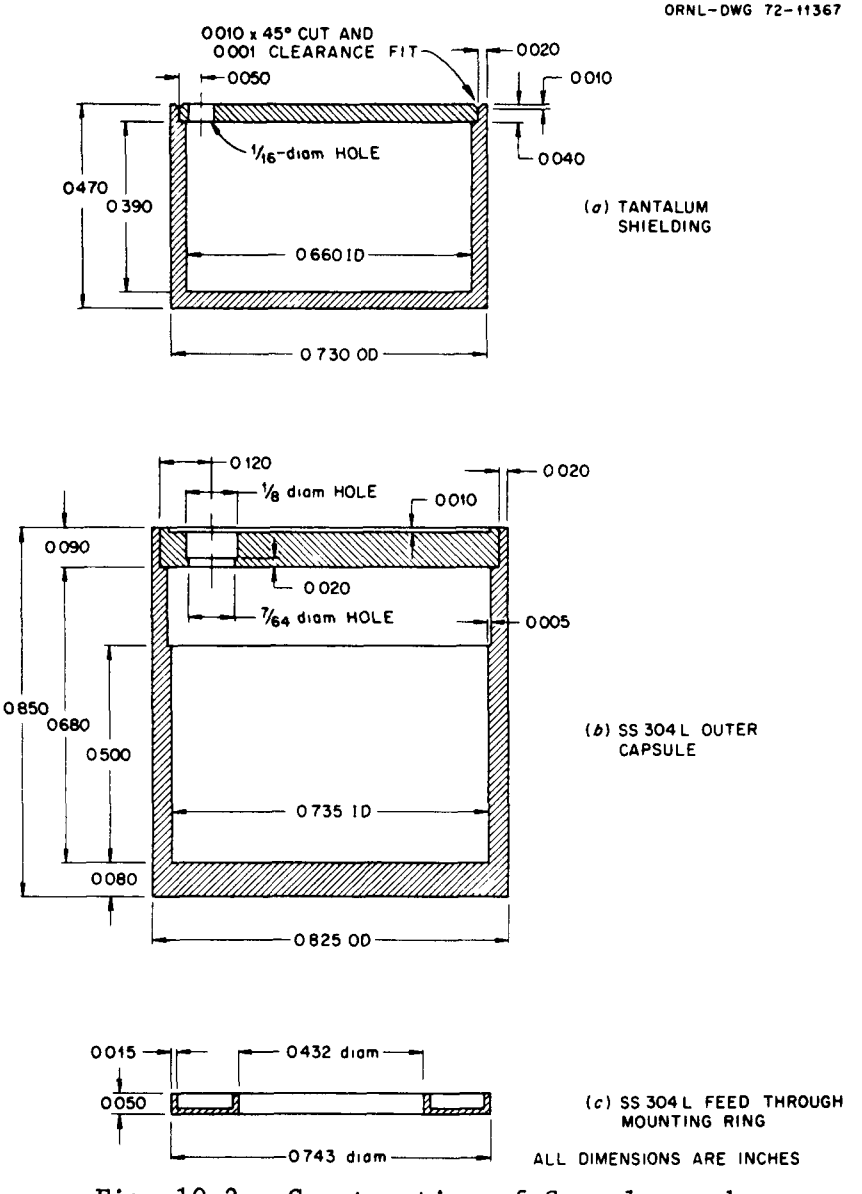

Fig. 10.2. Construction of Capsules and Feedthrough Mounting Ring.

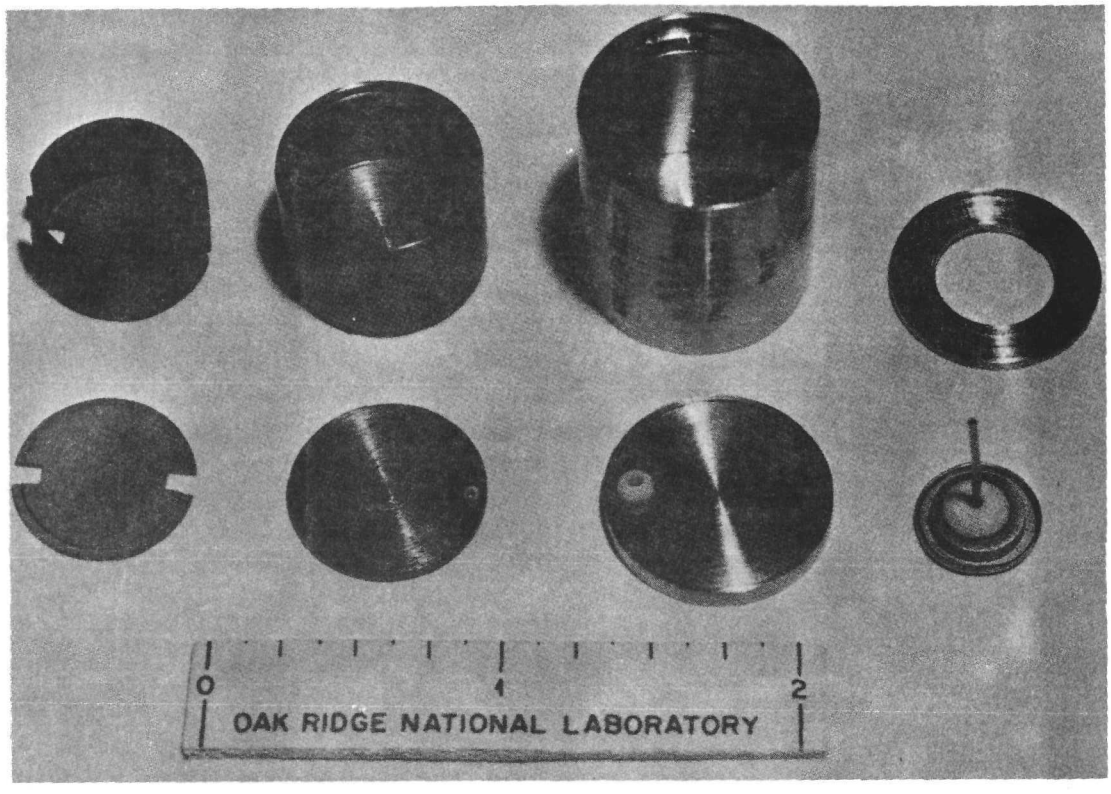

Fig. 10.3. Battery Capsules.

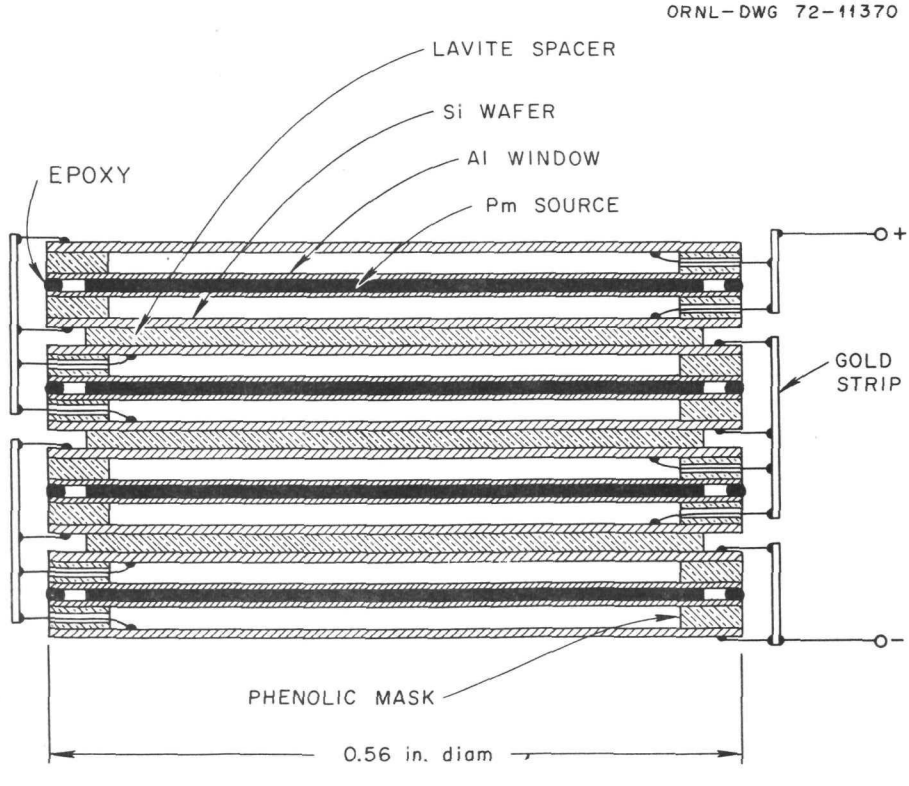

Fig. 10.4. Configuration of the Cell-Source Assembly.

Perforated gold ribbons were used to connect the leads of the cells. The leads were pushed through the perforations, bent, and then silver painted onto the gold ribbon as shown in Fig. 10.4. This method minimizes the force applied to the lead and reduces the possibility of the leads being detached from the Schottky cells.

A lavite can with two slots cut at the opposite sides of the can was used to contain the cell-source array. A hole was provided at the bottom of the can for the negative terminal to exit. Figures 10.5(b) and (c) show the lavite can and its cover. This lavite can was required to insulate the cells from the tantalum container. The lavite cover was epoxyed to the can.

The assembly of the cell-source array and the interconnections between the cells was carried out in a battery assembly jig shown in Fig. 10.6. Simulated radiation sources (made of teflon disks), insulation spacers, and

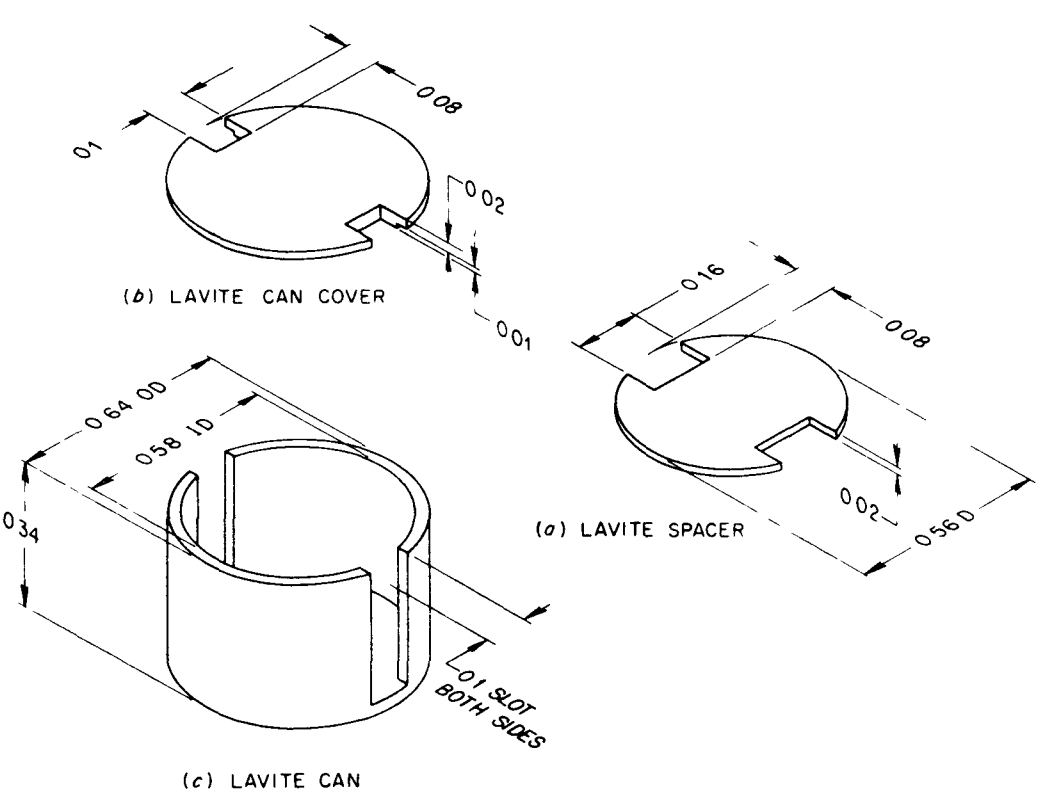

Fig. 10.5. Construction of Lavite Container and Spacer.

Schottky cells were loaded on the jig. The gold wires were then properly connected as described above. The whole assembly, after all interconnections were completed, was carefully moved to the inside of the glove box which contained the promethium metal foils. The simulated source was pulled out and the real source inserted into the same slot vacated by the simulated source. All replacement of sources was accomplished in a few minutes. This procedure of loading radioactive sources greatly reduced the radiation dose rate to the hands. The preassembly of the gold wire interconnections simplified the glove box operation.

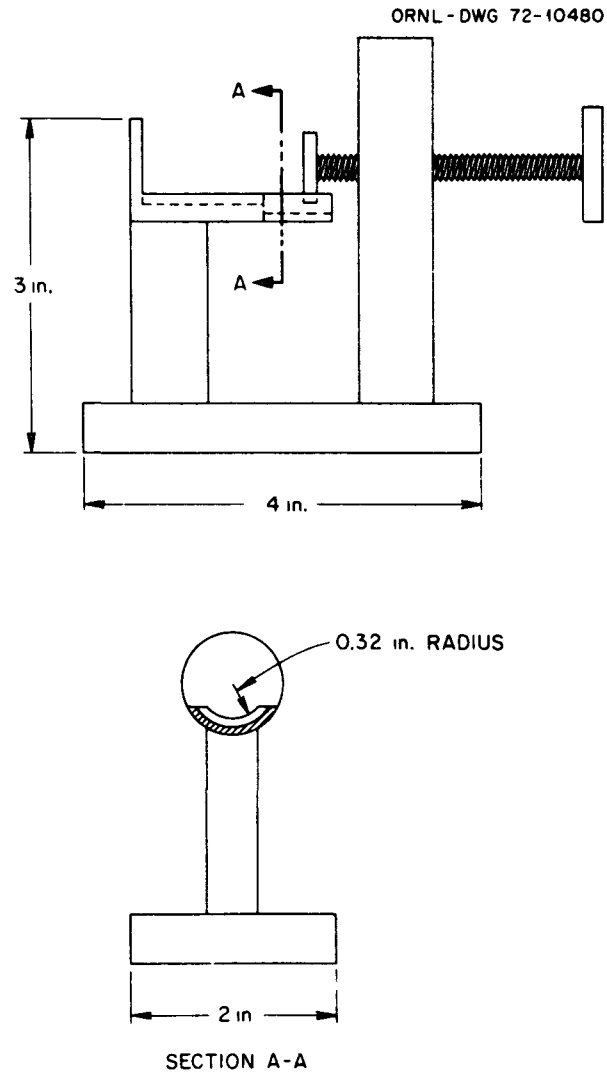

Fig. 10.6. Assembly Jig for Battery Cells.

10.3 Determination of Primary Shielding Thickness

Since this prototype battery was a laboratory device, considerations of the primary shielding thickness was based on the dose rate tolerances allowed in handling and experimentation with such a battery. The AEC regulations[45] specify the permissible total body exposure of individuals to radiation in unrestricted areas be less than 2 mrem/hr or less than 100 mrem/week. Since the occupancy time would be less than 40 hr/week, and the operation distances at least 2 cm, 10 mrem/hr at the surface of the battery was the governing criterion for shielding design. Since the dose rate is related to the distance between source and the dose point by an inverse square law, a large safety factor is involved when one considers the increase in distance from the surface of the battery to the sensitive organs of the body of an individual who is handling the battery.

The radiation dose rate from the bottom of the battery can be evaluated from the radiation shielding experiment described in Section 9.10. Figure 9.18 shows a dose rate of 12.5 mrem/hr per 10-Ci promethium source through a tantalum absorber thickness of 0.04 in. with a separation distance of 0.1 in. between the source and the dose point. The battery contains about 30 Ci of promethium, and the dose rate increases to about 40 mrem/hr. Additional shielding is provided by a 0.08-in.-thick stainless steel outer capsule. The reduction factor for stainless steel is 5 after being corrected for the differences in atomic number Z in bremsstrahlung production as indicated by Eq. 9.14. The predicted dose rate at the surface of the capsule is therefore 8 mrem/hr. This value is lower than the dose rate criteria. Therefore, a tantalum thickness of 0.04 in. was selected for shielding at the bottom of the battery. The selection of

the thickness of stainless steel based on structural integrity will be discussed in the next section. Similarly, a tantalum thickness of 0.04 in. was also selected for shielding on the top of the battery.

The cylindrical wall thickness of the tantalum shield was determined as follows: Because of geometry, the radiation travels a longer distance in the shield because of the slanting angle between the sources and the dose point, and the dose rate at the side is reduced by at least a factor of 2 compared to the dose rate at the top or bottom of the battery. Hence, tantalum thickness of 0.035 in. was selected for the side wall.

A detailed drawing of the tantalum capsule and its cover is shown in Fig. 10.2(a). Actual dose rate measurements for the assembled battery and the results are presented in Section 12.3.

10.4 Determination of Outer Capsule Thickness

Beyond 20 Ci of ^{147}Pm, DOT requires Type B packaging which is designed to contain the radioactivity when the package is subjected to a series of hypothetical accidents.[46] The detailed regulation requirements are discussed in Section 12.1. If the outer capsule of the battery can pass the hypothetical accident tests as specified by DOT, the battery should be able to contain the radioactivity under maximum credible accidents in the laboratory without causing any contamination problem to the environment. Therefore, the thickness of the stainless steel 304L outer capsule was based on the criteria established by DOT shipping regulations.

Savannah River Laboratory of Aiken, South Carolina, has conducted a series of stainless steel 304L capsule safety tests for their ^{252}Cf program.[47] One of the capsules has about the same dimensions as the battery outer capsule and has successfully passed all the tests required

by the regulations. A comparative study was done, as presentd in Section 12.2, to determine the capsule thickness based on the dimensions of the ^{252}Cf capsule. The results show that a battery outer capsule of 0.040-in. wall thickness and 0.080-in.-thick end plates would be at least as strong as the ^{252}Cf capsule. Figure 10.2(b) shows the construction and dimensions of the outer capsule. The step inside the capsule is for mounting the feedthrough. Welding penetration for the cover is set at 0.030 in. minimum, which is the same as required by ^{252}Cf capsules.

10.5 Electrical Feedthrough

In certain types of nuclear batteries, such as thermoelectric systems, the electrical feedthrough does not present a safety problem because the radiation source can be completely sealed in a welded fuel capsule which will absolutely contain the radioactivity under maximum credible accident conditions. For these batteries, the electrical feedthrough is involved only in the operational functions and is not related to the nuclear safety problem. However, for direct conversion systems, such as betavoltaic batteries, the electrical feedthrough has to penetrate to the fuel capsule which contains the radiation source. If the ceramic metal bonding of the feedthrough cracks under the fire test, the radioactive materials inside the capsule will find a leakage path to escape through the crack and contaminate the environment. Therefore, in order to construct a betavoltaic battery, it was necessary to find a miniaturized feedthrough which would remain vacuum tight at high temperature.

A commercial company, Ceramaseal, Inc. of New York, specializing in electrical feedthroughs, provided a feedthrough which was guaranteed to be vacuum tight at 1×10^{-9} cm^3/sec STP and able to withstand a temperature

of 1475°F.[48] The smallest feedthrough was 0.43 in. in diameter and 0.125 in. thick. Figure 10.7 shows the construction of the feedthrough. The advantage of this feedthrough is that a spring action is built in, and any difference in thermal expansion coefficient between ceramic and metal will be absorbed by the spring mechanism. Although this is a good system, it is relatively large in size compared to the size of the battery. A search for a more compact ceramic metal bond was initiated.

After consulting the Metals and Ceramics Division of ORNL, a furnace braze technique was tried. The main problem was the differences in the thermal expansion coefficients between metal and ceramic. Tantalum was selected for the metal because it has a much lower thermal expansion coefficient than most other metals,[41] and it is also a good radiation shielding material. Aluminum oxide (Al_2O_3) was selected as the ceramic because it has good mechanical, thermal, and electrical properties.[42,49] The alloy

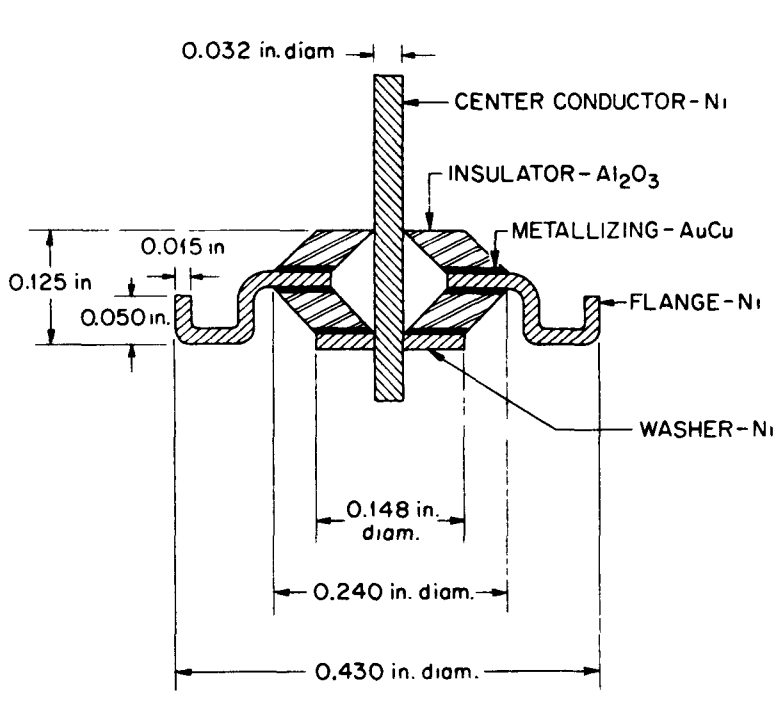

Fig. 10.7. Electrical Feedthrough.

TiCuBe (49 wt % Ti, 49 wt % Cu, 2 wt % Be) was used as the braze because of its good wetting properties. A tantalum disk 0.0625 in. thick with a hole in the center was machined to fit a ceramic ring (∿1/4-in. OD) to a clearance of about 0.002 to 0.003 in. A tantalum wire was placed at the center of the ceramic ring. Brazing alloy was added to the bonding area, and the assembly was then loaded into a vacuum furnace. After being heated to about 1850°F in high vacuum for several minutes, the assembly was allowed to cool down slowly in the furnace. A leak test of the ceramic metal bonding showed a leak of about 25 microns. A second test piece with an improved design was tried and it also showed a leak. It might be due to the microcracks formed during the heating-cooling temperature cycle. Prof. R. G. Wolfson of Dartmouth College has been consulted and no practical solution to direct bonding has been found at this time. Therefore, it was decided to use the feedthrough (shown in Fig. 10.7) supplied by Cermaseal, Inc., for battery assembly.

A stainless steel 304L mounting ring was required to mount the feedthrough. The construction and the dimensions of the mounting ring are shown in Fig. 10.2(c). The feedthrough was first welded to the inner flange of the mounting ring. After a leak test, the feedthrough-mounting ring assembly was set on the step of the outer capsule and welded. This barrier prevents radioactive material from escaping from the capsule in case of fire.

The positive terminal lead passes through two other metal covers: tantalum and stainless steel. Ceramic beads were used to fit inside the holes provided on the covers. The lead was passed through the center of the beads, and both beads and leads were epoxyed to the covers.

10.6 Welding

Welding is an important factor in both structural integrity and the containment of the radioactivity. The battery has three welded parts. The welding between the stainless steel cover and the outer capsule acts as a barrier against impact, puncture, and other mechanical forces. The weldings between feedthrough, mounting ring, and the outer capsule act as barriers against contamination. A TIG welding technique was used for all battery enclosures.

Two samples of stainless steel capsules and their covers were welded. The first welding used a current of about 30 amperes. After being leak tested at 10^{-10} cm^3/sec STP, the weld was sectioned. The penetrations were between 0.025 to 0.030 in. The current was increased slightly for the second welding, which showed a penetration of greater than 0.030 in.

10.7 Assembly of Battery

The assembly of the battery can be divided into three stages. The first stage is the assembly of cell-simulated source array and the interconnections of the leads of all cells. The next stage is done in the glove box. It is involved with replacement of the simulated source by promethium metal foil, epoxying the upper lavite can to the lower half, and loading it into the tantalum container. After the cover is epoxyed and the unit is decontaminated and life tested, the unit can then be taken out of the glove box and loaded into the stainless steel outer capsule and finally the cover can be welded under a hood.

The first stage was carried out with the help of the battery assembly jig, as shown in Fig. 10.6. Since there was no radiation source involved, this stage was done on the bench. Therefore, the interconnection between

the cells was handled and connected very carefully using magnifying glasses and the proper lighting conditions.

The lavite can and its cover were split into two halves. Each half of the cover was epoxyed to one half of the can. One epoxyed half was loaded on the jig. Simulated sources (teflon disks), spacers, and Schottky cells were placed inside the halved containers. The gold leads were then properly connected as described in Section 10.2.

The finished assembly from the first step, including the cell-simulated sources and the jig, was moved into the glove box which contained the promethium metal foil. The simulated source was pulled from the array and the real source was inserted into the vacated space. This was done one source at a time. When all sources were replaced, the other half of the lavite can was epoxyed to the bottom half. The tantalum container was placed on the lower step of the jig such that the lavite container could be slipped into the tantalum container. The inside wall of the tantalum container (except bottom) was lined with nylon tape to avoid the possibility of a short circuit. The tantalum cover was then epoxyed to the container. The negative terminal was grounded to the tantalum can. The positive terminal was exited through the ceramic bead and epoxyed to the tantalum cover. The power output of the battery assembly was monitored throughout the second stage operation so that the operation could be stopped if any abnormal behavior in power output occurred.

After completion of the second stage, the radioactive material was contained inside the capsule. The unit was decontaminated and set for life test. If the power output dropped, the container could be easily opened. The cell-source assembly could be inspected and repaired, if necessary.

The third stage was done in the hood. The tantalum capsule was removed from the glove box and loaded into the stainless steel capsule. After the positive terminal lead was connected to the feedthrough, the feedthrough and the mounting ring were welded to the capsule. Subsequently, the stainless steel cover was welded to the capsule. The positive terminal was epoxyed to the hole provided on the stainless steel cover.

11. BATTERY AND BATTERY CELL PERFORMANCES

11.1 Photovoltaic Response for Individual Battery Cells

Of the 14 cells supplied by UDT, the front leads of cells 13 and 14 were detached from the gold surface. These were sent back to UDT for repair. As will be discussed later in this section, due to the non-uniformity of the Schottky cell power output, UDT agreed to send six more cells free of charge along with the repaired cells. The second shipment was received two weeks after the initial shipment. Therefore, a total of 20 cells were tested for photovoltaic response. Construction of the battery cells has been discussed in Section 6.4. Since the cells were not mounted on BNC connections, they have to be handled very carefully. The front lead can be detached from the gold surface very easily. Tweezers must be used in handling them to avoid the gold surface being scratched.

The apparatus and procedures of the photovoltaic experiment were discussed in Section 9.2. The light intensity was set at 1 mW/cm^2. The V-I characteristics were measured by the measurement system consisting of two electrometers and an x-y plotter. This system was described in Section 8.1. Figures 11.1, 11.2, and 11.3 show the V-I characteristics and the power output of the photovoltaic response. The power outputs were calculated from the V-I curves. Table 11.1 tabulates the maximum power output, open-circuit voltage, and short-circuit current of the cells.

As shown in Table 11.1, the short-circuit current and the open-circuit voltage of most cells vary only slightly. On the other hand, some cells have a much higher power output than others. This is probably due to

the "shape factor" as discussed in Section 4.4. The relationship between current and voltage can be expressed as

$$I = I_s \quad (e^{qV/AkT} - 1) - I_L \qquad (11.1)$$

This equation has been described in Section 6.1. For ideal Schottky barrier cells, A = 1. Otherwise A is between 1 and 2. The curve for $e^{qV/kT}$ is much more square than the curve for $e^{qV/2kT}$. Since the maximum power output is dependent on the largest rectangle that can be fit under the curve in the fourth quadrant, the ideal Schottky cell with A = 1 yields a higher power output compared to the nonideal ones even though

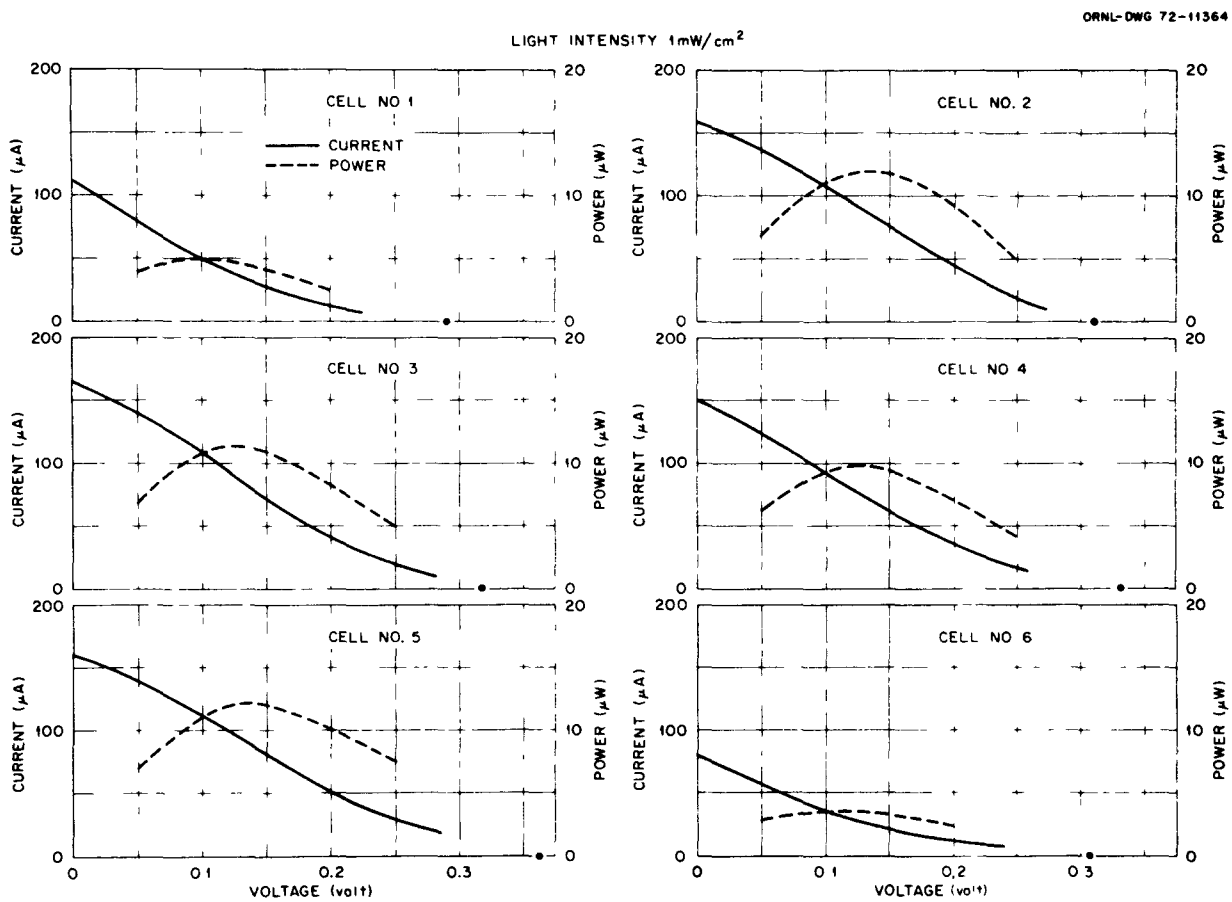

Fig. 11.1. V-I Characteristics of Battery Cells — Optical Response (Cells 1 to 6).

they all have the same short-circuit current and same open-circuit voltage. Examination of Figs. 11.1 to 11.3 confirms this prediction. Deviation from the ideal case may be due to surface states introduced during the production process.

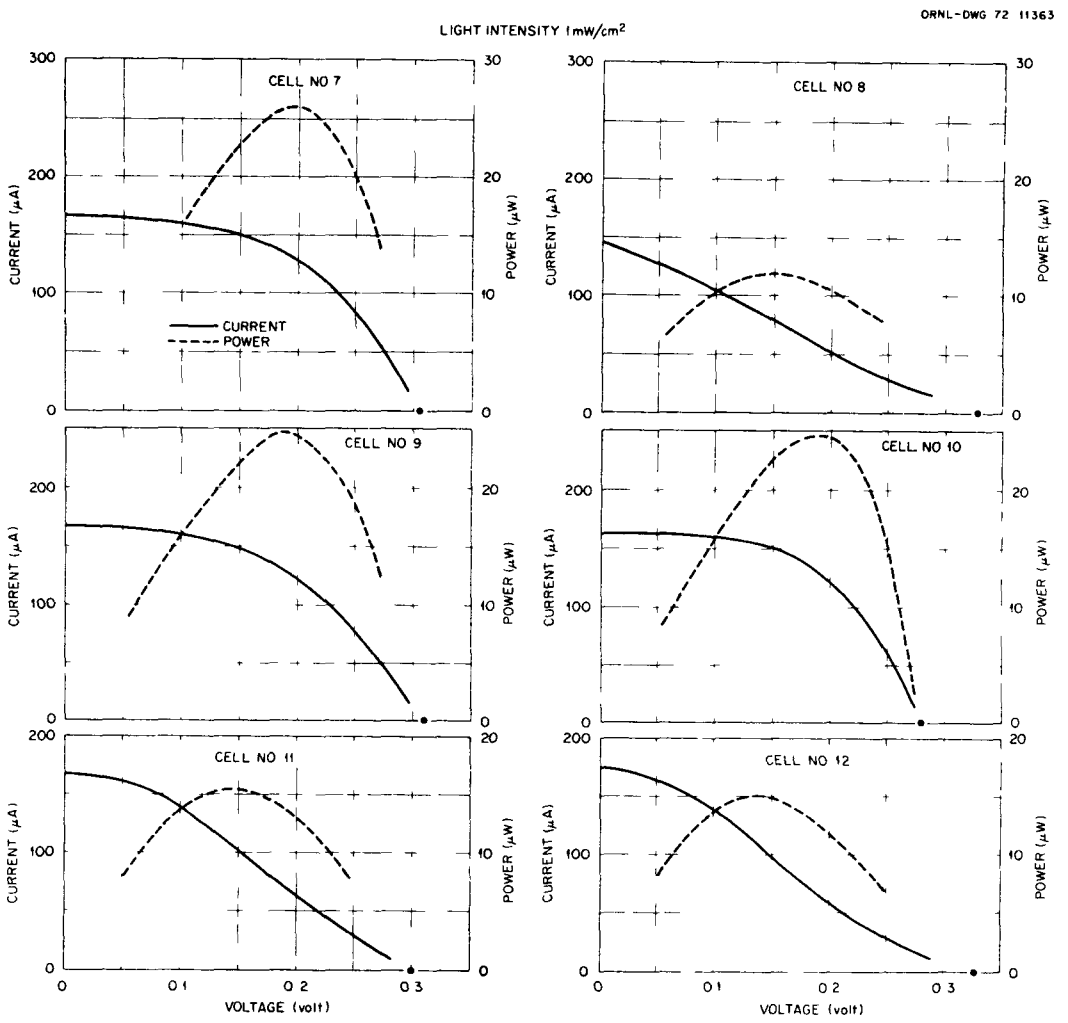

Fig. 11.2. V-I Characteristics of Battery Cells — Optical Response (Cells 7 to 12).

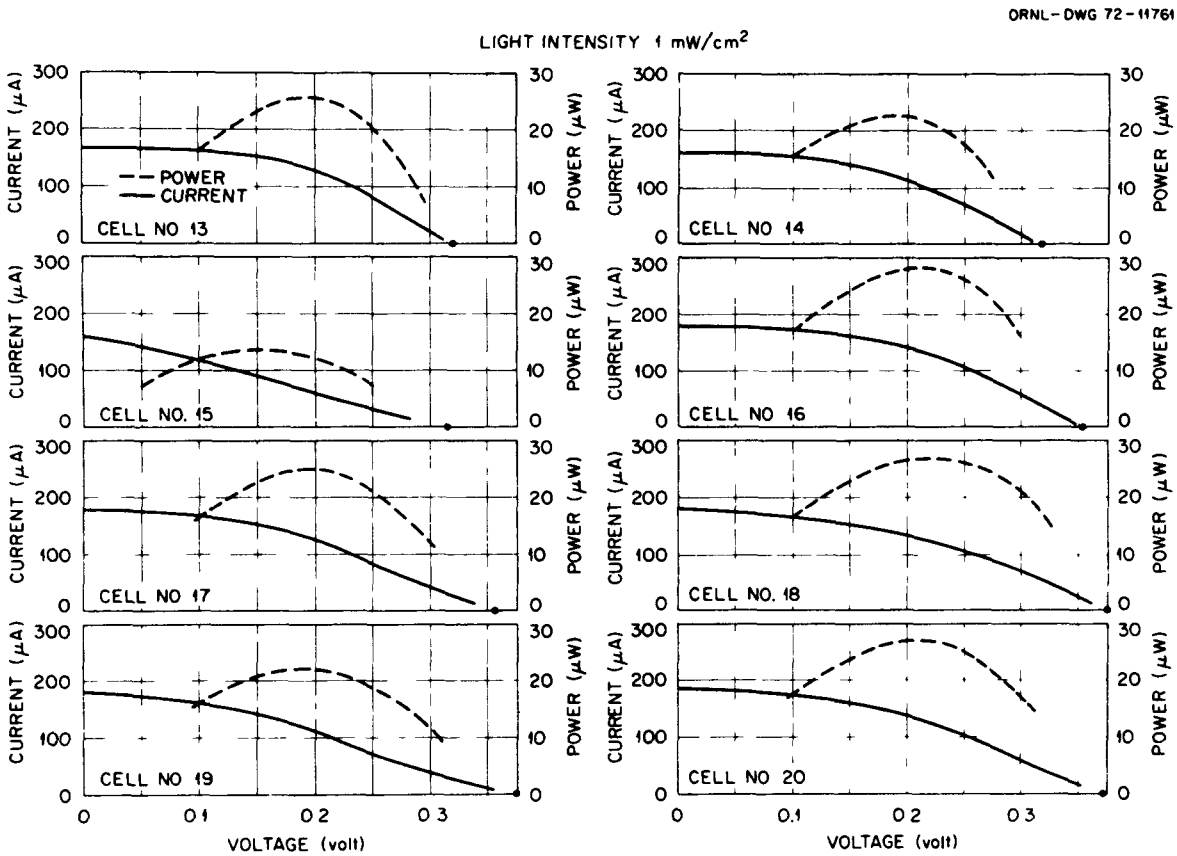

Fig. 11.3. V-I Characteristics of Battery Cells — Optical Response (Cells 13 to 20).

Table 11.1 Photovoltaic Response of Battery Cells

Light Intensity	1 mW/cm^2
Active Cell Area	1 cm^2

Cell No.	Maximum Power Output (μW)	V_{oc} (V)	I_{sc} (μA)
1	5	0.29	110
2	11.9	0.31	160
3	11.2	0.32	165
4	9.5	0.33	150
5	12.2	0.33	160
6	4	0.31	80
7	26	0.31	165
8	12	0.33	145
9	24.4	0.31	165
10	24.7	0.28	160
11	15	0.3	170
12	15	0.33	175

11.2 Photovoltaic Response for Combination of Cells

The optimization of the battery power density suggests that two cells be connected in parallel with radiation sources located between the cells. Four pairs can then be connected in parallel or in series. Cells 1 to 12 were used in this experiment.

The eight cells selected for parallel and series tests were 2 and 5, 8 and 9, 7 and 10, and 11 and 12. The V-I characteristics of each pair in parallel were measured. One pair, 7 and 10, was also measured in series. Figure 11.4 shows the V-I characteristics and power output of all pairs. From the results obtained from cells 7 and 10, one observes that the power output in series configuration is similar to that in parallel. However, the output voltage in series is twice as large. Subsequently, all four pairs were connected both in series and in parallel. Figure 11.5 shows the measured V-I characteristics, and it is evident from these curves that the total power output from the assembly is approximately equivalent to the sum of the power output of individual cells, whether they are connected in series or in parallel. The results of all cases are summarized in Table 11.2.

The Schottky cells selected for final battery assembly are tabulated in Table 11.3. The approximate power output for optical response was estimated by adding the power output of each individual cell. In the case of betavoltaic response, the power output can be estimated by using power ratios obtained in Table 9.6 of Section 9.9. Since the power ratio between the light source and the promethium source with 0.0015-in. aluminum window was about 16, the power output becomes 148/16 = 9.2 μW. However, if there is no alpha contamination, the power ratio between

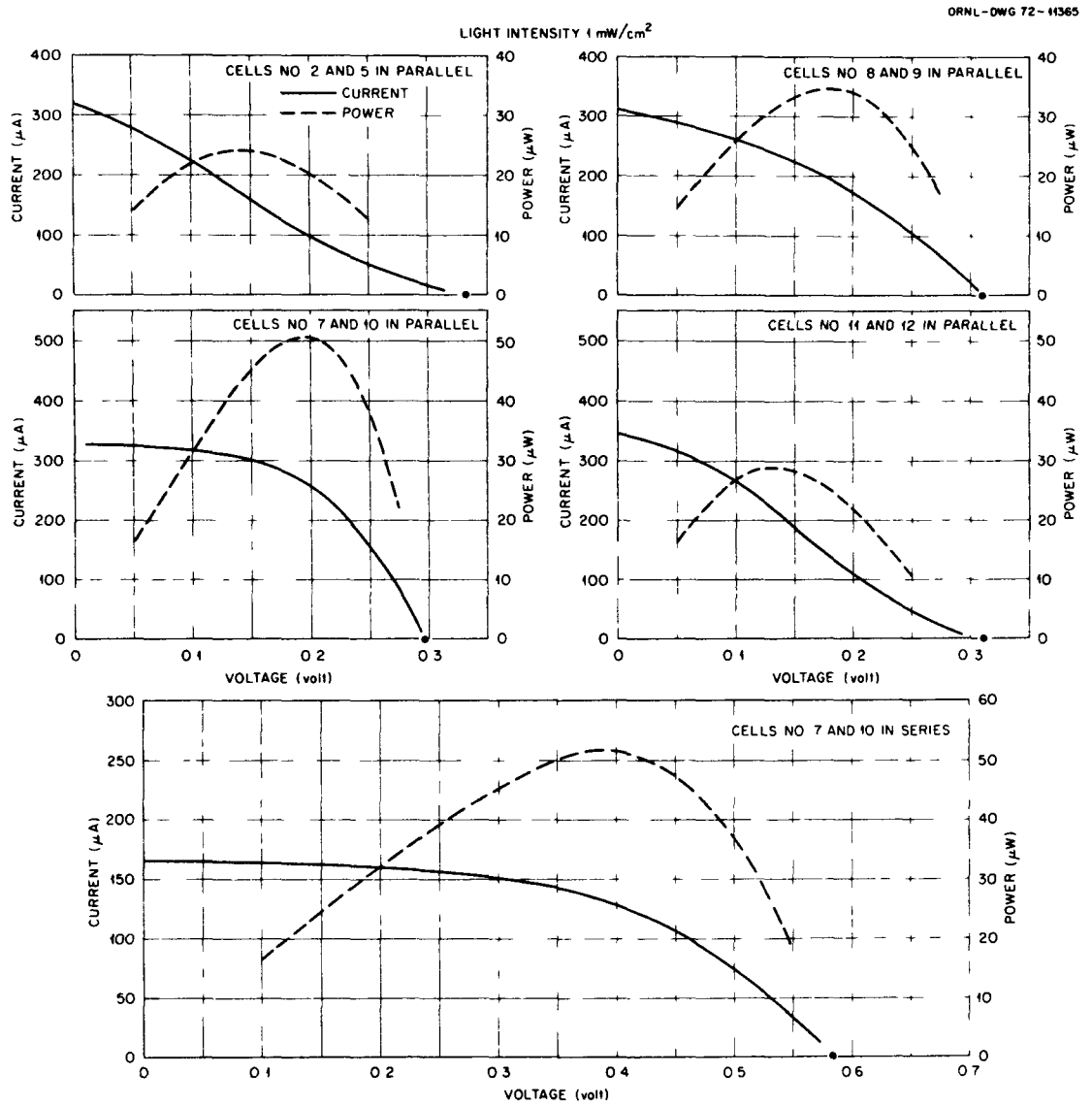

Fig. 11.4. V-I Characteristics of Battery Cells — Two Cells in Parallel or in Series.

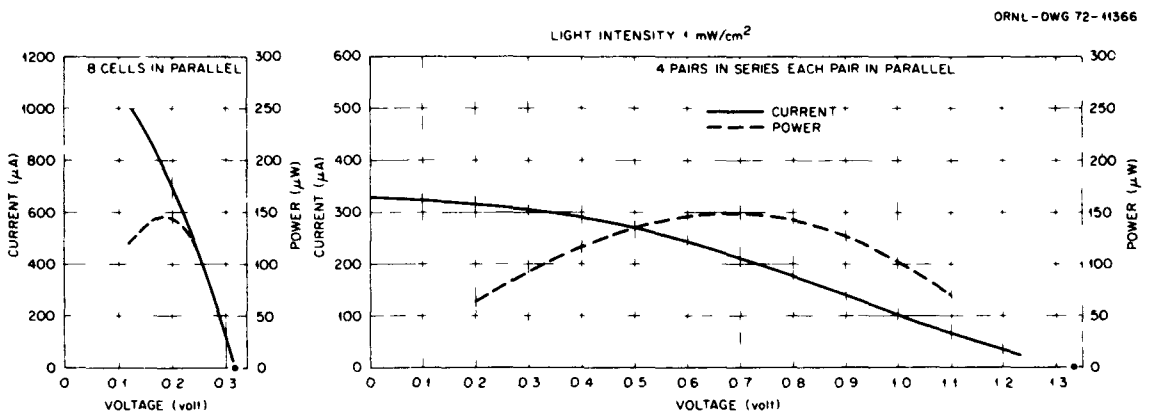

Fig. 11.5. V-I Characteristics of Battery Cells — Four Pairs in Parallel and in Series.

light source and bare promethium source should be used; the power output for betavoltaic response with bare promethium foil would be approximately 148/2 = 74 μW. In addition, if all eight cells were identical to cell 16, which has an optical power output of about 28 μW, the total optical output would be 224 μW. Hence, with bare promethium foil sources, the battery output would be approximately 110 μW.

Table 11.2 Parallel and Series Test Data

Light Intensity 1 mW/cm^2
Active Cell Area 1 cm^2

Cell No.	Individual Output		Parallel or Series	Total Output	
	Power (μW)	Voltage (V)		Power (μW)	Voltage (V)
11	15	0.15	Parallel	28.8	0.13
12	15	0.15			
7	26	0.2	Parallel	50.6	0.2
10	24.7	0.19			
7	26	0.2	Series	51	0.4
10	24.7	0.19			
8	12	0.15	Parallel	34.5	0.18
9	24.4	0.2			
2	11.9	0.15	Parallel	24	0.15
5	12.2	0.135			
4 pairs			Series	148	0.7
4 pairs			Parallel	146	0.18

Table 11.3 Power Output for Selected Cells for Battery Assembly

Cell	Optical Response		Parallel or Series
	Power (μW)	Voltage (V)	
10	24.7	0.18	Parallel
15	13.5	0.15	
13	25.8	0.2	Parallel
5	12.2	0.13	
8	12	0.15	Parallel
11	15	0.15	
19	22	0.2	Parallel
14	22.8	0.18	
4 Pairs	148[a]	—	Series

Estimated Betavoltaic Response:

1. Bare promethium foil sources[b]	74 μW
2. With 0.0015-in.-thick aluminum windows[c]	9.2 μW
3. With each of eight cells having 28-μW optical output and with bare promethium foils[d]	110 μW

[a]The sum of power outputs of eight individual cells.

[b]Optical power output is divided by a factor of 2 (see Table 9.6).

[c]Optical power output is divided by a factor of 16 (see Table 9.6)

[d]$8 \times 28\ \mu W/2 = 110\ \mu W$.

11.3 Power Output, Conversion Efficiency and Physical Characteristics of the Battery

The V-I characteristics of the battery were measured with the system described in Section 8.1. Figure 11.6 shows the V-I curve and the power output of the battery. The maximum power output of the battery was 8.7 μW at an output voltage of 0.65 volt.

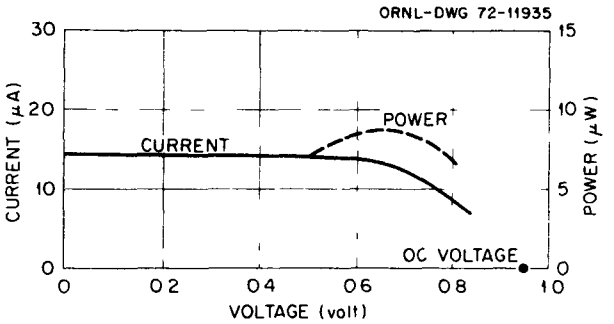

Fig. 11.6. V-I Characteristics of the Battery.

There are two factors which lowered the power output. The promethium sources were contaminated with alpha emitters. The 0.0015-in.-thick aluminum foils used to shield the Schottky cells against alpha particles also stopped the betas. The fraction of beta energy absorbed in aluminum has been discussed in Section 9.9. It shows that with 0.0015-in. aluminum foil, the power output would be reduced by a factor of 8 compared to the output of the same system without aluminum foil. The Schottky cells used in the battery assembly were not the best cells. Many good cells were damaged when the first and second assemblies of cell-simulated source array failed. If every cell in the battery had the same characteristics as cell 16, the power output would be increased by a factor of 224/148 = 1.5. Hence, if both problems can be removed, the power output of the battery would be increased to approximately 110 μW.

The conversion efficiency can be evaluated as follows. Each promethium foil used for battery source had an activity of 6.6 Ci. The total activity of four promethium foils is 26.4 Ci. The power input is 9.5 mW because the conversion factor for promethium is 2786 Ci/W. For the present battery, the power output was 8.7 μW, the conversion efficiency was about 0.09%.

If there is no alpha contamination of the promethium sources, and if all the Schottky cells had the same characteristics of cell 16, the power output of the battery would be about 110 μW. Therefore, the conversion efficiency would be about 1.2%.

The promethium sources were distilled in June 1972. The decay of the radioisotope follows the exponential law:

$$A = A_0 \, e^{-(0.693/T_{1/2})t} \tag{11.2}$$

where

A = activity at time t

A_0 = activity at time $t = 0$

$T_{1/2}$ = half-life

t = decay period

For promethium (2.62-year half-life), the decay period from June to October is four months, thus, $t = 1/3$ year. Therefore,

$$A = A_0 \, e^{-(0.693/2.62)(1/3)}$$

$$A/A_0 = 0.92$$

Therefore, the activity of the promethium source had been reduced by 8% in October 1972. Since the power output is proportional to activity, the battery power output also had been reduced. To obtain the power output and the conversion efficiency at the beginning of the life, all quantities described above should be divided by 0.92. On the other hand, the power output five years later would be reduced to 28% of the initial power output.

The physical and electrical characteristics of the battery are tabulated in Table 11.4. The radiation dose rate outside the battery was measured by TLD powder. The detailed results of the measurement are presented in Section 12.3.

Table 11.4 Characteristics of the Battery

Present Performance (with existing cells and shielded promethium sources)	
Maximum power output	8.7 μW
Voltage at maximum power	0.65 V
Open-circuit voltage	0.95 V
Short-circuit current	14.5 mA
Conversion efficiency	0.09%
Estimated Performance (with good cells and bare promethium sources)	
Maximum power output	110 μW
Conversion efficiency	1.2%
Physical Characteristics	
Diameter	0.825 in.
Height	0.85 in.
Weight	40 g
Promethium activity	27 Ci
Radiation Dose Rate	
At battery surface	9 mrem/hr

11.4 Battery Life Test

The battery was assembled on Friday, October 13, 1972. The power output was measured daily, and it was maintained at 8.7 μW for 3 days. On October 17, the battery ceased to operate. Both power output, short-circuit current and open-circuit voltage, had dropped to zero.

The failure mechanism might be due to the following. When the cell-simulated source array was assembled, gold leads were silver-painted to the gold bus bar. One possible failure mechanism was that the silver paint was damaged by radiation and the gold leads were disconnected from the bus bar, thus creating an internal open circuit. Therefore, no

voltage and current would be measured at the external terminals. The resistance of the battery was measured, and it showed an infinite resistance.

Based on the above failure mechanism, it would be possible at low temperature to re-establish the contact between the gold wire and the bus bar due to the contraction of the gold wire. The battery was chilled down to dry ice temperature (-78°C). The power output of the battery was resumed. After the cold trap was removed, the power output oscillated rapidly up and down. Vibration was applied to the battery until the battery output became stabilized and the battery continued to operate normally at room temperature. Figure 11.7 shows the V-I characteristics versus time. This observation supports the failure mechanism as discussed in the last paragraph.

An improved cell-source assembly will be suggested in Section 14.1. With the proposed assembly, all cells will be connected in series by pressure contact. Thus, the internal leads can be eliminated and the above difficulty can be avoided.

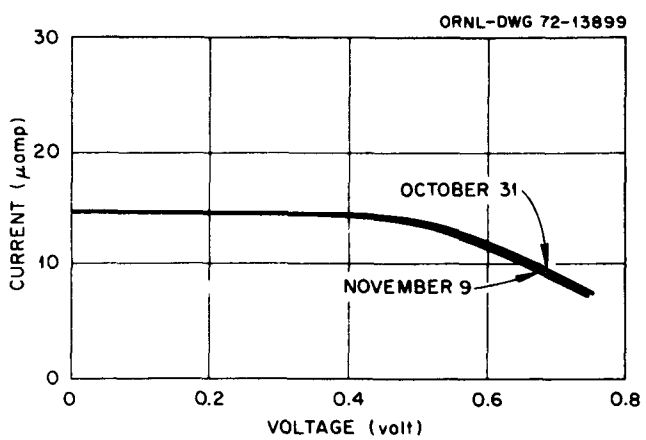

Fig. 11.7. Battery Life Test.

12. SAFETY CONSIDERATIONS

12.1 Shipping

The regulations governing the transportation of radioactive materials are implemented by the Atomic Energy Commission (AEC)[50] and the Department of Transportation (DOT)[46] in the United States and by the International Atomic Energy Agency (IAEA)[51] for international shipments. Safety is always the most important consideration in transporting radioactive materials. In general, the regulations require that the container must not release any radioactivity to the environment and must not have excessive radiation dose rates around the container after hypothetical accidents. There are three hypothetical accident conditions for nonfissionable radioisotopes. They can be briefly stated as follows: (1) free drop — a free drop through a distance of 30 ft onto a flat, essentially unyielding horizontal surface, (2) puncture — a free drop through a distance of 40 in. striking the top end of a vertical, 6-in.-diam, cylindrical, mild steel bar mounted on an essentially unyielding horizontal surface, and (3) thermal — exposure to a thermal test of 1475°F for 30 min.

The regulations specify that it is not necessary to conduct the actual tests if engineering evaluations or comparative experimental data can clearly show that the container would be capable of performing satisfactorily under the prescribed test conditions.

The outer capsule of the battery is designed to withstand the free drop and puncture tests, and the feedthrough is to withstand the thermal test. The design of the outer capsule against impact is derived from comparative experimental data of the ^{252}Cf capsule test program of

Savannah River Laboratory.[47] The thermal test of the feedthrough is obtained from test data provided by Ceramaseal, Inc.[48]

Although the battery is designed to comply with the DOT shipping regulations, it cannot be shipped as a package until a special transportation license is issued. The request for special license has to be reviewed and approved by various regulatory bodies. Generally, it will take from 4 to 6 months to get a license approved. Application for a transportation license is out of scope of this dissertation.

To transport the battery, a previously approved shipping container can be used. For example, USDOT Spec. 6M package has been approved for Type B shipments.[46,52] This container meets all the criteria specified in DOT and IAEA regulations. It can be used to ship any solid radioactive material whose thermal decay energy output is less than 10 W. The 6M drum has been authorized for all modes of transport. Figure 12.1 is a sketch of the 6M drum.

The drum must be clearly marked on the outside as follows: "DOT-6M Type B" and "Radioactive Materials."

12.2 Evaluation of Capsule Integrity

The design of the battery outer capsule against DOT hypothetical accidents was derived from comparative experimental data of ^{252}Cf capsule test programs performed by Savannah River Laboratory.[47] One of the capsules, SR-Cf-1000 series, has similar dimensions to the battery capsule. Both capsules use stainless steel 304L. The SR-Cf-1000 capsule has successfully passed all the tests required in DOT regulations. If it can be proven that the battery capsule is stronger than the SR-Cf-1000 capsule, the battery capsule can also pass all the tests prescribed by

the regulations. Table 12.1 tabulates the major characteristics for both capsules.

To compare two thin-walled (D/t > 10) cylindrical vessels under external forces, the most important criterion is to investigate the failure through elastic instability or buckling. A comparison between two capsules shows that the battery capsule is shorter in length, smaller in

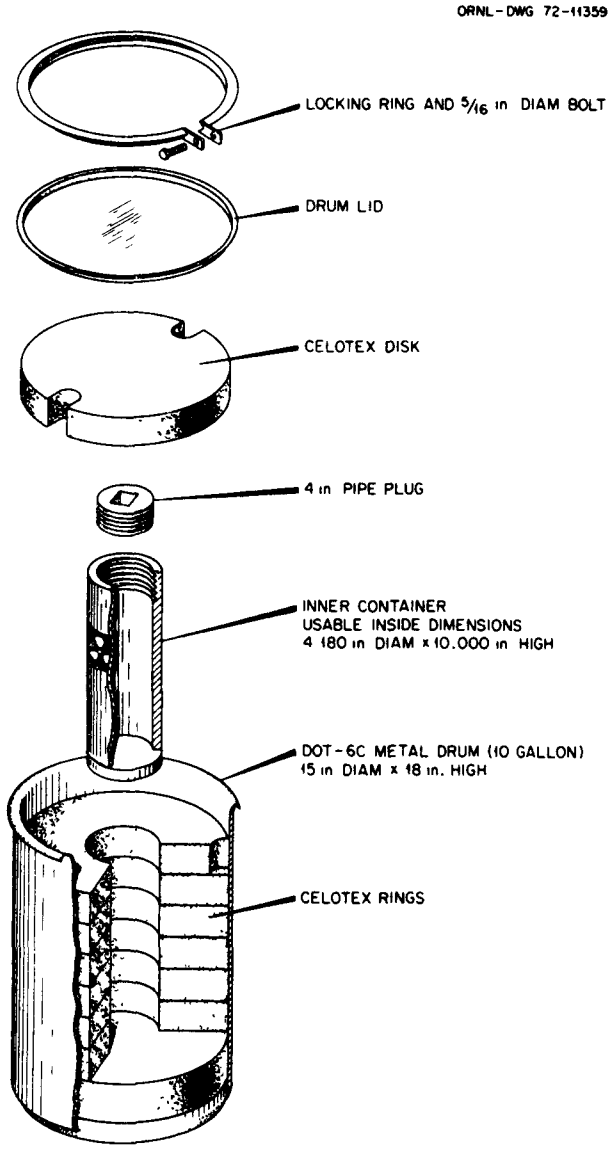

Fig. 12.1. USDOT Spec. 6M Package.

Table 12.1 Characteristics of SR-Cf-1000 Capsules and Battery Outer Capsule

Characteristics	SR-Cf-1000 Capsule	Battery Outer Capsule
Material	Type 304L stainless steel	
Length	3.75 in.	0.85 in.
Diameter	1.19 in.	0.825 in.
Wall thickness	0.035 in.	0.04 in.
End plate thickness	0.29 in.	0.08 in.
Minimum weld penetration	0.03 in.	0.03 in.
Diameter/thickness	34	21

diameter yet greater in thickness, and therefore more buckle-resistant than the ^{252}Cf capsule. An exact formula for buckling can be found in the literature.[53]

The second consideration is the meridional (S_m) and hoop (S_h) stresses. For uniform external pressure, the stresses can be determined approximately by

$$S_m = -pR/2t \tag{12.1}$$

$$S_h = -pR/t \tag{12.2}$$

where

p = external pressure, psi

R = radius, in.

t = wall thickness, in.

The negative sign denotes compressive stress. Since S_m and S_h are related by a factor of 2, only one stress needs to be investigated.

For the ^{252}Cf capsule

$$p = (t/R)S = (0.035/0.6)S = 0.06S \tag{12.3}$$

For the battery capsule

$$p = (t/R)S = (0.04/0.4)S = 0.1S \tag{12.4}$$

Since stainless 304L was used for both capsules, S is the same in both equations. Therefore, for the same stress, the battery capsule can sustain more pressure than the ^{252}Cf capsule.

The end plates of the battery capsule are 0.08 in. thick. They can be considered as fixed edges because they are welded to the cylindrical capsule. The maximum stress of a fixed edge circular plate with uniform load is

$$S = (3R^2p)/(4t^2) \quad \text{or} \quad p = [(4t^2)/(3R^2)]S \tag{12.5}$$

For end plates of the battery capsule, the thickness is 0.08 in. and the radius (the unsupported radius of the plate) is 0.36 in. Thus

$$p = \frac{4(0.08)^2}{3(0.36)^2} S = 0.065S \tag{12.6}$$

Compared to Eq. 12.3, the end plates of the battery capsule are stronger than the cylindrical wall of the ^{252}Cf capsule.

The minimum weld penetration is 0.03 in. for both battery and ^{252}Cf capsules. It has been proven that the weld joint of the ^{252}Cf capsule is adequate for all accident tests. Therefore, the weld should also be adequate for the battery capsule.

12.3 Radiation Dose Rate

The radiation dose rate at the surface of the battery was measured by TLD powder dosimeter. The principle of TLD dosimetry has been discussed in Section 9.10. The result shows a surface dose rate of about 9 mrem/hr. This is slightly lower than the dose rate criterion, but it is slightly higher than the predicted dose rate.

Since the dose rate is related to the distance between source and the dose point by an inverse square law, the absorbed dose at critical

organs received by an individual would be much less than 1 mrem/hr because the separation distance would be at least 5 cm. For this prototype battery, the radiation shielding appears adequate. For final design of the battery, the radiation dose rate at the surface of the battery should be less than 2.5 mrem/hr which requires an additional tantalum thickness of about 0.01 in.

12.4 Contamination Test

After the source-cell assembly was loaded into the tantalum can and the epoxy was dried, the can was decontaminated with detergent and water. Wipe tests showed only a trace of beta activity. No alpha activity was found. The tantalum capsule was then removed from the glove box and the decontamination procedures were repeated until no beta activity was found above the background level of the measuring system.

The same decontamination procedures were repeated with the stainless steel outer capsule after the cover was welded and no activity was found.

12.5 Leak Test

The electrical feedthrough supplied by Ceramaseal, Inc., was first leak tested and it showed a leak of less than 1×10^{-9} cm^3/sec STP. The feedthrough was then welded to the stainless steel mounting ring. Again, it showed a leak of less than 1×10^{-9} cm^3/sec STP. After the feedthrough was welded onto the stainless steel outer capsule, the assembly was set into a vacuum desicator which contains water. Under vacuum, the air from inside the capsule will escape and bubbles will be seen if there is a leak. No bubbles were seen when the assembly was tested under vacuum. It was concluded that the capsule was leak tight.

12.6 Marking of the Battery

To avoid accidental separation from the shipping cask or unintentional handling by unauthorized personnel, a radiation symbol was engraved on the outer capsule of the battery. The following letters were also engraved on the outside surface of the battery capsule for positive identification.

Nuclear Battery

ORNL

Pm-147 30 Ci 10/72

13. COST ANALYSIS

13.1 Cost of a Prototype Battery

It is difficult to estimate the cost of the first prototype battery because it has been heavily involved in research and development. However, if a second prototype battery were to be assembled, the approximate cost of such a battery could be estimated. Here, only the cost of material and labor are estimated.

The cost of various components of a 200-μW battery are tabulated in Table 13.1. Since each Schottky cell yields 15 μW power output, a total of 14 Schottky cells is required. The cost of one Schottky cell is $75 which makes the total cost about $1000.[54] The Pm_2O_3 can be purchased from AEC for about $0.50 per curie. If one assumes the conversion efficiency of the battery is 1%, the thermal power input would be 20 mW,

Table 13.1 Cost of a 200-μW Prototype Battery

Components		Cost ($)
Schottky Cells (14)		1050
Promethium Sources		
Pm_2O_3 (60 Ci)	30	
Reduction-distillation	500	
Rolling process	250	
Mounting, etc.	250	1030
Capsules		
Stainless steel outer capsule	40	
Tantalum inner capsule	60	
Lavite spacer and container	50	
Feedthrough	10	
Miscellaneous supplies	10	170
Assembly of Battery		500
Total		2750

corresponding to about 60 Ci of ^{147}Pm. The cost of 60 Ci of ^{147}Pm as Pm_2O_3 would be approximately $30. The reduction-distillation process to reduce the oxide to metal, rolling of metal foils, and mounting of foils may require four man-days, which may cost $1000. The material and machining cost for various capsules, components, and electrical supplies is estimated to be about $170. The assembly cost, which includes the interconnection of gold wires, welding, testing, and decontamination, is estimated for 2 man-days or $500. The sum of all these costs gives a price of about $2700 for a 200-μW nuclear battery.

13.2 Projected Cost for Future Batteries

If a large number of nuclear batteries are required in the future, the cost per battery will be reduced considerably. The estimated production cost for large quantities of Schottky cells will be reduced to about $10 per cell or less.[54] This item alone reduces the total battery cost by a factor of 2. Assuming the labor and material costs will be reduced by a factor of 3, the total cost of the battery would be $140 + $560 = $700. On the basis of dollars per watt-hour, the battery can be assumed to operate at least 2.62 years. The total energy delivered would be 4.6 watt-hours. Therefore, the nuclear battery would cost roughly $100 to $150 per watt-hour.

The cost of a battery with higher power output is not linearly dependent on the power output. Increase in power output will increase proportionally to the material cost but the cost of labor will remain approximately the same. Since most of the cost is labor, an increase in power output by a factor of two will increase the total battery cost by only about 20%. For a 5-year operation, the cost of a battery with initial power output of 850 μwatts would be approximately $1000.

13.3 Comparison With Chemical Batteries

As discussed in Section 13.2, the projected cost for nuclear batteries is expected to be of the order of about $100 per watt-hour. By comparison, the cost of chemical batteries is about $1 to $10 per watt-hour. Because of the complexity involved in a nuclear battery, and the requirements for safety and the absolute containment of the radioactive materials, the nuclear battery is inherently more expensive than the chemical batteries. However, for certain applications where inaccessibility can be established, cost comparison must include the expenses involved in the replacement of the battery in addition to the initial cost. In those applications where the shorter life batteries have to be replaced at a significant cost, the nuclear battery will be more favorable and more economical than chemical batteries.

For artificial pacemaker applications, for example, in-vivo residence time of the pacemaker is presently limited by the lifetime of the chemical battery. Nearly all pacemaker failures are the result of battery failure. By use of a nuclear battery, the residence time can be greatly extended. Apart from clinical advantages, a cost comparison between a 2-year chemical-battery- and a 5-year nuclear-battery-powered demand pacemaker can be estimated as follows. The initial cost of a chemical-battery-powered demand pacemaker is about $1000.[55] Within a 10-year period, four replacements plus initial implantation are needed. Each surgical operation for implantation requires about 4 days in the hospital.[56] The estimated cost for hospital and surgeon charges for each operation is about $600. Since the whole pacemaker (except the electrodes) has to be replaced during the operation, the total cost for a 10-year period would be $5 \times (\$1000 + \$600) = \$8000$. On the other hand, if a 5-year-life nuclear battery is used,

only two implantations will be required. Assuming the cost of a nuclear-battery-powered demand pacemaker is estimated at $2000, the total cost for a 10-year period would be 2 × ($2000 + $600) = $5200. Figure 13.1 shows the cost savings of a 5-year and a 10-year life nuclear pacemaker over a 2-year life conventional pacemaker.

Based on above figures, the cost savings can be estimated as follows. For a 5-year operation period, the cost to a patient would be $4000 if 2-year-life chemical powered pacemakers were used. On the other hand, if a 5-year-life nuclear powered pacemaker were used, the cost to the patient would be reduced to $2600. The net annual saving is approximately $300 per patient. Since 13,000 new pacemakers are required per year in the United States, the total savings in cost would be in millions of dollars annually.

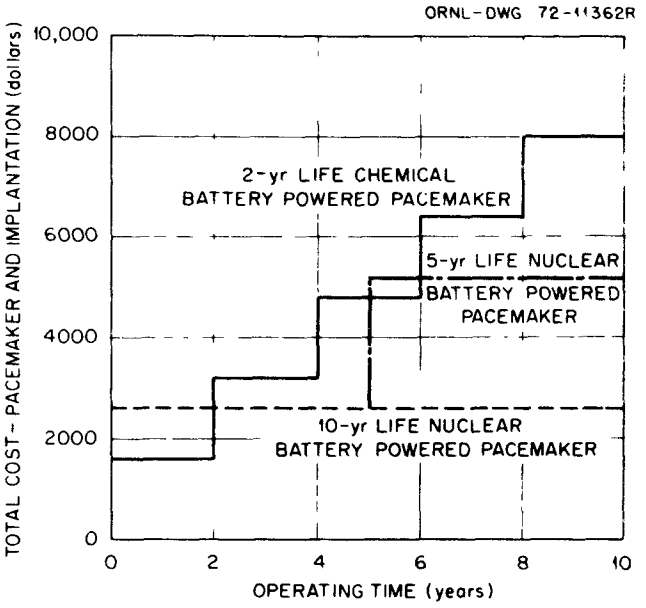

Fig. 13.1. Comparison of Total Cost Between Chemical and Nuclear Powered Pacemakers.

The cost of the battery as estimated above did not involve mark-up. It is difficult to say what the mark-up will be. If the mark-up is 2, there is still a cost advantage for a 5-year life battery. If the mark-up is 3, there is no cost advantage for a 5-year nuclear battery over mercury cells. However, due to the reduction in the number of operations necessary to replace pacemakers, the long-life battery would be beneficial to pacemaker patients even if there is no cost benefit. On the other hand, the battery manufacturers would perhaps like to sell more units by reducing the mark-up.

14. PROPOSED DESIGN OF THE BATTERY

14.1 Cell-Source Assembly

From experience obtained from the prototype battery, we have learned that the presence of the gold wire leads on the cells displayed many disadvantages. A phenolic mask, which increases the thickness of the Schottky cell by a factor of three, was required. This also increases the diameter of the assembly. If the internal leads can be eliminated and all cells are connected in series by pressure contact, one would have the following advantages: (1) the production of the Schottky cell is simplified because no mask and no leads are required for each cell except two terminal leads at the top and the bottom of the assembly; (2) a lavite spacer is not required because the cells are connected in series; (3) no interconnections are made between cells; (4) since all cells are in series, the output voltage is higher; (5) the power density is increased; and (6) the conversion efficiency is increased.

This improved system greatly increases the power density ($\mu W/cm^3$) of the battery due to the elimination of the phenolic mask (0.016 in. thick) and the lavite spacer (0.020 in. thick). Figure 14.1 shows such a system.

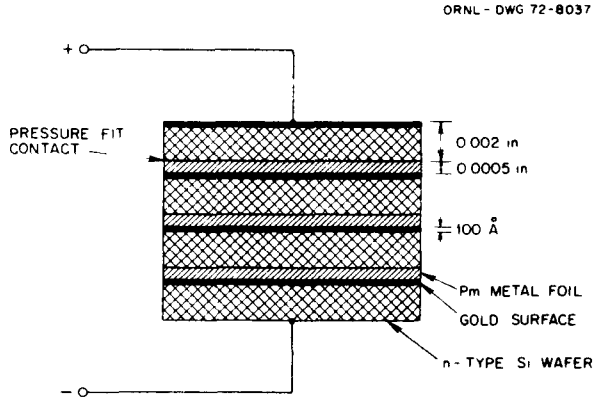

Fig. 14.1. Optimum Configuration for Cell-Source Assembly.

Here the Schottky cells must be thin in order to utilize the electrons emitted from both sides of the radiation source. If a cell delivers 15 μW from one side irradiation, it will deliver about 25 μW when irradiated from both sides (70% increase in power for the source on the back side).[14] A ten-cell battery will deliver approximately 250 μW with a voltage of about 1.5 V. The cross-sectional area of the cells is assumed to be 1 cm^2 and the thickness of the assembly is only about 0.1 cm. Under these assumptions, a flat disk-shaped battery can be built which is very suitable for pacemaker applications.

The conversion efficiency would be lowered if the two-side irradiation technique is used. However, there are two factors which increase the conversion efficiency and the net result makes the efficiency increase slightly. The first factor is the elimination of the phenolic mask, which in turn, eliminates the separation distance between the radiation source and the gold surface of the Schottky diodes. The reduction in beta flux due to the separation distance of 0.018 in. can be evaluated by the following equation[57]

$$G = \frac{1}{2}\left[\frac{1}{(1+\beta)^{1/2}} + \left(\frac{3}{8}\right)\frac{\beta\gamma}{(1+\beta)^{5/2}}\right] \qquad (14.1)$$

where

$\beta = b^2/a^2$

$\gamma = c^2/a^2$

a = distance from source to Schottky cells = 0.018 in.

b = radius of active surface of the cells = 0.23 in.

c = radius of active surface of the source = 0.23 in.

Substituting the values into the above equation, the reduction in beta flux is found to be

$$G = 0.054 \ .$$

Therefore, if the separation distance can be eliminated, the conversion efficiency would be increased by approximately 5%. The second factor is due to the loss of electrons through the phenolic mask. If the active source area is the same size as the active cell area, the diameter of the ^{147}Pm source would be reduced from 0.5 in. to 0.46 in. Thus, the power input would be reduced by 15%. This means an increase in conversion efficiency by 15%. From two side irradiation, the reduction in efficiency is 15%. The net effect of the improved cell-source assembly increases the conversion efficiency by approximately 5%.

There are two main problems to be resolved before such a battery can be assembled. The first is to make very thin silicon wafers. The chemical etching technique used for most commercial productions may not yield a thin wafer with flat surfaces. A grinding technique has been used by Bell Telephone Laboratories to obtain silicon wafers less than 0.001 in. thick.[58] Therefore, it should be possible to obtain thin silicon wafers commercially in the near future. The second problem is the electrical contact between the cells and the radiation sources. There are no data currently available for the electrical resistivity of promethium metal. Judging from the resistivities of other rare-earth metal recently published,[59] the electrical resistivity should be about 50 to 100 microhm-cm at room temperature. This is low enough for pressure contact between the cells and promethium metal, but the values should be verified.

14.2 Schottky Cells

It was evident from the experiments performed in this project that the Schottky cells are efficient betavoltaic converters. There were some difficulties involved in the handling of the front gold leads. The improved cell-source system, as discussed in Section 14.1, should eliminate such difficulties.

The major improvement required on Schottky cells is quality control. The maximum power output of the battery cells to optical sources varies from 12 μW to 28 μW. This variability is too large and it is unacceptable for commercial production. The use of short-circuit current as an indicator of cell characteristics proved to be inaccurate. Maximum power output, or the V-I characteristic curve, should be used to specify the variability of the cells. Strict quality control procedures would be required to achieve a variability of ±5% on maximum power output.

14.3 Promethium Radiation Sources

The promethium metal has been proved to be an excellent radiation source compared to promethium oxide. The metal has higher power density, and it can be rolled into foils of the desired thickness as well as uniform activity.

Alpha contamination was the major problem in the radiation sources. The origin of the contamination was traced to the rolling machine used for source construction. For future work, all equipment involved in source assembly should be thoroughly checked for alpha contamination.

14.4 Proposed Battery Design

With the improved cell-source assembly, quality controlled Schottky cells and ^{147}Pm metal sources without alpha contaminations, one should be able to design a practical battery which will satisfy the specifications required by a pacemaker battery.

The first quantity to be specified is the power level at the end of the life, i.e., after 5 years of operation. For demand pacemakers, the minimum power requirement is 200 μW. In 5 years, the promethium source would decay to approximately 28% of its original power output. Therefore, the power output at the beginning of life should be about 700 μW. Assuming the conversion efficiency of a dc-to-dc converter (from 3 volts to 6 volts) is 80%, the total power required should be about 850 μW.

The active area of the Schottky cells should be determined. Based on the requirement of the battery size, one would like to have a flat disk shape rather than a cubic shape. However, the surface area of the cells cannot be too large because the cells would be relatively thin and may be easily broken. A cell area of 2 cm^2 seems reasonable. The thickness of the cell should be 0.003 in. so that when both sides are irradiated by 5.55-mg/cm^2 ^{147}Pm sources, the power output would be

$$P = (15\ \mu W/cm^2)(2\ cm^2)(1.7) = 50\ \mu W$$

Note that 15 $\mu W/cm^2$ is the power output obtained from the betavoltaic measurement with the bare promethium foil of 5.55 mg/cm^2 thickness. The factor of 1.7 is the factor to account for irradiating both sides of the Schottky cell. For a 850-μW battery, 18 Schottky cells and 17 radiation sources would be required.

The radiation sources should also be 2 cm^2 in area and 5.55 mg/cm^2 ($\sim$0.0005 in.) thick. Each source will have an activity of approximately 10 Ci. A good glove box would be required for source construction. Argon should be used for all processes involving promethium metal to prevent oxidation of the metal.

Lavite cans should be used to contain the cell-source assembly. The thickness of the container may be reduced to about 0.010 in. The cell-source assembly can be loaded into the lavite can inside the glove box because there is no interconnection to be made between the Schottky cells.

A tantalum primary shield of 0.065 in. thickness is required to reduce the surface dose rate to less than 2.5 mrem/hr. The tantalum capsule would also be used for a barrier against mechanical forces. The stainless steel outer capsule with 0.025-in. wall thickness would be used to reduce the x-rays produced in the tantalum capsule.

The TIG welding technique deposited a large amount of heat into the capsule and caused some problems. Electron-beam welding should be used in future units. The electron beam can be collimated to a fine beam such that only the local welding area will be heated to high temperatures.

Figure 14.2 shows a sketch of the proposed design. The major characteristics of the battery are expected to be as follows:

Weight	30 grams	Diameter	2.1 cm (0.83 in.)
Volume	3 cm^3	Height	0.9 cm (0.35 in.)
Power output:	initial	850 μW	
	end of 5 years	240 μW	
Power density		300 $\mu W/cm^3$	
Output voltage		3 volts	
Conversion efficiency		1.1%	
Radiation dose rate		2.5 mrem/hr at the surface of the battery	

A parametric study has been performed to determine the power density versus battery power level. The results show that the power density increases as the battery power output increases. Figure 14.3 illustrates this relationship.

The characteristics of the proposed final design of the Schottky barrier nuclear battery are compared below to the specifications given in Chapter 2. Some comments about possible improvements of the battery performances are also discussed.

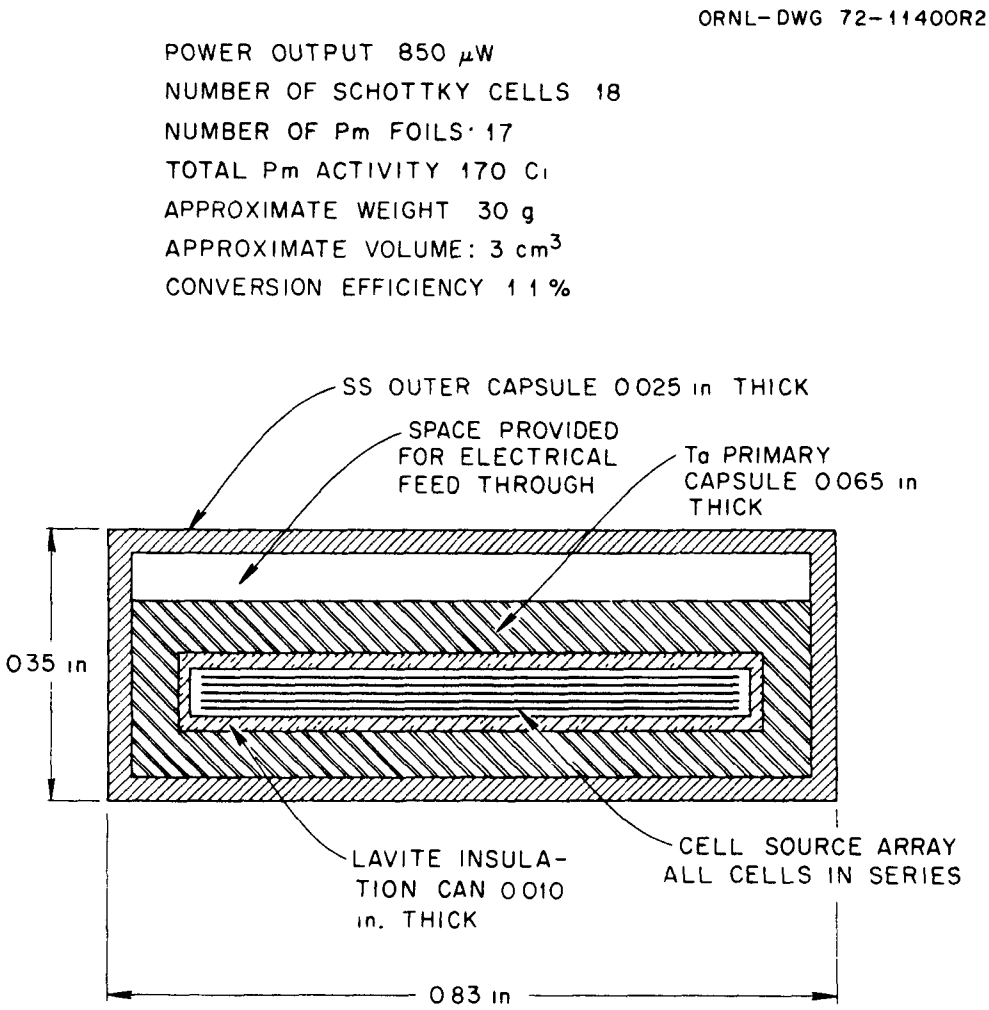

Fig. 14.2. Conceptual Design of an Optimized Betavoltaic Battery.

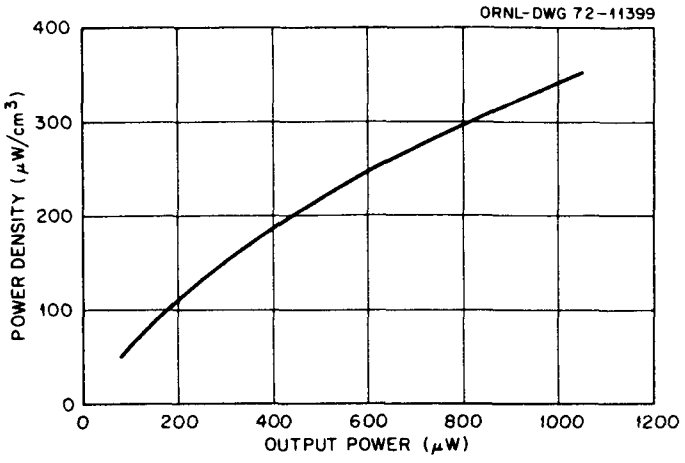

Fig. 14.3. Power Density for Optimized Nuclear Battery.

(1) Useful Life — The designed life of the battery is five years based on the energy content and the radioactive half-life of ^{147}Pm. This satisfies the specification but not the ultimate design goal. Improvement in useful life is expected if a longer lived radioisotope can be used. In this thesis, the radiation damage on Si-Au Schottky barrier cells limited the use of other radioisotopes with longer half-lives. If Schottky cells with more radiation resistance can be used, the probability of extending the useful life to 7 or 10 years is greatly increased. The true useful life of the final commercial prototype batteries should be verified by a long-term life test of such batteries.

(2) Reliability — It is very difficult to evaluate quantitatively the reliability of a new product except to test the product experimentally. In the design stage, however, efforts can be made to minimize or eliminate the possible modes of failure. In the case of this battery, for example, the electrical contact between Schottky cells is by area contact rather than point contact. Also, a lavite insulation container is used, instead

of chemical insulation material, to minimize the radiation damage to the insulation layer. It is expected that a Schottky barrier betavoltaic device is potentially more reliable than a thermoelectric device because of the large number of fragile electrical connections in the latter system. Before the battery can be commercialized, further experimentation is needed to prove the reliability of the device.

(3) Power Output and Output Voltage — The power output of the battery satisfies the specification. However, due to the relatively short half-life of ^{147}Pm, the mean power output is much higher than the required power level, i.e., an initial power of 850 μW dropping to about 240 μW at the end of 5 years. If a longer lived radioisotope can be used, the mean power will be decreased. The voltage output is about 3 volts, a dc-to-dc converter (80% from 3 volts to 6 volts) is needed to obtain the desired voltage to run the pacemaker. The output voltage of a betavoltaic device can be increased if the number of Schottky cells (in series) is increased. For example, 30 Schottky cells connected in series yields a voltage of about 6 volts. The tradeoffs are (1) Schottky cells become smaller in area and therefore more difficult to handle, (2) there may be an increase in the dose rate to the worker due to the increase in handling of more radiation sources during manufacture. The voltage can also be increased if a large barrier height Schottky cell is used. More experiments should be initiated to measure the betavoltaic effect on other metal—semiconductor junctions.

(4) Size, Shape, and Weight — The proposed battery has a disk shape with a volume of 3 cm^3 and a weight of 30 grams which matches the specifications. Since the major fraction of weight and size is related to

nuclear safety considerations, the weight and size of the battery are not expected to have large improvements except perhaps if a source with low radiation energy (such as tritium) can be developed.

(5) Maintenance — No maintenance is required for this device.

(6) Environmental Conditions — The device is designed to be unaffected by external conditions. Large temperature changes will have certain effects on the performance of Schottky cells. However, no wide temperature variation is expected when the device is used as a pacemaker battery. The operation of the battery should be unaffected by minor accidents (such as falls) which may be expected to happen to a patient during his daily life. This should be confirmed experimentally.

(7) Economics — The cost analysis suggested that the cost of a Schottky barrier nuclear battery is on the order of $1000. Compared to the break-even cost of a 5-year-life battery, this device would potentially have economic advantages over mercury cells. A more detailed economic analysis must await the development of a commercial prototype.

(8) Safety — The safety of a nuclear battery is the only specification which cannot be compromised. The radiation dose rate at the surface of the battery is less than 2.5 mrem/hr, which is the present European guideline (the U.S.A. has no regulations for nuclear pacemaker batteries at present). The battery is designed to meet the DOT and AEC transportation regulations. Experiments must be performed to assure the absolute containment of radioactivity under any foreseeable accident.

Although this proposed battery satisfies most specifications described in Chapter 2, the result of this work indicates only the feasibility of a

Schottky barrier betavoltaic conversion system, which is far from the completion of a commercial design. It is recommended that the second phase of the program will be to study the betavoltaic effect with various metal–semiconductor Schottky barrier devices in conjunction with various beta decay radioisotopes. It is expected that the final battery will have higher conversion efficiency, higher power density, and longer useful life than the prototype discussed in this thesis. If cost and reliability can be proven, the final microwatt betavoltaic device should be commercially marketable.

15. RECOMMENDATIONS

The need for a compact, reliable, long-life microwatt battery has been established. The feasibility of Schottky barrier betavoltaic energy conversion and the economics of such a battery have been demonstrated by this study. This result should lead one to further investigate this system. The following research programs are therefore recommended for study.

15.1 Schottky Cells

One of the major advantages of using Schottky barrier devices instead of pn junctions is the much wider choice of materials. The barrier height, diffusion length, mobility, and radiation-damage resistance can be optimized by a different combination of metals and n- or p-type semiconductors.

Most p-type semiconductors have not been investigated, perhaps because barrier heights observed and predicted from the surface states model are less than for the n-type materials. However, recent work[20] has shown that for the proper choice of metal this need not be the case. Also, theoretical considerations lead one to believe collection efficiency will be improved on p-type substrates. In the case of silicon, another advantage of using p-type semiconductors is the fact that p-type silicon is more radiation damage resistant than n type.[34]

A second area of research is to investigate compound semiconductors such as ZnS, $GaAs_5P_5$, GaN, etc.[19,60] In general, carrier lifetime decreases with increasing band gap. However, the indirect gap materials have much longer diffusion lengths than direct gap materials, independent of the band gap considerations. Therefore, indirect gap materials with

a reasonably high band gap and with heavy atoms seem most promising. Clearly the final selection should be made on the basis of test data.

15.2 Promethium-p Silicon Power Generating Cells

A particularly interesting program could be initiated with a radioactive hot evaporation, or sputtering, system. Suppose promethium metal could be deposited on p-type silicon, it would form a Schottky barrier with a barrier height of about 0.6 V. This is derived by comparison to the barrier height measured from a Gd-p silicon Schottky device.[27] The Pm-p silicon cell has a unique characteristic in that the wafer, by itself, is a small power generator. It would considerably simplify the battery assembly. In addition, such a configuration eliminates the use of gold; this would lead to higher conversion efficiency because the loss of electrons due to reflection at the promethium-gold interface would be absent.

15.3 Radiation Sources

The most important criteria for selection of radioisotope sources for betavoltaic microwatt battery applications are long half-life, low-dose rate, and no radiation damage to the Schottky devices. Thulium-171, promethium-147, and tritium were considered as potential sources. The area of research for each of the sources is outlined below.

The main problem with ^{171}Tm is the small amount of ^{170}Tm present in the source. The radiation dose rate becomes unacceptable if ^{170}Tm cannot be removed from the source. Many techniques, such as electromagnetic separation, radioactive decay, enrichment of target, etc., have been considered.[61] No satisfactory solution has been found.

Tritium is an ideal radiation source for betavoltaic energy conversion. It has a half-life of 12 years and a low maximum beta energy of 18 keV. The problem here is to find a suitable chemical form of tritium which has a high specific activity and does not release hydrogen atoms. A solution to this problem would greatly improve the characteristics of the betavoltaic battery.

At present, ^{147}Pm is the only working source for small solid-state conversion systems. One improvement that can be made on promethium sources is to reduce the radiation dose rates. The major dose rate contribution is not from ^{147}Pm, but from impurities and other isotopes of promethium remaining in the source. The other promethium isotopes, namely ^{146}Pm and ^{148m}Pm, are high-energy beta and gamma emitters. With a 43-day half-life, ^{148m}Pm decays to negligible amounts after the promethium has aged for 2 years or longer. Unfortunately, ^{146}Pm has a half-life of 5 years, which cannot be removed by decay. A major fraction of the dose rate from the present ^{147}Pm sources is from ^{146}Pm atoms.

Experiments have been performed in various AEC laboratories to reduce the ^{146}Pm content in ^{147}Pm sources. Neutron capture techniques, i.e., "burn-up," have been used to reduce the ^{146}Pm content to 0.1 ppm or less.[62] This means the radiation dose rate can be reduced at least by a factor of 2. Since the criteria for exposure of a human body to radiation is "as low as practical," a further reduction in ^{146}Pm content would be advantageous.

15.4 Electrical Feedthrough

Metallurgical studies should be performed to investigate the ceramic-metal bonding. The electrical feedthrough used in the prototype battery

is not sufficient because it is too large. A miniaturized, vacuum-tight ceramic-metal bonding, capable of remaining vacuum tight through high-low temperature cycles, is necessary for construction of a miniaturized betavoltaic battery.

15.5 Engineering Development

The results described in Chapters 9-11 showed that it is feasible to build Schottky barrier nuclear batteries in the microwatt range. To develop the batteries into a commercial product, the following practical engineering problems should also be investigated.

(1) Schottky Cells — Many Schottky cells used in this project have a large variability on their performances. The optical response showed a variation in maximum power output of cells ranging from 12 μW to 28 μW. Quality control of the manufacturing processes should be enforced to achieve a variability of about ±5% in maximum power output. Electrical leads attached to the Schottky cells always caused problems during battery assembly. These leads can be eliminated by using an area contact configuration. In this configuration, all cells are in series and the promethium metal becomes a part of the electrical circuit. Thin Schottky cells (∿0.002 in.) should be used in order to utilize the electrons emitted from both sides of the radiation sources. The present technique, chemical etching, is incapable of producing thin silicon wafers with flat uniform surfaces. A grinding technique may be used, but some development effort may be necessary.

(2) Radiation Sources — The major problem with radiation sources is to minimize the radiation exposure to the hands of the workers. Remote

processing should be used whenever possible. Another problem is to avoid cross contamination from distilling, rolling or punching equipment; they should be thoroughly checked and monitored before service.

(3) Battery Assembly — Battery assembly should be performed in an air tight glove box under an argon atmosphere. Care must be taken to avoid oxidation of the promethium metal foil, which will greatly increase its electrical resistivity. Another problem is to develop a procedure for loading the Schottky cell-radiation source array such that there will be no scratching of the sensitive surface of the Schottky cells during assembly.

(4) Electrical Feedthrough — A miniaturized electrical feedthrough, i.e., ceramic-metal bonding, capable of remaining vacuum tight through high-low temperature cycles (simulating an accident involving a serious fire) and an impact test is necessary. This is required to prevent any spread of radioactive materials through the metal-ceramic bonding which may crack during fire or other impact accidents such as an automobile or airplane crash.

(5) Reliability and Long-term Life Test — Although it is expected that the useful life of the device is 5 years, this should be confirmed experimentally.

(6) Operational Safety — The operation of the battery should be unaffected by external conditions. The battery should be tested against vibration, impact, etc., to simulate minor accidents, such as falls, which may happen to a patient.

(7) Nuclear Safety — Nuclear safety can be divided into two parts: (a) radiation exposure to the patient and to the general population and

(b) contamination by radioactive materials due to the rupture of the capsule or the electrical feedthrough. The radiation exposure can be minimized with the proper design of shielding. The contamination problem is more serious. Severe accident conditions such as cremation, fire, airplane and automobile crashes, gun shot, and other foreseeable accidents should be considered. Battery capsules should be tested against puncture, impact, fire, and other simulated test conditions to assure the integrity of the capsule under an foreseeable accidents.

(8) Commercial Prototype — With Si-Au Schottky barrier cells, the battery has, including cost, characteristics comparable with a silicon pn junction betavoltaic battery which is now commercially available. The main advantage of the Schottky barrier betavoltaic conversion system is the potentially much wider choice of semiconductor materials. For example, Schottky barriers with larger barrier heights may increase the conversion efficiency of the device, and Schottky barriers with higher radiation resistance may allow one to select a radiation source with longer half-life. Therefore, the emphasis in further research should be directed towards investigation of the betavoltaic effect of other metal–semiconductor junctions (such as those listed in Table 4.1) rather than the production of a commercial prototype with Si-Au Schottky barrier cells.

16. SUMMARY AND CONCLUSIONS

The need for a long-life, high-power density, reliable, and compact microwatt battery was established. Various conversion systems were studied. The betavoltaic-effect with Si-Au Schottky barrier cells was selected for detailed investigation.

To optimize the battery power output, characterization experiments were performed to determine the silicon resistivity and the thickness of the radiation source — ^{147}Pm metal foil. Photovoltaic measurements were also made to compare the results from betavoltaic systems.

Primary shielding was designed to minimize radiation dose rates. Experiments were performed to determine radiation dose rates versus absorber thicknesses. The battery outer capsule was designed to contain the radioactivity under maximum credible accident conditions specified by DOT and AEC transportation regulations.

A prototype battery was built and tested. The economics of such a battery were analyzed and showed that the nuclear battery is favorable for special applications. The design of a practical battery was proposed. Further research areas were recommended.

The results of this study can be concluded as follows:

(1) A betavoltaic conversion system using Si-Au Schottky barrier cells has been proven to be feasible. The conversion efficiency is between 1 to 2%.

(2) A 100-$\mu W/cm^3$ system can be built for a battery with a power level of 200 μW.

(3) Based on economics, the nuclear battery is more favorable than the chemical battery for special applications such as artificial pacemakers.

(4) Commercial development should await the results of research to study the betavoltaic effect on other Schottky barrier cells. The Si-Au battery is likely to be barely competitive with existing silicon p-n junction betavoltaic batteries.

REFERENCES

1. John H. Gibbon, Jr., "Surgery of the Chest," Chapt. 38, *Cardiac Pacemakers and Heart Blocks*, William M. Chandack, W. B. Saunders Company, Philadelphia, Pa., 1969.

2. M. J. Poole, J. Wyatt, A. W. Penn, and M. H. Brown, "Miniature Nuclear Batteries — A Review of the Work in the UK," *Trans. Amer. Nucl. Soc.* 13(2), 508-09 (1970).

3. R. Berger, R. Boucher, B. Jampsin, and M. Hot, "^{238}Pu Sources for Cardiac Pacemakers," *Inform. Bull. Isotop. Generators* 10, 3-21 (November 1970).

4. M. Alais, R. Berger, R. Boucher, and P. Laurens, "^{238}Pu Isotope Generator for Implantable Electro-Systolic Cardiac Stimulator," (in French) *Bull. Inform. Sci. Tech.* (Paris) 142, 31-8 (November 1969).

5. P. Laurens, "French Nuclear-Powered Pacemaker Program," *Trans. Amer. Nucl. Soc.* 13(2), 508 (1970).

6. Nuclear Materials and Equipment Corporation, *Radioisotope Powered Cardiac Pacemaker Program*, Midterm Report, Phase I, NUMEC-3731-13 (April 1968).

7. *Nuclear News* 15(7), 59 (July 1972).

8. B. W. Johansson, "Complete Heart Block," *Acta. Med. Scandinav.* 180, 15 (1966).

9. W. F. Windle, "Microwatt Radioisotope Energy Converters," *IEEE Trans. on Aerospace* 2(2), 646 (April 1964).

10. George W. Sutton (ed.), *Direct Energy Conversion*, McGraw-Hill Book Company, New York, 1966.

11. H. J. Gerwin, *Selected Thermoelectric, Thermionic, and Electron-Voltaic Energy Conversion Device Characteristics*, SC-ARPIC-1011, Sandia Laboratories (May 1969).

12. P. Rappaport, J. J. Loferski, and C. G. Linder, *The Electron-Voltaic Effect in Germanium and Silicon p-n Junctions*, RCA Review, p. 100 (March 1956).

13. H. Flicker, J. J. Loferski, and T. S. Elleman, "Construction of a ^{147}Pm Atomic Battery," *IEEE Transaction on Electron Devices*, ED-11, No. 1, p. 2 (January 1964).

14. W. F. Windle, *^{147}Pm Silicon Betavoltaic Battery Feasibility*, SC-RR-65-671, Sandia Laboratories (January 1966).

15. Russel H. Barnes, R. L. Ritzman, J. F. Kircher, and D. N. Sunderman, *Fabrication Studies on ^{147}Pm Betavoltaic Batteries*, BMI-1709, Battelle Memorial Institute (January 1965).

16. L. C. Olsen, "Betavoltaic Properties of Silicon n-p Junction Devices," Donald W. Douglas Laboratories, presented to American Physical Society, Dallas, Texas, March 1970.

17. M. Lewis and S. E. Seeman, "Performance Experience with Prototype Betacell Nuclear Battery," Donald W. Douglas Laboratories, presented to American Nuclear Society, Miami Beach, Florida, October 1971.

18. A. Y. C. Yu, "The Metal Semiconductor Contact: An Old Device with a New Future," *IEEE Spectrum* 1(3), 83 (1970).

19. S. M. Sze, *Physics of Semiconductor Devices*, Wiley-Interscience, New York, 1969.

20. A. N. Saxena, "Hafnium-Silicon Schottky Barriers: Large Barrier Height on p-Type Silicon and Ohmic Behavior on n-Type Silicon," *Applied Physics Letters* 19(3), 71 (1971).

21. G. S. Pinkham, *The Betavoltaic Effect*, Bachelor of Engineering Thesis, Thayer School of Engineering, Dartmouth College, Hanover, N. H. (September 1970).

22. R. Kalibjian and K. Mayeda, "Photovoltaic and Electrovoltaic Properties of Diffused and Schottky Barriers as Diodes," *Solid State Electronics* 14, 5-29 (1971).

23. David K. Ferry and D. Ronald Fannin, *Physical Electronics*, Addison-Wesley Publishing Company, Reading, Mass., 1971.

24. W. E. Matheson, "Nuclear Batteries," *2nd International Fair and Technical Meeting for Nuclear Industries, Basel, Switzerland, October 1969*, CONF-691018 (1970).

25. A. Scharman, "A Photoelectric Radionuclide-Battery and Its Limits," *Proc. Intl. Sympos. Industrial Applications of Isotopic Power Generators*, AERE, Harwell, September 1966.

26. Charles A. Low, Jr., *High Voltage Generation with a Beta Electrogenerator Cell*, NASA TM X-5-2776, Lewis Research Center, NASA (1970).

27. Peter Roitman, *Betavoltaic Effect in Silicon Schottky Barriers*, MS Thesis, Dartmouth College, Hanover, N. H., 1972.

28. J. J. Loferski and P. Rappaport, "Electrovoltaic Study of Electron Bombardment Damage and Its Thresholds in Ge and Si," *Phys. Rev.* 98, 1861 (June 1955).

29. P. Rappaport and J. J. Loferski, "Threshold for Electron Bombardment Induced Lattice Displacements in Si and Ge," *Phys. Rev.* 100, 1261 (November 1955).

30. R. W. McKee, *An Evaluation of the Prospects for Large-Scale Production of ^{147}Pm*, BNWL-310, Pacific Northwest Laboratories (1966).

31. L. Lidofsky, P. Macklin, and C. S. Wu, "The Beta-Spectrum of ^{147}Pm," *Phys. Rev.* 76, 1888 (December 1949).

32. E. J. Wheelwright, *Preparation of ^{147}Pm Metal and Determination of the Density and Melting Point*, BNWL-959, Pacific Northwest Laboratories (1969).

33. E. H. Kobisk and W. B. Grisham, "Application of Reduction-Distillation Method for Preparing High-Purity Rare-Earth Isotope Metals," *Mater. Res. Bull.* 4, 651-62 (1969).

34. H. Flicker, J. J. Loferski, and J. Scott-Monck, "Radiation Defect Introduction Rates in n- and p-Type Silicon in the Vicinity of the Radiation Damage Threshold," *Phys. Rev.* 128(6), 2557-63 (December 1962).

35. Douglas S. Billington and J. H. Crawford, Jr., *Radiation Damage in Solids*, Princeton University Press, Princeton, N. J. (1961).

36. Claude Finley Williamson *et al.*, *Tables of Range and Stopping Power of Chemical Elements for Charge Particles of Energy 0.05 to 500 MeV*, Rapport CEA-R3042, Centre D'Etudes Nucleaires De Saclay, 1966.

37. J. J. Fitzgerald, G. L. Brownell, and F. J. Mahoney, *Mathematical Theory of Radiation Dosimetry*, Gordon and Breach, New York, 1967.

38. Robley D. Evans, *The Atomic Nucleus*, McGraw-Hill Book Company, New York, 1955.

39. J. H. Jarrett and H. H. Van Tuyl, *Promethium Isotopic Power Data Sheets*, BNWL-1309, Pacific Northwest Laboratories (May 1970).

40. W. H. McMaster, N. Kerr Del Grande, J. H. Mallett, and J. H. Hubbell, *Compilation of X-Ray Cross Sections*, UCRL-50174 Sec. II, Rev. I, Lawrence Radiation Laboratory (May 1969).

41. *Metals Handbook*, Vol. 1, 8th Ed., American Society for Metals, Novelty, Ohio, 1961.

42. *Engineering Properties of Selected Ceramic Materials*, American Ceramic Society, Columbus, Ohio, 1966.

43. J. R. Cameron, N. Suntharalingam, and C. N. Kenney, *Thermoluminescent Dosimetry*, The University of Wisconsin Press, Madison, 1968.

44. H. W. Taylor and A. H. Kukoc, "A Coincidence Study of the Decay of ^{146}Pm," *Nucl. Phys.* A122, 425-30 (1968).

45. Title 10, *Code of Federal Regulations*, Part 20, "Standards for Protection Against Radiation."

46. Title 49, *Code of Federal Regulations*, Parts 170-190.

47. Savannah River Laboratory, *Californium-252 Source and Shipping Capsule Assembly Design and Test Information*, Jan. 21, 1972.

48. E. Sawin, Ceramaseal, Inc., New Lebanon Center, New York, private communication, 1972.

49. "Ceramaseal High-Temperature Terminals and Assemblies," Catalog 661A, Ceramaseal, Inc., New Lebanon Center, New York.

50. Title 10, *Code of Federal Regulations*, Part 71, "Packaging of Radioactive Material for Transport."

51. International Atomic Energy Agency, *Regulations for the Safe Transport of Radioactive Materials*, Safety Series No. 6, Vienna, 1967.

52. R. D. Seagren, *ORNL Isotopes Division Guide for the Packaging of Radioactive Materials for Transport*, ORNL-TM-2769, Oak Ridge National Laboratory (March 1970).

53. R. J. Roark, *Formulas for Stress and Strain*, 4th Ed.,McGraw-Hill Book Company, New York, 1965.

54. Steve Kahn, United Detector Technology, Santa Monica, California, private communication, 1972.

55. Tom Barrows, Medtronic, Inc., Minneapolis, Minnesota, private communication, 1972.

56. Knoxville Cardiovascular Group, Knoxville, Tennessee, private communication, 1972.

57. B. P. Burtt, *Nucleonics* 5(2), 28 (1949).

58. S. M. Sze, D. J. Coleman, Jr., and A. Loya, "Current Transport in Metal-Semiconductor-Metal Structures," *Solid State Electronics* 14, 1209-18 (1971).

59. *Handbook of Chemistry and Physics*, Chemical Rubber Publishing Company, 1971-1972, p. B-233.

60. C. A. Mead, "Metal Semiconductor Surface Barriers," *Solid State Electronics* 9, 1023 (1966).

61. J. K. Poggenburg, *A Study of Thulium-171 as a Power Source for Circulating Support Systems*, ORNL-4283, Oak Ridge National Laboratory (May 1969).

62. Division of Applied Technology, *Isotope Development Programs — Research and Development, 1971*, TID-4067, U. S. Atomic Energy Commission (1972).

BIBLIOGRAPHY

Archer, R. J. and T. O. Yep, "Dependence of Schottky Barrier Height on Donor Concentrations," *J. Appl. Phys.* 41(1), 303 (January 1970).

Cameron, J. R., N. Suntharalingam, and C. N. Kenney, *Thermoluminescent Dosimetry*, The University of Wisconsin Press, Madison, 1968.

Chang, C. Y. and S. M. Sze, "Carrier Transport Across Metal Semiconductor Barriers," *Solid State Electronics* 13, 727 (1970).

Corliss, W. R. and D. G. Harvey, *Radioisotopic Power Generation*, Prentice-Hall, Inc., New Jersey, 1964.

Cowley, A. M. and S. M. Sze, "Surface States and Barrier Height of Metal-Semiconductor Systems," *J. Appl. Phys.* 36(10), 3212 (October 1965).

Crowell, C. R., *et al.*, "Surface State and Interface Effects in Schottky Barriers at n-Type Silicon Surfaces," *J. Appl. Phys.* 36(12), 3843 (December 1965).

Everhart, T. E. and P. H. Hoff, "Determination of Kilovolt Electron Energy Dissipation vs Penetration Distance in Solid Materials," *J. Appl. Phys.* 42(13), 5837 (December 1971).

Fitzgerald, J. J., *Applied Radiation Protection and Control*, Gordon and Breach, New York, 1969.

Garrett, Alfred B., *Batteries of Today*, Research Press, Inc., Dayton, Ohio, 1957.

Kahny, D., "Conduction Properties of the Au-n Type Si Schottky Barrier," *Solid State Electronics* 6, 281 (1963).

Kaye, J. and J. A. Welsh (eds.), *Direct Conversion of Heat to Electricity*, John Wiley & Sons, Inc., New York, N. Y., 1960.

Kidwell, Walter, *Electrical Instruments and Measurements*, McGraw Hill, New York, 1969.

Luppold, David S., *Precision DC Measurements and Standards*, Addison-Wesley, Reading, Mass., 1969.

Miley, George H., *Direct Conversion of Nuclear Radiation Energy*, American Nuclear Society, 1970.

Milnes, A. G. and D. L. Fencht, *Heterojunctions and Metal-Semiconductor Junctions*, Academic Press, New York, 1972.

Morse, J. G., "Energy for Remote Areas," *Science* 139(3560), 1175 (March 1963).

Pinajian, J. J. and J. F. Allen, "The (n,γ) Absorption Cross Section of ^{146}Pm for Reactor Neutrons," *J. Inorg. Nucl. Chem.* 29, 2117 (1967).

Price, William J., *Nuclear Radiation Detection*, McGraw-Hill, New York, 1964.

Rupp, A. F. and J. J. Pinajian, "Isotopes," *Encyclopedia of Physics*, revised edition, Robert M. Besancon (ed.), Reinhold Publishing Company, New York, August 1972.

Sheppard, J. C. and H. H. Van Tuyl, *Hanford ^{146}Pm Burnout Experiments*, BNWL-1270, Pacific Northwest Laboratories (January 1970).

Wheelwright, E. J., *et al.*, "Calorimetric Determination of the Mean β Energy and Half-Life of ^{147}Pm," *J. Phys. Chem.* 69, 1220-23 (1965).